PETROGENESIS AND LITHOSTRUCTURAL ANALYSES OF SINGHBHUM GROUP OF METASEDIMENTS AT SOUTHERN EXTREMITY OF SINGHBHUM SHEAR ZONE AND THEIR POTENTIAL FOR U-CU MINERALIZATION IN KESHARPUR-KUSUMBARI-TILOGORIA-DUMURDIHA TRACT, MAYURBHANJ DISTRICT, ODISHA.

by

ANKUR KUMAR

ENGG1G201801009

Bhabha Atomic Research Centre, Mumbai

A thesis submitted to the
Board of Studies in Engineering Sciences

In partial fulfillment of requirements

for the Degree of

MASTER OF TECHNOLOGY

of

HOMI BHABHA NATIONAL INSTITUTE

February, 2021

Homi Bhabha National Institute

Recommendations of the Thesis Examining Committee

As the members of the Thesis Examining Committee, we recommend that the thesis prepared by **Mr Ankur Kumar**, entitled "**Petrogenesis and Lithostructural analyses of Singhbhum Group of metasediments at southern extremity of Singhbhum Shear Zone and their potential for U-Cu mineralization in Kesharpur-Kusumbari-Tilogoria-Dumurdiha tract, Mayurbhanj district, Odisha**" be accepted as fulfilling the thesis requirement for the degree of Master of Technology.

	Name	Signature
Member-1	Dr. D. K. Sinha	DKSinha
Member-2	Dr. T. S. Sunil Kumar	
Member-3	Dr. Navin Goyal	
Member-4	Dr. Pranesh Sengupta $	P. Sengupta
Member-5	Dr. A. Rama Raju	
Technical advisor	Shri B. K. Tripathi	Brajesh Kumar Tripathi
Examiner	Prof. R. Krishnamurthi $	R. Kmi
Guide & Convener	Dr. Kalyan Chakrabarti	Chakrabarti
Chairman	Prof. Vivekanand Kain $	

$ Participated through video conferencing

Final approval and acceptance of this thesis is contingent upon the candidate's submission of the final copies of the thesis to HBNI.

I hereby certify that I have read this thesis prepared under my direction and recommend that it may be accepted as fulfilling the thesis requirement.

Date: 11-02-2021

Place: Hyderabad

Dr. Kalyan Chakrabarti

(Project Guide)

DECLARATION

I, hereby declare that the investigation presented in the thesis has been carried out by me. The work is original and has not been submitted earlier as a whole or in part for a degree/ diploma at this or any other Institution/University.

(ANKUR KUMAR)

ACKNOWLEDGEMENT

I sincerely thank Dr. D. K. Sinha, Director, Atomic Minerals Directorate for Exploration and Research, Hyderabad for permission and providing me an opportunity to pursue the M.Tech. Programme. I would like to express my heartfelt gratitude to my guide Dr. Kalyan Chakrabarti, Regional Director, Atomic Minerals Directorate for Exploration and Research (AMD), Eastern Region, Jamshedpur and technical advisor Shri B.K. Tripathi, Deputy Regional Director, Atomic Minerals Directorate for Exploration and Research (AMD), Eastern Region, Jamshedpur for their invaluable guidance, comments, and suggestions throughout the course of the project.

I am thankful to competent authority Homi Bhabha National Institute (HBNI) for providing me opportunity to pursue M.Tech. I acknowledge Prof. P.R. Vasudeva Rao, Vice-Chancellor, HBNI and Prof. Vivekanand Jain, Dean-Academic, Engg. Sci. Stream-I, Head MP & CED, BARC.

I would also like to thank Shri. S. Hamilton, Additional Director (Operations-I), Shri. B. Sarvanan, Additional Director (Operations-II), and Dr. T.S Sunil Kumar, Additional Director (R&D) and Dr. Rama Raju, In-Charge, BARCTS for their encouragement, administrative support, and conducting this entire M. Tech. programme.

I extend my gratefulness to Mrs V S Akhila for their constant and fruitful guidance and patience during long hours of petrological studies and discussions, Shri Vijay Kumar, In-Charge Chemical Laboratory, AMD, Eastern Region, Dr. Joydeep Sen In-Charge, XRF Lab, AMD, Hyderabad, Dr. Ajay Kumar, In-Charge, XRF Lab, AMD, Nagpur, Dr.Vishwanathan XRD Lab, AMD Hyderabad, and Dr, Chancghal Sarbajna, In-Charge EPMA lab, AMD Hyderabad for their extensive laboratory support.

I thank Shri Debashis Bhatacharya, Incharge, Singhbhum Shear Zone East Investigations, AMD, Eastern Region for their cooperation and support. I am extremely grateful to Shri B S Panigrahi, Technical Secretary, AMD, ER, Jamshedpur for providing me the infrastructural facilities available in the department. I acknowledge Shri Aneesh VJ, SO/D, Shri Nithil Pillai, SO/D, Shri Atanu Mukherjee SO/E, Shri Parvej Alam SO/C, Shri SP Upadhyay for their genuine support and guidance.

I am indebted to the entire exploration team of Singhbhum Shear Zone (East) Investigations for their constant encouragement, genuine criticism and guidance at different stages of this work.

CONTENTS

SYNOPSIS

Early to middle Proterozoic uranium mineralisation is a major episode of uranium metallogeny felt across the globe. Development of uranium Province in Singhbhum Shear Zone (SSZ) also took place within the above said age bracket. The Singhbhum Shear Zone formed the part of the supercontinent 'Ur' that latter is believed to be accreted to various mobile belts during Grenville Orogeny (1.0 Ga). The evidence of Grenville Orogeny are manifested in the form of Proterozoic granitoid bodies throughout the world, which known to play significant role as host and source for uranium mineralization which is facilitated by hydrothermal alteration, intensive leaching, metasomatism, and migmatization. Throughout the Singhbhum shear zone sporadic patches of albitized/metasomatized schists have been reported in close association with Soda Granite. These granitic bodies and albitized rocks, like the feldspathic schists are known to host the uranium and copper mineralization in the Singhbhum Shear Zone. Various metallogenic models have been proposed to explain the uranium and copper mineralization in feldspathic schist. The present project attempts to investigate and verify those proposed models at south-eastern tip of Singhbhum shear zone near Kuliana sub-district, Mayurbhanj district, Odisha.

In the present study Singhbhum metasediments, Romapahari Granite, and associated feldspathic rocks occurring on the south-eastern tip of Singhbhum shear zone (SSZ) have been mapped geologically from the Kesharpur in the North to the Dumurdiha in the South. Structural elements preserved in the granites, and associated metasediments, were studied in order to decipher the structural history of the area. A stratigraphic order for the different lithounits in the area has also been suggested.

Detailed petrological variations within the Romapahari Granite and associated metasediments of the shear zone have been studied. The XRF analysis, XRD study, and EPMA analysis of a few mineralized samples were carried out to understand the genetic aspect of uranium and copper mineralization. Based on analytical data the chemical characters of a granitic rocks and associated metasediments have been determined.

Considering the mineralogical, chemical, textural and structural criteria, a high temperature origin of the radioactive feldspathic rocks has been inferred. It has been pointed out that the high temperature sodium rich magmatic/pegmatitic fluids which are possibly generated by the partial melting of the Singhbhum Granite during intense shear movements could cause feldspathization.

Copper-sulphide and uranium mineralization occurring in close association with the feldspathic schists have also been studied. A close relationship between feldspathic schist and ore mineralization has been established. It is also suggested that the country rocks through which the high temperature sodic solutions passed through might have contributed a significant amount of Cu, U, Ni, Cr etc. to these solutions to give rise to sulphide and oxide mineral phases which formed the ore minerals.

LIST OF FIGURES

LIST OF TABLES

CHAPTER 1

INTRODUCTION

1.1 Thesis Introduction

The Singhbhum shear zone (SSZ) is an arcuate, polymetallic and polymetamorphic belt (Banerji, 1981) that has been prominently developed at the contact of Proterozoic fold belt of North Singhbhum and the Archaean craton of Singhbhum Granite (Mukhopadhya and Deb, 1995). It is northerly dipping high strain zone which is believed to come into existence after overthrusting of older rocks from the north against the younger rock of south (Dunn, 1937; Dunn and Dey, 1942). The shear zone is continued for about 200 km strike length, along E-W direction in western part to NNE-SSE direction in the southeastern part (Mukhopadhya and Deb, 1995). The belt is well known for rich deposits of copper (Cu), uranium (U), apatite-magnetite, and kyanite.

SSZ has been associated with several generations of folds, cleavages and lineation with characteristic geometry due to distinctive structural history. These structures can easily be observed at macroscopic as well as microscopic level and could be interpreted as a product of major ductile deformation (Sengupta & Ghosh, 1990, 1997). Despite being the fact that the developed structures in SSZ shared similar structural evolution, the observed deformation is highly heterogeneous, and can be attributed to the spatial variation in shear intensity (Sengupta & Ghosh, 1997).

Earlier researchers like Dunn & Dey (1942) mapped and discretized SSZ based on the distribution of granophyres that were grading to biotite-granite-gneiss and suggested Gourmasahi as a Western end, and Bharagora as Southern end of SSZ. Later many workers re-examined the parts of the Singhbhum Shear zone and came up with different opinions related to the continuation of the Singhbhum Shear zone. Naha (1954, 1956) has suggested that SSZ extends further Southwards than was formerly believed (Dunn & Dey 1942). Later it has been further proposed by Naha (1977) that the Kendua fault can be considered as southern extension of SSZ. Sengupta & Ghosh (1997) has also advised to trace the continuation of SSZ based on spatial distribution of mylonites and phylonites that have been formed due to shearing of mica-schist, quartzite, granite and amphibolite. However, these aspects have not yet been fully investigated at southern extremity of SSZ and it has been aimed to study in the present work. Therefore one of the prime objective of present study is to addresses the gap related to the nature of shearing and its correlation with Singhbhum Shear Zone at the proposed study area (Fig 1-1).

The SSZ has not only known for its structural complexity rather its workable deposits of Copper (Cu) and Uranium (U) has always taken an attention of exploration geologists. Because of numerous deposits of Copper minerals, SSZ has also been referred to as 'The Singhbhum Copper belt' (Ghosh, 1972). The curiosity to know the close association of Cu and U with SSZ has always been major concerned to many of the field geologists. In order to cognize the genetic aspects of Cu and U mineralization in SSZ many ideas have been propounded by different researchers. It has been founded that these ideas are highly controversial and differs widely.

Earlier researchers like Dunn (1937) and Bhola (1965) described Cu and U mineralization based on epigenetic hydrothermal model, while Banerji (1962, 1974, 1981), Talpatra (1968), and Ghosh (1972) were in favor of metosomatic hydrothermal origin. Meanwhile Sarkar et al., 1971 and Sarkar and Deb (1974), linked these deposits to exhalative volcanogenic layer type deposit. Since most of these studies were carried out in parts of SSZ where Soda-granite and ore minerals are closely associated, therefore, most of the proposed models were tempting to hypothesize the role of soda-granite in Cu and U mineralization (Ghosh, 1972). The present study area is lying on southern extremity of SSZ where continuation of SSZ is ambiguous and no soda-granite body is exposed on the surface. Although the recent subsurface investigation by AMD (unpublished AMD annual report FS-2019/20) indicates the presence feldspathic schist, a schistose variety of soda granite. However, those metallogenic models that have been proposed in main SSZ have not yet been tested in the present area. Therefore, there is a scope for verification of the existing opinions and understanding the genetic aspects of Cu and U mineralization within the limited scope of present M.tech dissertation work.

1.2 Objectives of the study

Present work has been carried out on metasediments at southeastern extremity of Singhbhum craton in Kesharpur-Kusumbari-Tilogoria-Dumurdiha tract, Mayurbhanj district, Odisha pursuing the following objectives.

1. To decipher lithological and structural dispositions of different litho-units exposed over an area of 10sq km on a scale of 1:5000RF.
2. To study the continuation of SSZ at its southern end.
3. To elucidate sequence of events including phases of deformation, shearing events.
4. To understand the uranium and copper mineralization with reference to the structure and other controlling factors.
5. To propose a genetic model for U- Cu mineralization in this area.

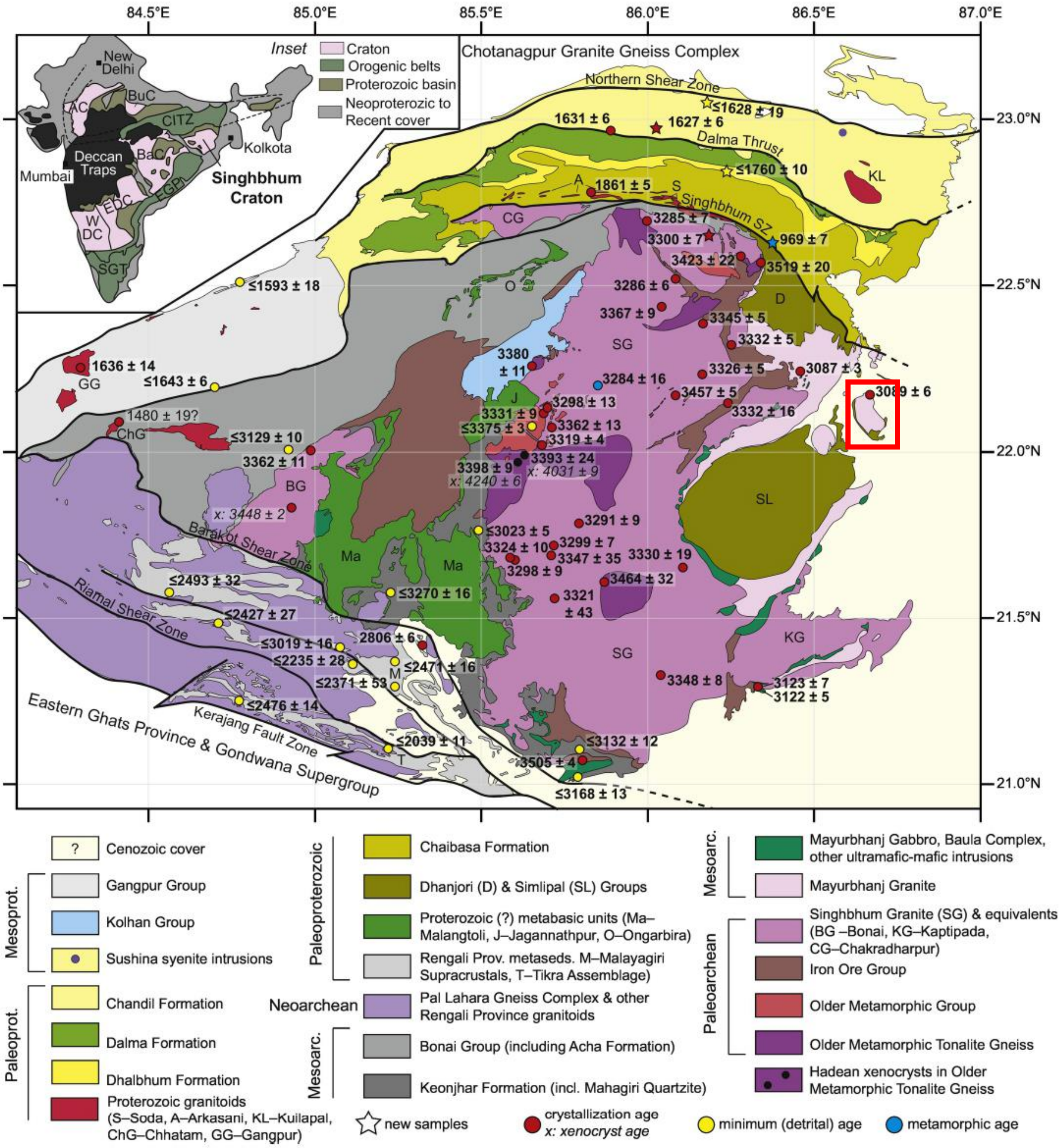

Figure 1.1 Geological map of Singhbhum craton and supracrustal province after Olierook, (2019); open red-rectangle marks the present study area.

1.3 Methodology

The Methodology for the present study divided into three steps. The first step is the field investigation which involves the detailed litho-structural mapping of 32 sq km area to deliante the different lithounits, potential radioactive zones, and to carry out systematic sampling. The second step will be lab investigation which includes physical assay, petromineralogical study, and geochemical analysis of the collected samples. The final step is the data integration for the comprehensive understanding of the area as well as to establish the genetic coherence of uranium and associated mineralization in study area. The detail associated with each step is given below.

1.3.1 Satellite data Interpretation and Field Investigation

- Study of geomorphological features in satellite imagery and digital elevation model (DEM).
- Detailed litho-structural mapping over 32 sq km area (1:5000 RF) to delineate the litho-units and their contact-relationship displaying evidence of multiple deformational history.
- Structural mapping of selected area to elucidate the structural disposition of the litho-units and understand the deformation pattern.
- Delineation of radioactive zone and establishment of the field controls on U mineralization vis- a-vis the Cu- mineralization.
- Systematic sampling from the mineralized as well as non-mineralized zones for petrographic, petrofabric (microstructural and micro-textural studies) and geochemical analyses.

1.3.2 Laboratory Investigation

Physical Assay

- Physical assay of radioactive samples for estimation of eU_3O_8, U_3O_8 (β-γ), ThO_2, and K in Physics laboratory, AMD, Eastern Region.
- Study of disequilibrium for uranium mineralization in the study area.

Petrography

- Petrofabric (microstructural and micro-textural studies) and Petro-mineralogical study to characterize different rock types, micro-structures of the shear zone and identification of radioactive and associated mineral phases respectively.
- Study of mode of occurrence and textural features of U & Cu mineral phases to understand the paragenetic relationship, under optical microscope (*polarizing microscope, E-600, Nikon with Biovis image analysis system, version 1.50 for photomicrography*).
- High Resolution Electron microscopy of a few selected samples under EPMA study for minero-chemical analysis. Understanding relationship between uranium and associated mineral phases.

Chemical Analysis

- Analyses of host rocks for major and trace elements by WDXRF (*MagiX Pro PW 2440 (PAN analytical); ARL PERFORM'X 4200 (Thermo Fisher Scientific)*) & ICP-OES.
- Analyses of Ore-Zone samples for major and trace elements by XRF and other analytical techniques.
- Characteristics of minerals (ore and gangue) by XRD (*GE-XRD-3003*) and EPMA (*Cameca (France) make SX-100*) studies.

1.3.3 Data processing and Interpretation

- Interpretation of lithological and structural data for understanding geological controls of mineralization.
- Interpretation of geochemical data of the host-rocks in terms of its elemental concentrations and their redistributions during hydrothermal alteration, if any.
- Interpretation of petro-mineralogical, petrofabric (microstructural and micro-textural studies) and mineral chemistry data of the mineralized zones.
- Integration of all the above data for comprehensive understanding of the genetic coherence of uranium and associated mineralization in study area.

1.4 Study Area

The present study area is located in eastern part of Kuliana tehsil of Mayurbhanj district, Odisha belonging to SOI toposheet no- 73J/12. It is bounded by latitude 22°01'58.23"N - 22° 6'25.10"N and longitude 86°39'52.99"E - 86°41'23.11"E. It presents rugged and plain topography, residual hills trending NE-SW direction. The area mostly covered with soil and agricultural land with flat topography. Different rock types exposed in the area are hornblende-biotite granite, hornblende-biotite-qaurtz schist, biotite-chlorite-sericite-quartz schist, fuchsite quartzite, kyanite quartzite, ferrugenized quartzite, metabasalt, gabbro and dolerite with multiple small scale quartz veins. The general strike of the lithologies varies from NNE-SSW direction in eastern part to NNW-SSE direction in western part with moderate to steep dips towards northerly direction forming a synformal disposition.

1.5 Location and accessibility

The study area is 5 km from Kuliana tehsil connected through metalled road and 22 km from district headquarter Baripada connected by NH-18 up to Kuliana tehsil. The nearest railway station is Buramara railway station situated on Roopsa-Bangariposi broad gauge. The study area is 285 km in NE direction from the state capital Bhubaneshwar and can be accessed through Cuttack- Bhadrak- Balesore- Baripada route from south. Within the study area the major villages are well connected by metalled road while remote localities are well connected through pakka road and foot tract.

1.6 Physiography and drainage

The mapped area presents a rugged and plain topography. The Budhabalanga River is the main river system flowing in western part of the area. The flow direction of the river is from north to south. The eastern part of the Budhabalanga River constitutes sub-peneplained surface with a few small mounds and linear ridges with prominent ridges trending along NE-SW direction and rising up to 168m above msl with general ground level is about 100 m above msl. The monotonous vast expanse of the plain country is mostly covered with soil and alluvium with scanty exposures occuring around Madansahi-Kesharpur-Buramara area forming small mounds. The plain country is drained by several ephemeral nalas flowing into the Budhabalanga River. All the tributaries of the area join the higher order Budhabalanga River.

1.7 Climate and rainfall

The climate of the area is tropical to sub-tropical. The area is experienced by high and well distributed rainfall during monsoon. The average annual rainfall is about 1500mm. most of which is precipitated between June and October. The relative humidity in the area is varies from 26 to 84°C. The general temperature ranges from 5°-7°C in winter to 40°-45°C in summer.

1.8 Flora and fauna

The area has moderated density of forest cover with thick dense growth of sal trees with thorny bushes and shrubs. The varied types of plant include sal, jackfruit, acacia, papal, neem mango, java plum, etc. Most of the plain area is cultivated with mustard, rice and seasonal vegetables. Natural fauna comprises of snakes, fox, goat, wild lizard, rabbits and scorpion.

1.9 Infrastructure and environment

The area is well connected by metal road with district headquarter and other major localities. The private bus services provide good transport facilities in the area. The sub-tehsil Kuliana is a small town with good facilities for locale marketing. There is a govt. hospital in kuliana providing medical facilities in the area. Water facility is good and well connected through pipeline supply from Budhabalanga River to the major localities both for agriculture as well as for drinking purpose. In eastern part of the area Haldia dam is major reservoir. However remote localities are dependent on borewell and dugwell. People are mainly dependent on farming, mostly sowing summer and winter crops.

CHAPTER 2

REGIONAL GEOLOGY

The Eastern part of Indian Precambrain Shield exposes 200km long, an arcuate, polymetallic and polymetamorphic mineralized zone known as Singhbhum shear zone (SSZ) (Banerji, 1981). Dunn (1937) and Dunn and Dey (1942) defined SSZ as zone of overthrusting along which older rocks from the north thrust against younger rock from south. According to Banerji (1969, 1974, 1981) SSZ was primarily a zone of deep seated fractures and volcanism, however, later thrusting of North Singhbhum fold Belt (NSFB) against the southern Archean platform (Singhbhum craton) turned it into shear zone. Banerji (1981) further concluded that because of thrusting, change of temperature and pressure has resulted a geochemical alteration causing albite metosomatism, biotitization, chloritization etc., and ultimately resulted in the formation of the ore deposits.

2.1 General Geology

SSZ marks the boundary between NSFB and Singhbhum craton (SC) of the Archean age (Fig 2.1). The nucleus of Singhbhum craton made up of Older Metamorphic Group (OMG) and Older Metamorphic Tonalite Gneiss (OMTG) that seems to be deformed 3200 m.y. ago (Sarkar, 1969). OMG and OMTG form the basement for group of older metasediments consisting of moderate to high grade argillites, calc-magnesian, metasediments, and arenites. These older metasediments along with older metamorphic Group (OMG and OMTG) get further intruded by Singhbhum Granite (SBG) around 2900 m.y. ago (Saha, 1979). More than 12 magmatic bodies of Singhbhum Granite complex have been reported from the craton (Saha, 1994, Meert et al., 2010). Singhbhum Granite (SBG), in turn, has been further intruded by Newer Dolerite Dyke swarm.

The age of the rocks within Singhbhum craton varies from Paleoarchaean to Neoproterozoic. Younger rocks are found toward north. Isotopic data suggest that the Singhbhum craton contains rocks ranging in age from 3500 Ma to 900 Ma (Mazumder et al., 2012a). The Singhbum craton is a result of 2.1 billion-year cratonization process, and within that time it has undergone collision with mobile belts (3.0 Ga), suturing with continents and formation of supercontinent 'Ur' (1.5 Ga), and rifting during dispersal of Rodinia (0.6 Ga) (Rogers, 1996; Sarkar and Gupta, 2012). In addition, it has experienced two other orogeny events: Grenville and Pan-African orogeny (Table 2.1).

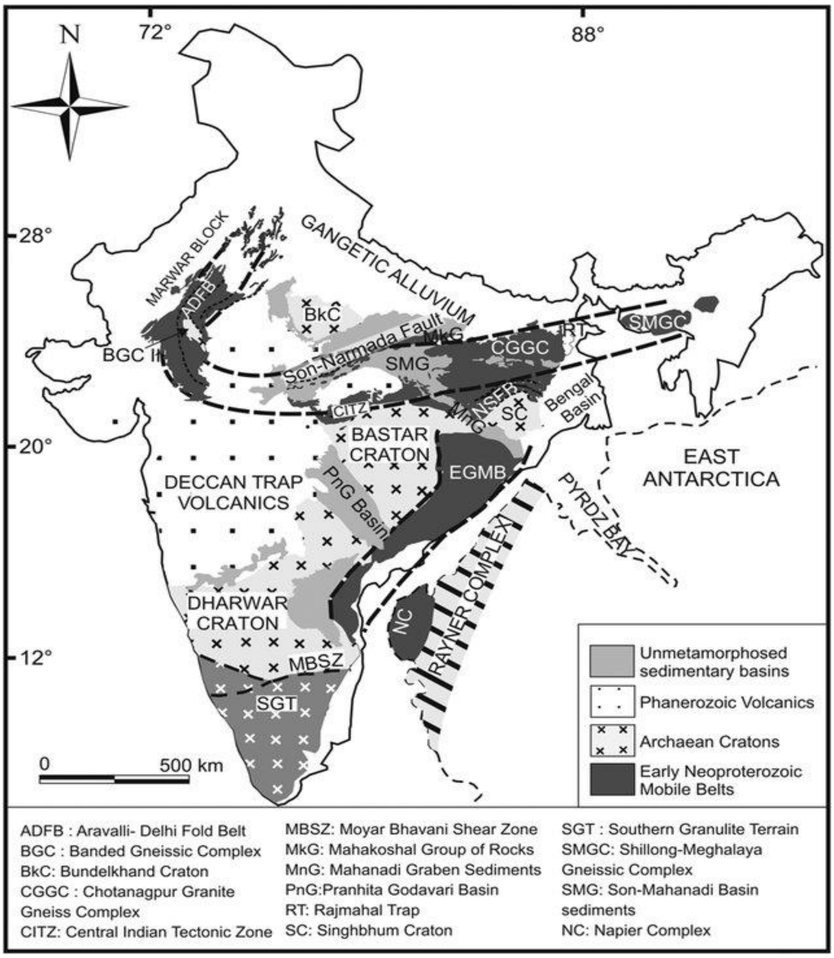

Figure 2.1 Generalized tectonic map of Indian subcontinent during Rodiana: modified after Dasgupta and Sengupta (2003).

The Singhbhum Granite body is enveloped by four groups of younger rocks which together constitute the Iron Ore Super-group (Banerji, 1977). The oldest member of the super-group is Gorumahisani Group, which mostly occurs to the north and east of the Singhbhum granite and majorly consists of epidorite, hornblende schist, gritty and cherty quartzite, and hematite shale-phyllite. This group is unconformably overlain by quartzitic conglomerate, chloritic and carbonaceous tuff, and phyllite locally called Dhanjori Group. The Dhanjori Group further lain by thick sequence of tholeiitic lava known as Dhanjori lava. The Dhanjori Group and Dhanjori lava are further intruded by Mayurbhanj Granite (Saha, 1975). The next member of the supergroup is Noamundi Group (younger than Mayurbhanj granite), occurs in the western part of the platform, and consists of thick sequence of tuffaceous shale-phyllite. This group is overlain by sandstone-conglomerate, shale and limestone, called Kolhan group (Banerji, 1981), which formed in an intracratonic rift basin related to the fragmentation of Rodinia (Bandopadhyay and Sengupta, 2004; Mukhopadhyay et al., 2006). These rocks were deformed into a series of tight folds, overturned to the south, along the northern border of the platform, but the folds gradually open out toward the east and west, in which directions the intensity of deformation decreased (Banerji, 1964).

The North Singhbhum fold belt (NSFB) is made up of Singhbhum, Porhat and Gangpur Groups, spanning over a time range between 2,000 to 850 m.y. (Banerji, 1975). The oldest of these rocks called the Singhbhum Group (Chaibasa Formation and Dhalbhum Formation) (Mazumder, 2005), consists of garnet-staurolite-, kyanite- and occasionally sillimanite-bearing mica schist and quartzite, and innumerable bodies of schistose and massive amphibolite. The rocks show various sedimentological features similar to those of flysch deposits and are considered to have been deposited under eugeosynclinal conditions (Mathur, 1964; Naha, 1965; Iyengar and Anandalwar, 1965;

Bhattacharyya, 1966). They have been affected by four successive phases of, coaxial deformation and metamorphism (Bhattacharyya, 1978; Bhattacharyya et al., 1976, Banerji., 1981).

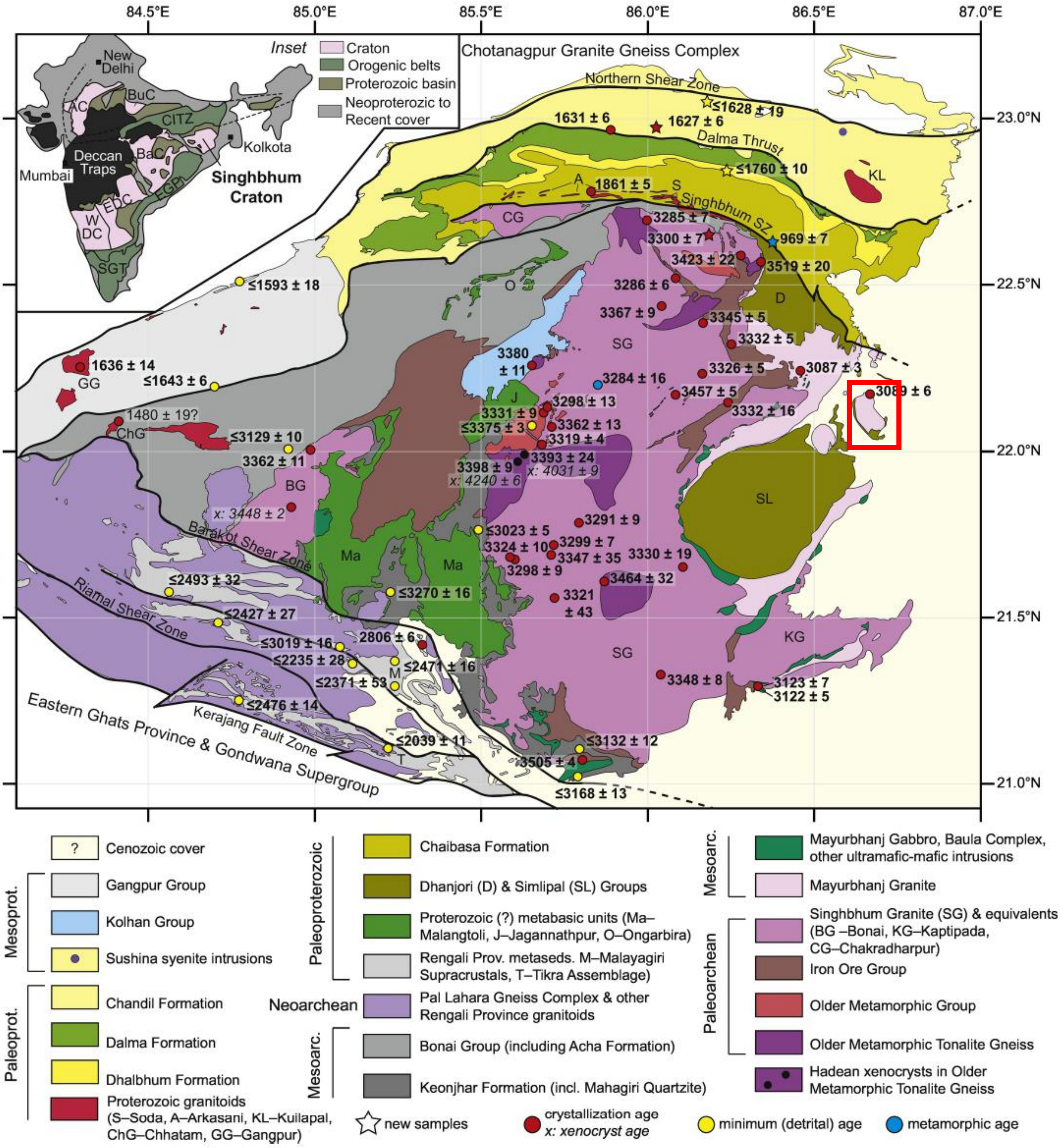

Figure 2.2 a Geological map of Singhbhum craton and supracrustal province, Olierook, (2019); open red-rectangle marks the present study area.

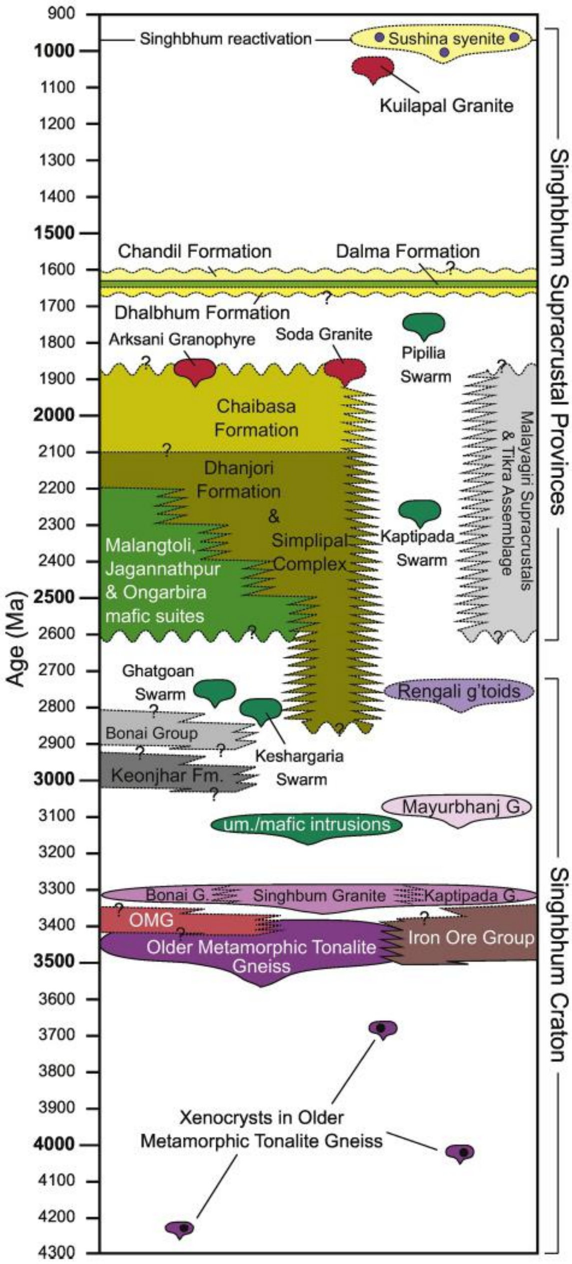

Figure 2.2 b Stratigraphic succession of the Singhbhum Craton and Singhbhum Supracrustal province. Olierook, (2019)

Rocks of the Dhalbhum Formation show fine laminations throughout with occasional cross bedding in the quartzite in the lower part, indicating that the eugeosyncline had stabilized considerably during their deposition. Tuffaceous shale-phyllite and quartzite overlie these rocks in the western part of the area and constitute the Porhat Group. Bedding is well preserved in these rocks over which a cleavage and a strain-slip cleavage are superimposed indicating the effects of two phases of deformation in contrast to the three three phases in Dhalbhum Group. The youngest member of the Singhbhum Supergroup is called the Gangpur Group.

2.2 Archaean nucleus

The Archaean nucleus of Singhbhum craton is represented by three major components, the first and oldest one is Older Metamorphic Group (OMG) and Older Metamorphic Tonalitic Gneiss (OMTG). The second major component is massif of Singhbhum Granite, Bonai Granite, Kaptipada Granite and Pallahara Gneiss. The last component is younger supracrustals that include iron ore basins (Mukhopadhyay, 2001). Other than that granitic activity of slightly younger ages are represented by Tamperkola Granite, Rengali-Raimal Granulite, and Mayurbhanj Granite. Singhbhum Granite is further intruded by intersecting sets of 'Newer Dolerite Dyke Swarm' (2.6 Ga).

2.2.1 Older Metamorphic Group (OMG) - Older Metamorphic Tonalite Gneisses (OMTG)

One of the oldest unit of Archean nucleus is the Older Metmorphic Group (OMG). It basically consists of amphibolite facies, pelitic schists, quartzites, banded calc-gneisses, cummingtonite schists, and quartz- magnetite (Mukhopadhyay, 2001). Origin of OMG is slightly controversial, recovered zircons from siliceous-aluminous sediments indicates granitic origin and further suggesting the existence of older sialic microcontinents (Mukhopadhyay, 2001). The Pb^{207}-Pb^{206} ages of zircon grains cluster around 3.55Ga, 3.4Ga, 3.2 Ga (Goswami et al., 1995; Mishra et al., 1999; Mukhopadhyay, 2001). However, rounded to sub-rounded zircon belonging to 3.55 Ga group suggests detrital origin, whereas the subhedral zircons belong to younger age group point towards metamorphic origin (Mukhopadhyay, 2001). Tonalite-

Trondhjemite Gneisses (TTG) are also present at the contact with amphibolites (Meert et al., 2010).

OMG rocks are intruded by OMTG (Mukhopadhyay, 2001) which consists of mostly tonalite-trondhjemite with some granodiorite. OMTG has been derived from partial melting (20%) of OMG amphibolites and partially from older crustal rocks (Mukhopadhyay, 2001). TTG in OMTG suggests slab melting in a subduction model at shallow depth (Sarkar and Gupta, 2012; Foley et al., 2002; Martin and Moyen, 2002). An igneous crystallization age of 3380 ±11 Ma based on $^{207}Pb/^{206}Pb$ dates of zircon has been obtained (Nelson et al., 2007). Both OMTG and OMG have been affected by major metamorphic event that occur around 3.2 Ga.

2.2.2 Singhbhum Granite (SBG)

Singhbhum Granite intruded into OMG-OMTG and younger metasedimentary rocks in polyphase emplacement (Naqvi and Rogers, 1987). SBG has been outcropped in form of atleast 12 separate magmatic bodies. Geochronological data suggest that these 12 bodies were emplaced in three successive steps: earliest intrusion at 3.45-3.5 Ga, followed by 3.3 Ga and 3.1 Ga emplacement (Saha., 1972, 1994; Acharya et al., 2008; Mishra et al., 1999; Mondal et al., 2007; Meert et al., 2010).

Three phases of SBG termed as phase I, II, and III. These rocks have been found to vary from biotite granodiorite to adamellitic granite and some rare gradation of granodiorite to trondhjemite (Mukhopadhyay, 2001). The rocks of phase-I intrusion are relatively K-poor granodiorite-trondhjemite, and phase-II and phase-III rocks are granodiorite grading to adamellitic granite (Saha, 1972; Saha et al., 1984; Saha et al., 1988; Saha, 1994). Each of the phases is compositionally distinct in terms of both major and trace element geochemistry.

Based on REE patterns Singhbhum Granite is classified into two distinct types: type A and type B. Type-A patterns have gently sloping REE pattern with relatively enriched LREE and similar to OMTG whereas type-B shows moderately enriched LREE and flat HREE. Samples from phase I and II shows type-A pattern and those of phase III shows type-B pattern. Hence the oldest phase of Singhbhum Granite is as old as OMTG, but the xenoliths of banded OMTG in the former indicates an age difference (Saha et al., 1984). Based on geochronological evidence Moorbath and Taylor (1988) have proposed that the protolith of OMTG and SBG were extracted from the mantle at same time and their age difference is of the order of 150 Ma.

The presence of banded xenoliths of OMTG with in SBG-A indicates that OMG and OMTG were deformed earlier before its emplacement (Mukhopadhyay, 2001).Enclaves of OMG amphibolites and OMTG are reported within SBG-A, while in SBG-B enclaves of IOG rocks are common (Sarkar and Gupta, 2012).

2.2.3 Other Granitic bodies

2.2.3.1 Bonai Granite (BG)

Small ovoid body (700 km²) of Bonai Granite is separated from SBG by a belt of IOG rocks of Jamda-Koira-Noamundi basin. The modal composition of the pluton is granite-granodiorite and rarely tonalite; the pluton contains xenoliths of TTG, banded migmatites, quartzite, BIF, and mafic-ultramafic rocks (Mukhopadhyay, 2001). REE pattern of host granitoids have flat HREE pattern, moderately enriched LREE, and negative Eu-anomaly which is similar to SBG-B. U-Pb age of subhedral to nearly euhedral zircon has given an age of 3.4 Ga as its upper intercept on discordia line (Sengupta et al., 1991; Sengupta et al., 1996).

2.2.3.2 Kaptipada Granite (KG)

Kaptipada Granite (KG), also known as Nilgiri Granite, is found in the east of the southern part of Singhbhum Granite, and it is surrounded on all sides by supracrustal and intrusive rocks. Compositionally it is tonalite-granodiorite-granite massif (Sarkar and Gupta, 2012). Similar to Singhbhum Granite and Bonai Granite; xenoliths of amphibolite and migmatite are found within high Al_2O_3 tonalite-trondhjhemite granodiorite which shows a fractionated REE pattern without Eu-anomaly (Mukhopadhyay, 2001). This pluton is thought to have been derived by partial melting of amphibolite source and has produced Rb-Sr age of around 3.3Ga (Vohra et al., 1991).

2.2.3.2 Mayurbhanj Granite (MBG)

Mayurbhanj Granite (MBG) occurs as small body east of the Singhbhum Granite and is intrusive into the latter. It is a K_2O rich rock which is believed to be anorogenic (Saha, 1994). MBG was dated by Rb-Sr whole rock isochron to be 2.2Ga and 1.9 Ga (Iyenger et al., 1981; Vohra et al., 1991) and Pb-Pb zircon age have given an age of 3.1 Ga (Mishra et al., 1999) suggesting that emplacement of Mayurbhanj Granite was coeval with the emplacement of SBG-B.

Another granitic bodies like Pal-Lahara Gneiss (Sarkar et al., 1990) plots in the 'Granite field'. Charnockitic bodies occur within the Pala Lahara Gneiss. They have been named as 'Rengali-Raimal Granulite' and dated as 2.74 Ga by Rb-Sr whole rock isochron method. 'Tamperkola Granite' associated west of Bonai granite BG has high K_2O/Na_2O and K_2O+Na_2O/SiO_2 ratios (Mahalik, 1994), it is believed to be anorogenic granite. Associated with granite are acidic rocks which closely resemble the granitoid rocks in composition. The Tamperkola Granite has yielded Pb-Pb zircon age of 2.8 Ga (Bandyopadhyay et al., 2001).

2.2.3.3 Soda-Granite

All along the length of Singhbhum Shear Zone, lenticular patches of Soda Granite hosts rich deposits of apatite-magnetite, copper sulphides, and uraniferrous minerals (Banerjee, 1962). It is an inequigranular rock with quartz and plagioclase (An_{9-15}) being the dominant minerals along with chlorite, biotite, epidote, tourmaline, muscovite, magnetite, amphibole in varying proportions and apatite and zircon as rare accessories (Saha, 1994). Different views exist about the origin of Soda-Granite. Dunn and Dey 1942 were in opinion that the Soda-Granite is a product of residual sodic melt which replaces more pottasic granite, however, a Migmatitic origin of the Soda Granite produced by the progressive replacement of the shear zone schists through introduction of feldspathic material have been proposed by Banerjee and Talapatra (1966). Some authors opine that ore-bearing hydrothermal solutions generated from a cooling magma led to the formation of Soda Granite (Bhola et al., 1966). The Rb/Sr isocron age of Soda-Granite varies from 1633 to 1677 Ma (Sarkar et al., 1986 and Ghosh and St. Lambert, 1986). Since many economic deposits of Cu and U are hosted by Soda-Granite many theories have been propounded to understand its influence on different ore deposits. Bhola et al. (1966) proposed that the uranium mineralisation is hydrothermal in nature and the hydrotherms were produced by cooling Soda Granite.

2.2.4 Younger Supracrustal Rocks

Cratonization of Singhbhum-Orissa craton includes the formation of greenstone-gneiss terrane known as Iron Ore Group (IOG) (Meert et al., 2010). IOG rocks composed of Banded Iron Formation (BIF), basic volcanic rocks and clastic rocks

(Sarkar and Gupta, 2012) and occur on western, eastern, and southern sides of Singhbhum Granite (Fig. 2.2). IOG rocks are found in three belts: Jamda-Koira valley, Gorumahisani-Badampahar, and Tomka-Daitari (Mondal et al., 2007), BIF in all these belts are associated with mafic lavas. IOG rocks are metamorphosed to low greenschist facies.

IOG rocks have been divided into two units: older IOG and younger IOG. Singhbhum Granite Phase III is intrusive into the IOG rocks, while phases I and II are older than IOG (Saha et al., 1988; Saha, 1994).

2.2.5 Banded Iron Formation (BIF)

There is still controversy regarding whether the BIFs of the different IOG basins are of same age or not. Some authors support that they belong to three different sequences: first sequence extends from Gorumahisani-Badampahar southwards to Nausahi and Sukinda continuing eastwards to Malayagiri; second sequence is exposed in Tomka-Daitari region; Jamda-Koira-Noamundi belongs to the youngest third sequence (Banerjee, 1977; Banerjee, 1982; Acharya, 1984). BIF of the first sequence is unconformably overlain by that of the second sequence in Malayagiri Hill and the second sequence in turn is unconformably overlain by gritty quartzite in Tomka-Daitari belt (Acharya, 1984). The Gritty quartzite underlies the BIF of third sequence. Also, Some differences in mineralogy, geochemistry, and lithological association of BIFs in three belts have been reported by authors (Mukhopadhyay, 2001).

In all the three IOG basins, the base starts with Sandstone-conglomerate followed upwards by ferruginous shale, tuff, lava and BIF (Murty and Acharya, 1975; Chakraborty and Majumder, 1986). Clay mineralogy and heavy mineral assemblage in shale point toward a granitic provenance and non-marine condition of deposition.

Geochemistry of chert associated with BIF has shown fresh water environment (Dasgupta et al.,1999) and a lot of sedimentary structures have been reported from BIF (Rai et al., 1980) that suggest a shallow water environment with current action and occasional desiccation under subaerial condition.

BIFs are not amenable to dating by robust geochronological methods. Indirect age can be inferred from the mafic-ultramafic rock complex, which is intrusive into the IOG rocks (Sarkar and Gupta, 2012). Bangur gabbro, a member of Baula-Nausahi Complex has yielded ^{207}Pb-^{206}Pb age of 3119 Ma and Sm-Nd age of 3205 Ma (Auge et al., 2003). Sm-Nd whole rock isochron age of Singhbhum Granite intruding the IOG rocks of Gorumahisani-Badampahar has been dated to be 3120 Ma (Auge et al., 2003; Sunder-Raju et al., 2015).

2.2.6 Mafic-Ultramafic Rocks

Mafic-ultramafic rocks are common in IOG sequence and occur as dyke like bodies within Singhbhum Granite in Gorumahisani-Badampahar and Baula-Nausahi area (Sarkar and Gupta, 2012). Based on its major element compostion, they can be divided into tholeiitic basalt, calc-alkaline basalt, and high-Mg tholeiitic basalt/basaltic Komatiite (Sengupta et al., 1997). There are flows of lava south of Jamda-Koira valley and to the east of Noamundi, known as Malangtoli and Jagannathpur lavas respectively (Saha, 1994).

2.3 Proterozoic Supracrustals

Oval shaped Archaean nucleus (OMG, OMTG, SBG and other related granitic bodies, and the IOG rocks) is surrounded by Proterozoic rocks both to the north and south (Fig. 2.2) (Saha et al., 1988; Saha, 1994; Mukhopadhyay, 2001). The

Paleoproterozoic supracrustal rocks (Chaibasa, Dhalbhum, and Dalma Formations), occurring to the north of Archaean nucleus have been deformed and metamorphosed to greenschist and amphibolite facies, this entire sequence constitutes the North Singhbhum Mobile Belt (NSMB) (Dasgupta, 2004; Sengupta and Chattopadhyay, 2004). NSMB is sandwiched between Singhbhum Granite Batholith to the south and Chottanagpur Granite Gneissic Complex (CGGC) to the north (Bose, 1994; Saha, 1994; Mukhopadhyay, 2001).

2.3.1 Dhanjori Formation/Group

It constitutes of two members: lower member is composed of the phyllites, quartzites, and conglomerate and the upper member is rich in volcanic and volcaniclastic rocks. Lower member and its conglomerate-sandstone association has been interpreted as the distal fringe of an alluvial fan deposit, whereas the upper member represents channel and mass-flow deposits (Mazumder and Sarkar, 2004; Mazumder, 2005).

Sandstone bodies within Dhanjori Formation are massive to cross-bedded, poorly sorted, compositionally immature, and locally granule rich with matrix content of 10-12%. In addition to all these, unimodal paleocurrent pattern indicate that Dhanjori Sandstone is a fluvial deposit (Mazumder et al., 2015).

2.3.2 Chaibasa Formation

Dhanjori-Chaibasa contact represents terrestrial to marine transition which establishes a sequence boundary between them (Mazumder, 2005; Mazumder et al., 2012). Chaibasa Formation constitutes the interbanded sandstone, a heterolithic (a very fine sandstone/siltstone-mudstone) and shale facies.

The Sandstone is cross-stratified with mud drapes and it suggests a subtidal setting. Heterolithic facies shows wave generated structures including hummocky cross-stratification which was formed in a shelf setting between fair weather and storm wave base (Mazumder et al., 2012). The lower shale facies generally contain thin and rarely very thick sandstone beds showing penecontemporaneous deformation structures (Mazumder et al., 2015; Bhattacharya, 1991) and formed in a shelf setting below the storm wave base (Bose et al., 1997; Mazumder, 2005; Mazumder et al., 2004; Mazumder et al., 2012). The upper shale facies show superimposed ripples and desiccation cracks (Bhattacharya, 1991). The upper Chaibasa shale facies was formed in an intertidal setting (Mazumder, 2005; Bhattacharya, 1991).

The Dhanjori –Chaibasa contact is marked by a sheet conglomerate which represents a lag deposit (Mazumder, 2005). Lower Chaibasa shale facies to upper Chaibasa transition indicates sea-level fall and shallowing of the depositional setting (Mazumder, 2005; Mazumder et al., 2012).

2.3.3 Dhalbhum Formation

Dhalbhum Formation unconformably overlies the Chaibasa Formation, and it is made up of sandstone and shales (Mazumder et al., 2015). Dhalbhum Sandstone is compositionally immature, coarser grained, poorly sorted in nature. Fining upward, and unimodal paleocurrent pattern indicates that they are fluvial in origin (Mazumder, 2005; Mazumder et al., 2012). Chaibasa-Dhalbhum contact is a sequence boundary (Mazumder, 2005; Mazumder et al., 2012).

2.3.4 Dalma Formation

Dalma formation comprises of a thick sequence of mafic-ultramafic volcanic rocks with basic agglomerate lenses (Bose, 1994). Pillow structures are common within the basalts (Mazumder et al., 2012). Different workers have proposed different tectonic setting for Dalma Formation, ranging from continental rift (Dunn and Dey, 1942; De, 1964) to island-arc (Naha and Ghosh, 1960) and even back-arc (Bose and Chakrabarti, 1981; Bose, 1994; Bose, 2009).

2.3.5 Chandil Formation

The Chandil Formation includes quartzites, mica schists, carbonaceous slate/phyllite, weakly metamorphosed felsic volcanic and volcaniclastic rocks (Mazumder et al., 2015). Compositional and textural immaturity of the sandstone constituting the Lower Chandil Formation, combined with poor sorting, lenticular geometry, and unimodal cross-strata orientation suggest terrestrial (fluvial) origin (Mazumder, 2005). The uppermost sandstones are shallow marine and/or lacustrine (Chatterjeee al., 2013).

2.4 Singhbhum Shear Zone

Singhbhum Shear Zone (SSZ), a narrow zone situated north of the Archaean nucleus, is northward dipping shear zone with thrust movement toward south. Shear sense indicators in SSZ suggest that the northern block has gone up (Sengupta and Chattopadhyay, 2004). Shearing (1600 ma) has affected Dhanjori Formation (2600 2100 Ma) and Chaibasa Formation (2200 Ma) (Vinogradov et al., 1964; Sarkar et al., 1986; Sengupta and Chattopadhyay, 2004, Acharyya et al., 2010).

SSZ exposes chloritic schist, basic volcanics (+ tuff-greywacke assemblage), Soda Granite/feldspathic schist, Arkasani granite-granophyre, quartzite (Kyanite bearing at places), tourmalinite, conglomerate (both oligomictic and polymictic), sericite and biotite schists and amphibolite (Sarkar and Gupta, 2012). Shearing has mylonitised Soda Granite, quartzite, quartz schists and vein quartz, while quartz kyanite rocks and basic rocks have become phyllonite. Soda granite in the field vary from feldspathic biotite-chlorite-quartz schist to migmatite (Saha, 1994).

2.5 Geology of the present Study area

The present study area lies on the south-eastern tip of the Singhbhum shear zone (SSZ). The area exposes the large synformal structure plunging towards north. The core of the synform occupied by the Romapahari Granite, whereas, the outer part consists of metamorphites of Singhbhum Group. The age of the Romapahari Granite is 1895$\pm$46ma (C. P. Vohra, 1981) with initial 87Sr/ 86Sr ratio of 0.765. Misra, 1993, 1999, 2002 consider the Romapahari Granite as easternmost extension of the Mayurbhanj Granite. Two different varieties of Romapahari granite occur in the area, one is coarse grained, highly foliated hornblende-biotite granite, and the other is relatively fine grained massive to poorly foliated apltic granite. Further south of the Romapahari Granite the area is occupied by the metasediments of Dhanjori and Chaibasa formation. Hornblende-chlorite-biotite-quartz schist, biotite-chlorite-quartz schist, chlorite-biotite schist and constitute the part of the Chaibasa Formation, whereas the fuschsite quartzite, kyanite quartzite, and ferrugenized sericitic quartzite constitute the upper part of Dhanjori Formation. The presence of feldspathic schist in the area is relatively younger phenomenon and relates to the granitization of shear zone metasediments (Ghosh, 1972). The South eastern part of the area emplaced by the relatively younger, undeformed, medium to coarse grained gabbroic body. The entire area intersected by fine grained dolerite bodies. The overall metamorphic grade in the area varies from greenschist to lower amphibolite facies. Primary structures marked by depositional bedding are represent by colour and compositional bandings in quartzite. Secondary structures are represented by asymmetric folds, foliations, fracture, joints and linear structure. The most prominent secondary foliation encountered in the area is NNE-SSW to NNW-SSW trending and dipping towards easterly direction

2.6 Discussion on Regional Geology

The Singhbhum craton and supracrustal provinces experienced a protracted Hadean to Neoproterozoic geological history. Plume-facilitated magmatic intrusions drove the evolution of the Singhbhum craton from the Hadean to the Mesoarchean. Both juvenile input and crustal recycling played a role in shaping the early magmatic history of the craton, starting with dominantly TTG-type composition and evolving to granitoid composition more akin to present-day granites. Sedimentation was dominantly on the periphery of the craton. Predominantly alkalic magmatism and minor sedimentation attested to cratonization at ca. 2.8 Ga and, a change from ephemeral subduction to permanent subduction in a plate tectonic regime. Sedimentation and mafic volcanism occurred in the latest Archean to early Paleoproterozoic in the Singhbhum craton and along the Rengali Province to the south of the craton. Volcanosedimentary deposition may also have coincided with the amalgamation of the Singhbhum craton within the broader Peninsular Indian region. Later Paleoproterozoic sedimentation and volcanism after ca. 2.1 Ga moved outboard of the Singhbhum craton into the North Singhbhum Mobile Belt. Sedimentation ceased by the end of the Paleoproterozoic, at which point accretionary processes extend further towards north. Reamalgamation of Peninsular India then followed at ca. 1.0 Ga with significant metamorphism and minor alkalic magmatism, all of which attest to the final stabilization of the Singhbhum craton.

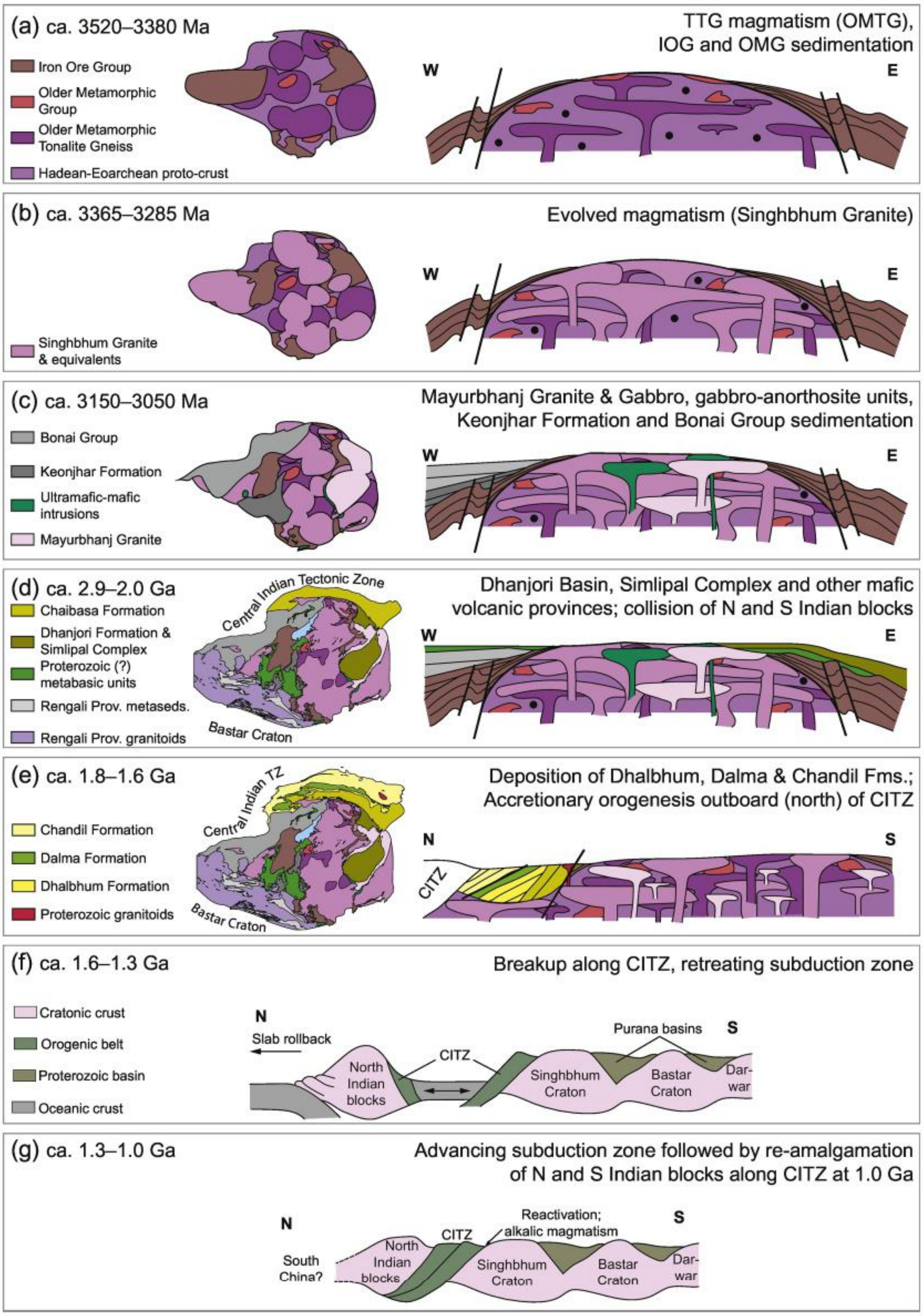

Figure 2.3 Schematic diagrams detaling the proposed evolution of the Singhbhum Craton and supracrustal province from its establishment in the Paleoarchean to the final tectonic activity in the early Neoproterozoic. Olierook, 2019.

CHAPTER 3

PREVIOUS WORK

The present area has been studied by only a few researchers as a result a very limited geological understanding has been developed so far. Earlier researchers like ***Prof.*** *Saumitra Misra* and A.K. *Saha* have devoted a valuable part of their study to develop an initial geological understanding of the area. The major part of their study was focused on Romapahari Granite which is a large igneous body, occupying a significant portion of the area. Other than those, most of the existing literature which directly or indirectly related to the present area is in the context of Mayurbhanj Granite. The present chapter will deal with very brief discussion on the structural and geochemical aspects of the area which has been studied and published by earlier researchers.

3.1 Geological Setup of the Area

The present area is a part of large synformal structure lying in Southern extremity of Singhbhum Shear Zone (SSZ). The northern part of the area is represented by large igneous body known as Romapahari Granite (Iyengar and Murthy, 1982), whereas the southern part exposes metamorphites belonging to Singhbhum Group. The tongue shaped Romapahari Granite occupies the core of the synform whereas the outer part of the synform is represented by the Singhbhum metasediments (Misra, 1993). The large igneous batholith of Mayurbhanj Granite lying in close proximity with the study area and has been separated from the Romapahari Granite by a 20km long north-south trending Kendua fault (Misra, 1993). Naha (1960) purposed to consider Kendua fault as a southern extension of SSZ.

3.2 Tectonic History of the Area

The second phase of Deformation (D_2) was a period of lateral compression which resulted in many mesoscopic and macroscopic folds (Saha et al., 1977). According to Mukhopadhya (1979) the presence of synformal structure in present area can also be attributed to same deformation (D_2). It has been further shown by Misra (1999) that S-pole distribution of genetic foliations (S_g) developed on the surface of Romapahari granite do not show any harmony with S-pole distribution of singhbhum metamorphites lying on outer part of synform. Therefore emplacement of Romapahari Granite can be considered as a post-tectonic with respect to folding (D_2). Moreover, the Romapahari Granite has also been crosscut by some sheared fracture cleavages. These fractures probably formed after D_2 and get sheared during third deformation (D_3). Therefore emplacement of Romapahari Granite can be considered as post-tectonic with respect to D_2 and pre-tectonic with respect to D_3 (Misra, 1999).

3.3 Mayurbhanj Granite and its Field Relationship with Romapahari Granite

The Mayurbhanj Granite (MBG) consists of three different units with two fine grained units which intruded earlier and one major coarse grained unit (Saha, 1977). The oldest one is fine-grained (~0.67mm), biotite-hornblende microgranite with a granophyric texture (Phase I). The second one is moderately coarse-grained (~0.88mm), hypidomorphic to allotromorphic, subequigranular, ferrohastingsite-biotite granite (Phase II). The youngest one is unsheared biotite-microgranite phase (Phase III). The coarse grained variety of MBG can be traced upto Romapahari granite (Misra, unpub. Ph.D. Thesis-1993). Based on these field relationships and Geochemical similarities, Misra, (1999) has purposed to consider Romapahari granite as easternmost extension of MBG that has been separated from main batholith by N-S trending Kendua fault.

3.4 Petrography of Singhbhum Metasediments

Singhbhum Group of metasediments lying in the outer part of the regional synform belongs to Chaibasa Formation. They include muscovite-garnet-chloritoid-chlorite schist, staurolite-muscovite-chlorite schist etc (Mukhopadhya, 1979). Quartzite in the area consists of polygonal quartz grains, interlayered with fine mica flakes at places. A few biotite, apatite and sphene crystals are present as accessories. Mica-schists of this area are medium to coarse grained and greyish white in color. Flaky muscovite, flattened opaques and quartz grains define the schistosity. Lenticular and xenoblastic quartz grains such as deformation lamellae, subgrains, strong undulose extinction are observed. Large relict of porphyroclastic grains are also common.

3.5 Petrography of Romapahari Granite

Misra, (unpub. Ph.D thesis, 1993) has studied coarse ferrohastingsite biotite granite Microcline, Plagioclase and Quartz are very common constituents; Magnetite, biotite, sphene, and apatite occur in varying proportions; Stilnomelane and garnet as rare accessories. Microcline occurs in the form of large phenocrysts, circular inclusions in quartz and locally shows graphic intergrowths. Plagioclase occurs as subhedral/ anhedral/ elongated grains, and as inclusion within microcline. Quartz occurs as anhedral equant grains with sutured contact, often elongated parallel to foliation, and in granophyric intergrowth with microcline. Magnetite and sphene occur as subhedral square and subhedral rhombic outline and occur within close association. Apatite occurs as small grains in close association with mafic minerals, inclusion of apatite within hornblende is also common. Exsolution lamellas of microcline and soda feldspar, alteration of plagioclase into muscovite and sericite have also been noticed.

3.6 Geochemistry of Romapahari Granite

Misra, (2002); Saha, (1977,1984) presented representative analyses of the micro- and coarse granite phases of the Bangriposi-Romapahari area which area plotted within the alkali-feldspar granite and syenogranite quadrants of Q-A-P diagram. The three phases of the granite are similar in modal composition, as well as SiO_2, Al_2O_3, Na_2O, K_2O and CaO chemistry. They are also found to have overlapping FeO_t and MgO contents with minor variation in the TiO_2 contents. Similarity in trace element chemistry among the phases is reflected in their Rb versus Sr and Y/Nb versus Ga/Al plots. In Both the diagrams there is an overlap between all the three phases. However, a little variation in the major element composition of the three phases, depletion of compatible (Sr) and enrichment of incompatible (Rb & Zr) elements indicates that the granite originate by partial melting process. Higher Larsen Index and A/CKN ratio, high HFS, U, Th and Rb contents, low MnO + MgO + CaO and Sr content, high total REE and very high intial 87Sr/ 86Sr suggested by Vohra (1991) indicate that the granite has been derived from partial melting of Sialic crustal source. Misra, (2002) further suggested that unlike other A-type granites, the comparatively low REE content in this granite can be attributed to the fact the source of the granite must be residual sialic source from which A –type granite had previously been extracted.

3.7 Geochronology of Romapahari Granite

The ferrohastingsite Granophyres of Simlipal (a part of the MBG) has been dated by Iyenger, (1981) by Rb/Sr method. The Rb/Sr isochron age of these

Granophyres found to be 2084±70 Ma with an intial 87Sr/ 86Sr ratio of 0.745. Vohra, (1981) dated MBG around Nilgiri which yielded a Rb/Sr isochron age of 2366± 126 Ma with initial 87 Sr/86 Sr of 0.725, while the Romapahari Granite, eastern most extension of the MBG, provide an age of 1895±46 Ma with initial 87Sr/ 86Sr ratio of 0.765. Recently MBG has been dated by Misra (1999) by in situ $^{207}Pb/^{206}Pb$ dating of single zircons, using a ion microprobe. These detrital zircons recovered from MBG was dated ~3.09 Ga, representing the youngest phase of acid plutonism (Misra, 2002).

3.8 Petrogenesis of Romapahari Granite

It has been suggested by Misra, (2002) that all the three phases of MBG (also includes Romapahari Granite) has been originated by batch partial melting of sialic crust source possibly of Singhbhum Granite Phase III. Misra, (1999) had further suggested that the partial melting took place in relatively anhydrous conditions (~0.1 wt%) at high temperature (~980 °C) and at low pressure (4 to <2 kbar). The necessary heat for partial melting provided by gabbroic body that intruded into Singhbhum Granite phase III. Misra, 2002 had noticed the higher oxidation index for microgranite and apologranite, therefore he suggested that the said phases evolved in high oxygen fugacity (fO_2) whereas coarse granite evolved in low fO_2. In order to explain the late stage formation of hydrous phases (biotite, hornblende, ferrohastingsite) in coarse granite, Misra, (2002) has suggested a limited amount of assimilation of metasedimentary country rock into the parent magma of the coarse granite phase may provide relatively H_2O-rich environment. Misra, (unpub. Ph.D thesis, 1993) suggested that N-S trending Kendua fault may act as a possible channel way for intrusion of basic magma into SBG phase III. The first phase of partial melting of SBG III produced the granophyric micro granite followed by second phase of MBG. Under the existing tensional stress the magma rapidly rose through crust to a depth of nearly 4km, where it largely crystallised and later intrude into Chaibasa Formation (solid state emplacement). Lastly a minor partial melting SBG III gave rise to the last phase of MBG (aplogranite).

3.9 Uranium and Copper Mineralization in the area

The government agencies like *Atomic Mineral Directorate* (**AMD**) and *Geological Survey of India* (**GSI**) have been working in this area for U and Cu mineralization. According to GSI (unpub. Annual report FS 19-20) the copper mineralization is hosted by hornblende biotite schsit and also structurally controlled by foliation and secondary shear fabrics in the form of disseminations, stringers and vein filling at places. The major copper mineral is chalcopyrite associated with pyrite, pyrrhotite and magnetite at places. According to AMD (unpub. Annual report FS 2018-19) the area host both primary and secondary U- mineralization. U-mineralization is structural control with the grade and thickness varying from 0.013 to 0.034 %eU_3O_8 in Kusumbari area. The recent investigation by AMD (unpub. Annual report FS 2019-20) in Tilogoria area, has also indicated the uranium hosted feldspathic schist. In addition to that an elevated concentration of Cu (upto 3.8%), Ni (upto0.38%), Mo (upto 0.084%) and ΣREE (upto 0.99%) have also been identified by AMD, which raised the potentiality of area for polymetallic mineralisation.

CHAPTER 4

SATELLITE AND GEOPHYSICAL DATA INTERPRETATION

4.1 Data Products used

Digital Elevation Model (DEM) image from CARTOSAT-1 with 1 arc sec resolution (~30m) inflated into three dimensions model (Fig. 4.2). The image processed in ArcScene 10.3.1 reveals how the geomorphology is related to its lithology. The data of magnetic survey carried out by AMD during in field season 2017 has also been incorporated to correlate the geophysical signature of different lithounits present in the study area.

4.2 Regional Geological Map of the Area.

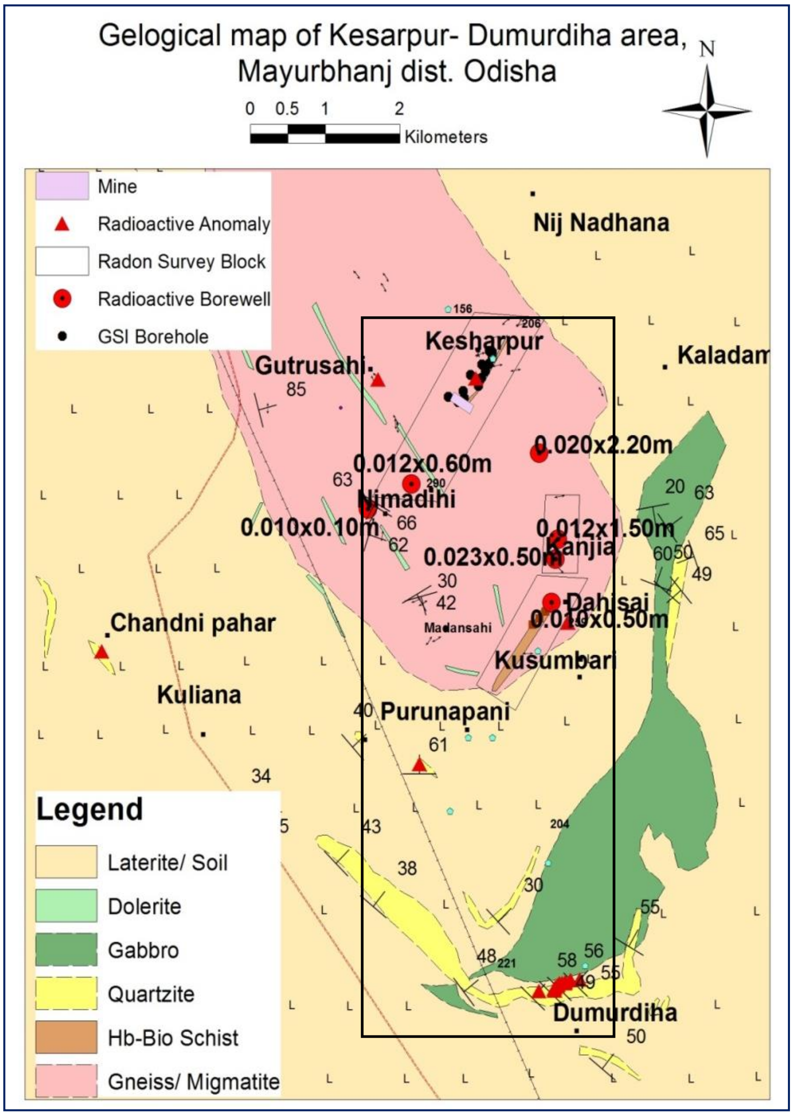

Figure 4.1 The regional geological map of the area based on the survey carried out during field season 2017. The open black rectangle marks the present study area.

4.3 Satellite Data Interpretation

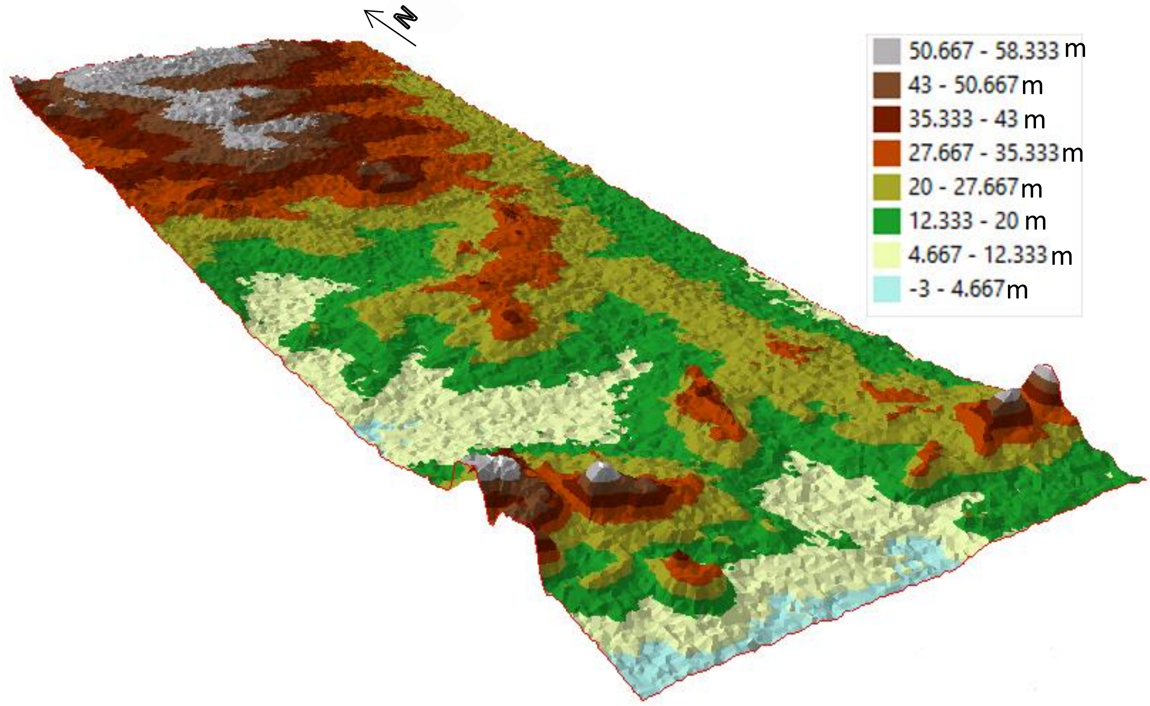

Figure 4.2 3D elevation model of the area based on DEM data of Cartosat-1. Vertical exaggeration 7.5 x

The Digital Elevation Model (DEM) indicates the presence of regional fold, whose closure can be observed in southern part of the area. When compared with the geology of the area, the high elevation in the northern part represents the granitic body (Romapahari Granite), whereas the high elevation in the southern part represents the ferruginous quartzite. The lower elevation in the central part represents soil cover area. In the southern part the closure represented by the ferruginous quartzite is exposed in the Dumurdiha village. In the northern part the Romapahari Granite is emplaced in the Singhbhum Group of metasediments at the core of the regional synform.

4.4 Drainage Pattern

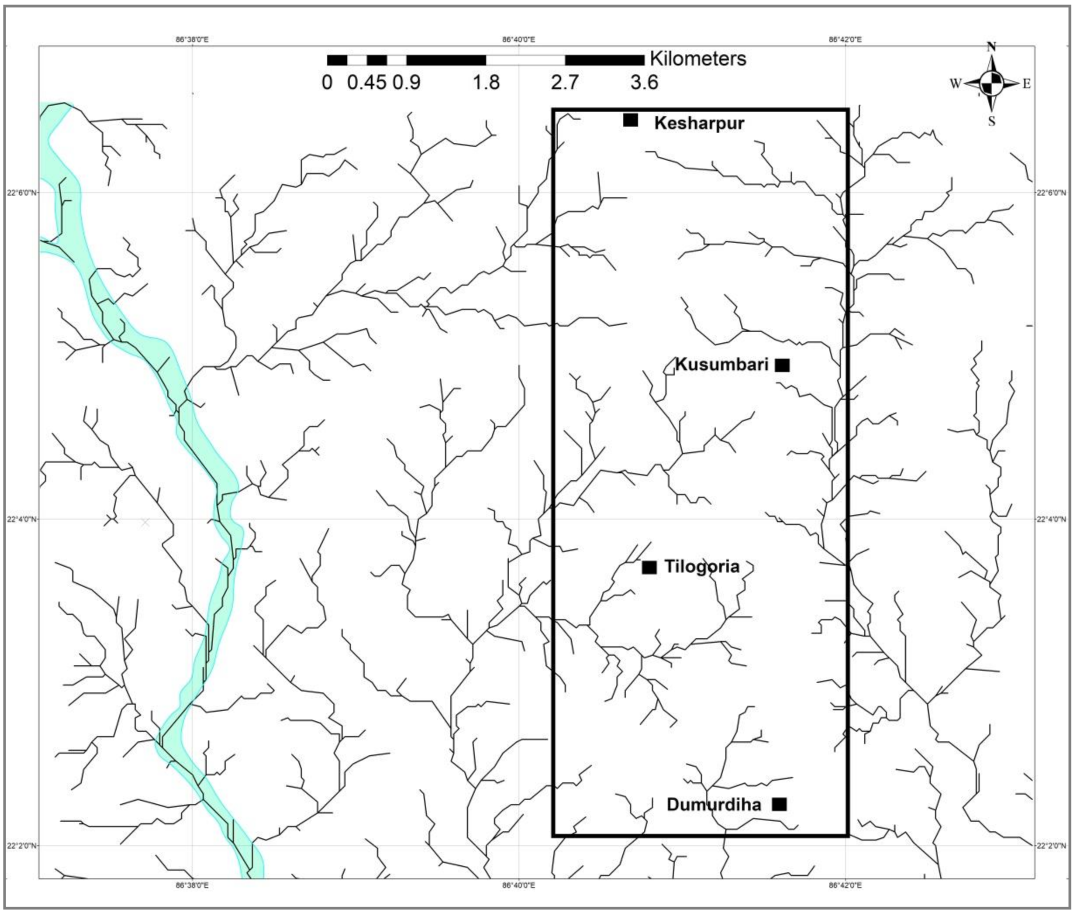

Figure 4.3 Drainage pattern of the area, rectangle marks the study area, large area is incorporated while processing for better understanding of the drainage pattern.

The drainage pattern of the study area is extracted from digital elevation data. The data is processed in ArcMap 10.3.1. The overall drainage pattern of the area appears to be dendritic in nature. The budhabalang river in the west is 4^{th} order stream.

4.5 Geophysical data interpretation

The result of the magnetic survey carried out by AMD during FS 2017 has been incorporated in the present study. Total Magnetic Intensity of the earth's magnetic field is measured with proton precision magnetometer (GEM System) and corrected for diurnal variation of the field. The observed anomalies with reference to the base are contoured and shown in Figure 4.4(a).

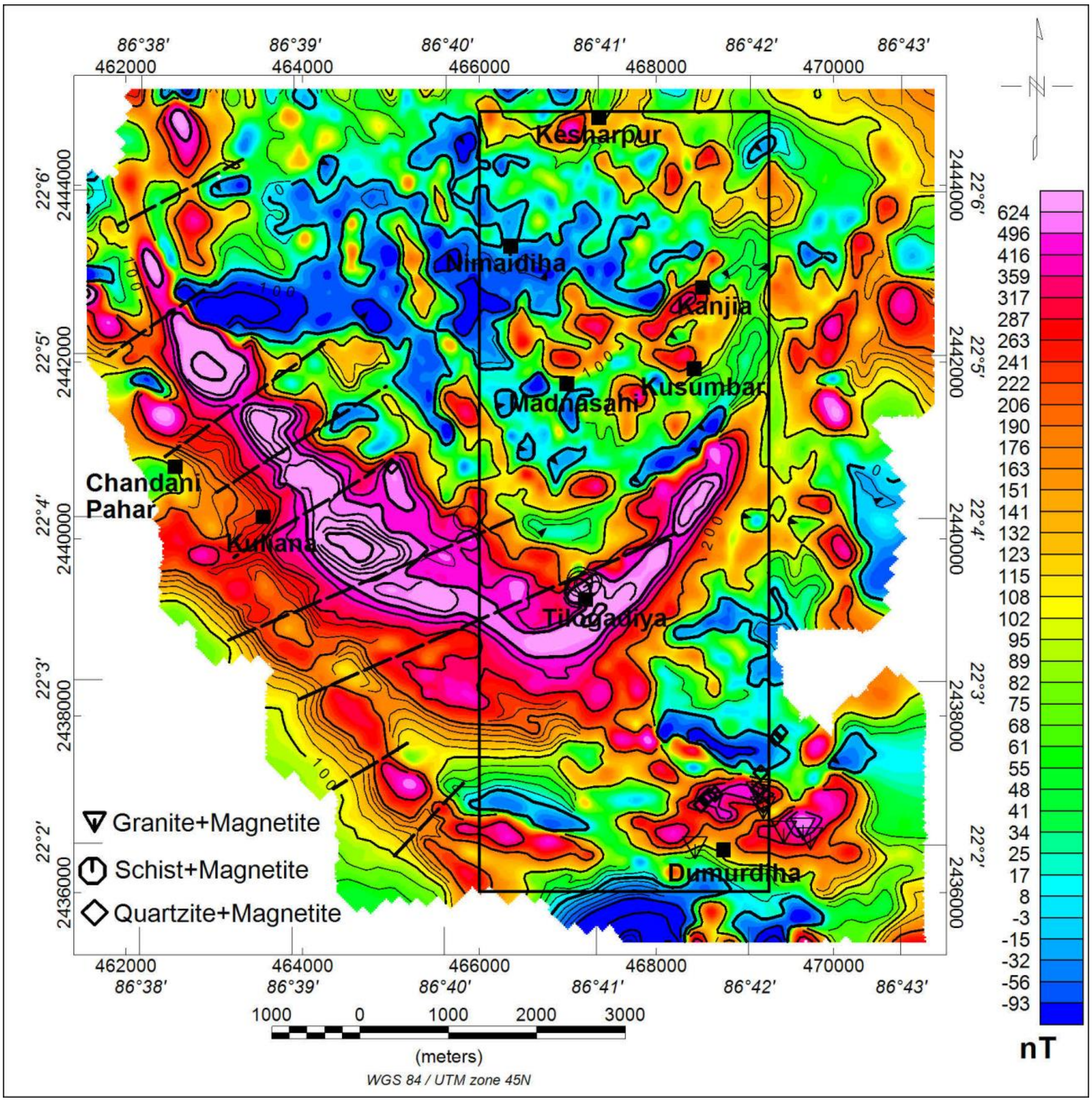

Figure 4.4 a Total magnetic intensity map of the area, rectangle marks the present study area

The observed anomalies with reference to the base are contoured and shown in Figure 4.4 a. Very high order magnetic anomalies are forming a folding pattern with axial plane trending in N-S direction. In the central part, the fold shape high magnetic unit is coinciding with highly susceptible (~50-100 x 10^{-3} SI units) magnetite rich schist exposed near Tilogoria. In the southern part, the similar signature was observed for magnetite rich quartzite exposed in Dumurdiha village. Terminations of the contours are demarcated by black dashed lines representing lineaments in the NE-SW direction.

High magnetic anomalies in Dumurdiha village can be attributed to the magnetite rich quartzite. Similarly, high magnetic anomalies in the southwestern corner of the map (figure 4.4 (a)) is due to magnetite rich granite exposed with in-situ susceptibility in the range 3-12 x 10^{-3} SI units. Tilt map of TMI is also prepared that enhances weak anomalies to the level of strong anomalies. The Tilt map is shown in Figure 4.4 b where another linear folded high magnetic anomaly parallel to the central linear folded anomaly is visible between Tilogoria and Dumurdiha villages and passing through Kuliana. This fold unit coincides with the folded magnetite-rich quartzite in Dumurdiha area to be following the trend of magnetite rich quartzite exposed in Dumurdiha.

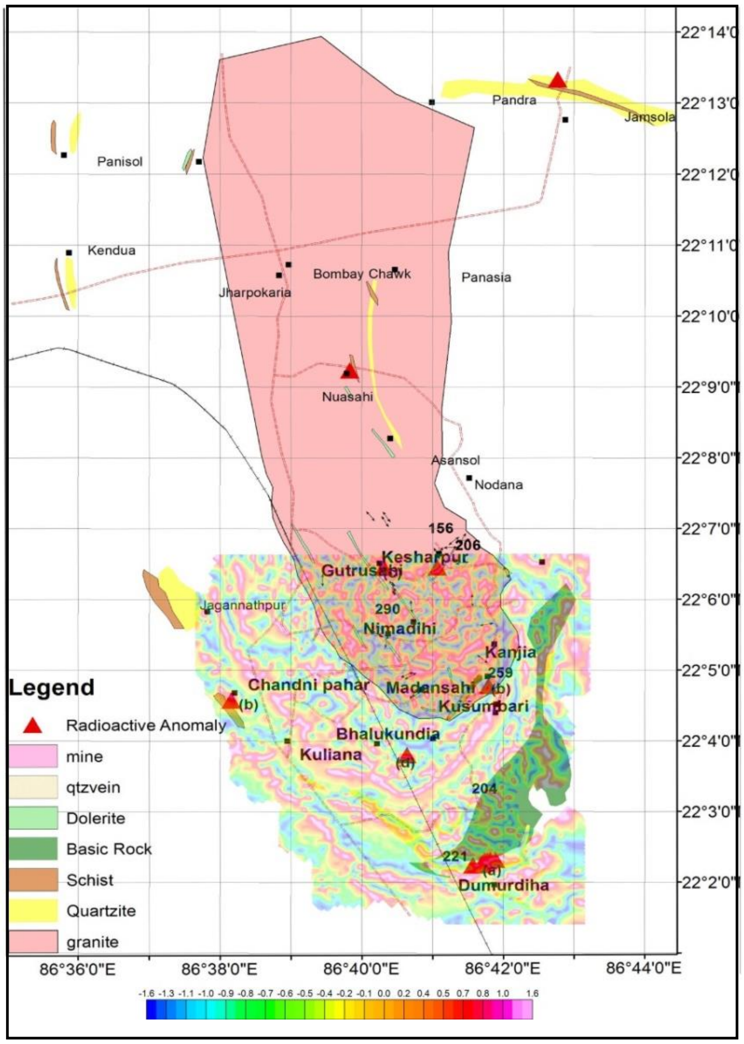

Figure 4.4b Tilt map superposed over geological map of Kesharpur area, Mayurbhanj dist., Odisha.

4.6 Discussion

DEM model when compared with the geology of the area, shows the high elevation in the northern part represents the granitic body (Romapahari Granite), whereas the high elevation in the southern part represents the ferruginous quartzite. The lower elevation in the central part represents soil cover area. In the southern part the closure represented by the ferruginous quartzite is exposed in the Dumurdiha village. The drainage pattern extracted from DEM model shows the overall drainage pattern in this area is dendritic in nature with 4^{th} order Budhabalang River flowing in the western part of the area. The Geophysical data obtained from the magnetic survey shows high order magnetic anomalies are forming a folding pattern with axial plane trending in N-S direction. In the central part, the fold shape high magnetic unit is coinciding with highly susceptible magnetite rich schist exposed near Tilogoria. In the southern part, the similar signature was observed for magnetite rich quartzite exposed in Dumurdiha village. Tilt map obtained from total magnetic intensity map further enhance the weak signals to the level of strong anomalies.

CHAPTER 5

Detailed Geological Mapping

Detailed geological mapping was carried out over a scale of 1:5000 to decipher lithological and structural dispositions of different lithounits exposed over an area of 32 sq Kilometre. The mapping was carried out from Kesharpur in the north to Dumurdiha in south. The major lithounit exposed over northern part of the area is Romapahari granite. The granitic body intrudes into Singhbhum Group of metasediments (metamorphosed to greenschist and amphibolite facies) which includes biotite-sericite-chl-quartz schist, hornblende-biotite-chlorite-quartz schist, feldspathic schist (schistose sodagranite), magnetite bearing quartzite, kyanite quartzite, and fuchsite quartzite. The comprehensive geologic map has been given in the Plate 1.

5.1 Romapahari Granite

The Mayurbhanj Granite (MBG) Pluton consists of four mappable units (Saha, 1994). Out of four, the main MBG unit occurs to the north of the Simlipal volcano-sedimentary complex (considered to be equivalent to Dhanjori Group, Saha, 1994). The tongue shaped Romapahari granite is the easternmost extension of the main MBG unit (Misra, 1999, 2002). The Mayurbhanj Granite consists of three intrusive phases, emplaced in successive order (Saha, 1977; Misra, 1993). These are

a) Relatively fine-grained, biotite-hornblende microgranite with a granophyric texture (Misra, 2002). The phase is not exposed in the present study area and majorly occurs in the northwestern part of the main MBG pluton.

b) Moderately coarse grained, subhedral, to anhedral, subequigranular, hornblende-biotite granite, grading to alkali-feldspar granite (Misra, 2002). The described phase is exposed both in main MBG unit as well as in the present study area. In main batholithic part it is massive to crudely foliated, whereas in the present Romapahari area the said phase is strongly sheared along NNW-SSE in the western part and NNE-SSW in eastern part. In the Romapahari area the granite is characterised by grey coloured rounded quartz grains standing out with in dull white feldspathic base. At most of the exposures the sheared granite contains feldspar megacrysts varying between ~4mm to 2cm in size, which are generally elongated in the foliation direction and have tail drawn out into parallelism with the foliation. At a few places the Augens of somewhat different nature have also noticed (Khardiasol, western part of Kesharpur) (Fig 5.1). They are of the order of 3 to 5cm and elongated parallel to foliation, with pressure shadow zones produced at its ends.

c) A fine- grained, unsheared biotite-aplogranite phase, of the pluton in the Romapahari area, within the coarse granite phase, as small irregular veins and tongues. The rock is equigranular, allotriomorphic and consists of microcline, quartz and plagioclase; with subhedral square magnetite, biotite and zircon as accessories. The major exposure of this unit is in south Kanajia area.

Figure 5.1 Field photograph showing the outcrop of coarse grained Romapahari granite, showing feldspar augens (~5 cm) with strain fringes aligned along foliation plane of granite, Khardiasol (western part of Kesharpur), Mayurbhanj, Odisha.

5.1.1 Contact relationship of coarse and fine granite

Near Kesharpur at a few places the contact of coarse grained granite and fine grained aplogranite has observed. At contact the surface of coarse granite bears the intense shearing along NE-SW direction whereas the aplogranite is massive to crudely foliated (Fig 5.2(a) & (b)). The contact is very sharp and do not show any chemical alteration due to intrusion of latter phase.

Figure 5.2 The outcrop of Romapahari Granite showing **(a) & (b)** contact of coarse grained biotite granite and fine grained aplitic granite, Kesharpur, Mayurbhanj, Odisha.

5.2 Sector-wise Distribution of Singhbhum Metasediments

5.2.1 Kusumbari and Kesharpur Area

The enclaves of schistose rocks are exposed both in Kesharpur in the north and Kusumbarai in the north eastern part of the area. In Kesharpur area hornblende-Chlorite-biotite-quartz schist exposed in trenches as the main host rock for Cu and U mineralization. It also occurs as enclaves within Romapahari Granite. It has NE- SW strike which coincides with the shear trend in eastern part of area. In the Kusumbari area, two type of schistose bodies have observed, one is hornblende-chlorite-biotite-quartz schist, trending NE-SW with dip due west, which has been encountered in the trenches (Fig: 5.3 (a) & b)). Another is biotite-chlorite-sericite-quartz schist observed in the southern part of the Kusumbari area.

Figure 5.3 The field photograph showing **(a)** outcrop of chlorite-biotite-quartz schist exposed in trenches, **(b)** oriented hand specimen of the same rock type, Kusumbari, Mayurbhanj dist., Odisha

5.2.2 Tilogoria Area

Tilogoria lies in the south western part of the study area near to the closure of synform. Ferrogenized Quartzite (Fig 5.4 (a)), biotite-chlorite-sericite-quartz schist, feldspathic schist (schistose soda granite), and metabasalt bodies (chlorite-biotite schist and amphibolites) are the main litho-units present in the study area. Small Outcrops of highly crenulated biotite-chlorite-sericite-quartz-schist has exposed near Tilogoria (Fig 5.4 (b) & (c)). In the schist the schistosity plane is defined by the micaceous minerals (sericite, chlorite, and biotite). Quartzite at places shows kyanite and micaceous (sericite) minerals. It also gets intruded by magnetite veins. Based on color banding the bedding planes are also indicated with in ferrugenized quartzite (Fig 5.4 (d) & (e)). They are preserved with strike of N70, dipping 45° toward NW direction. The subsurface data also indicates the presence of magnetite and tourmaline bands in the schist. The strike of schist varies from N10°E (Eastern part of area) to S40°E (western part of area) and dipping towards NW to NE direction, indicates the first generation of folding. The second generation of deformation in the area represented by

Figure 5.4 The field photograph showing **(a)** ferrugenized quartzite exposed in Tilogoria area, **(b)** highly crenulated outcrop of chlorite-sericite-quartz schist in the Tilogoria (pen size 14cm), **(c)** oriented sample of chlorite-sericite-quartz schist of Tilogoria area, Mayurbhanj dist., Odisha.

asymmetric folds and crenulation cleavages, with axial plane lying along N40°E and dipping towards NW at angle of 30 ° degree.

Fig 5.4...(Contd.) The outcrop of ferrugenized quartzite showing **(d)** & **(e)** color bending, indicates bedding planes, Tilogoria, Mayurbhanj dist., Odisha. (Pen size 12cm)

The feldspathic schist (schistose sodagranite) is also present in the Tilogoria area (fig 5.4 (f) & (g). However, the said lithounit is not exposed on the surface. Its establishment has been defined based on subsurface data. The major phases present are albite, plagioclase, quartz, chlorite, and biotite. The feldspathic schist in this area host radioactive phases (uraninite) along with sulphides (chalcopyrite, pyrite) and oxides (Magneite, ilmenite).

Fig 5.4…. (Contd.) photograph of subsurface borehole core sample of feldspathic schist showing **(f)** minor crenulations along foliation planes, **(g)** along with sulphide mineralization, Tilogoria, Mayurbhanj, Odisha (Pen size 12cm)

5.2.3 Panijia area

Panijia village lies in the central part of survey area towards south of Tilogoria. Though majority of the survey area is covered by paddy field and soil cover, NE-SW trending small hillocks of quartzite are also present. Main lithounits encountered in the area are kyanite quartzite, fuchsite quartzite, biotite-chlorite-sericite-quartz schist, gabbroic rock, and amphibolite.

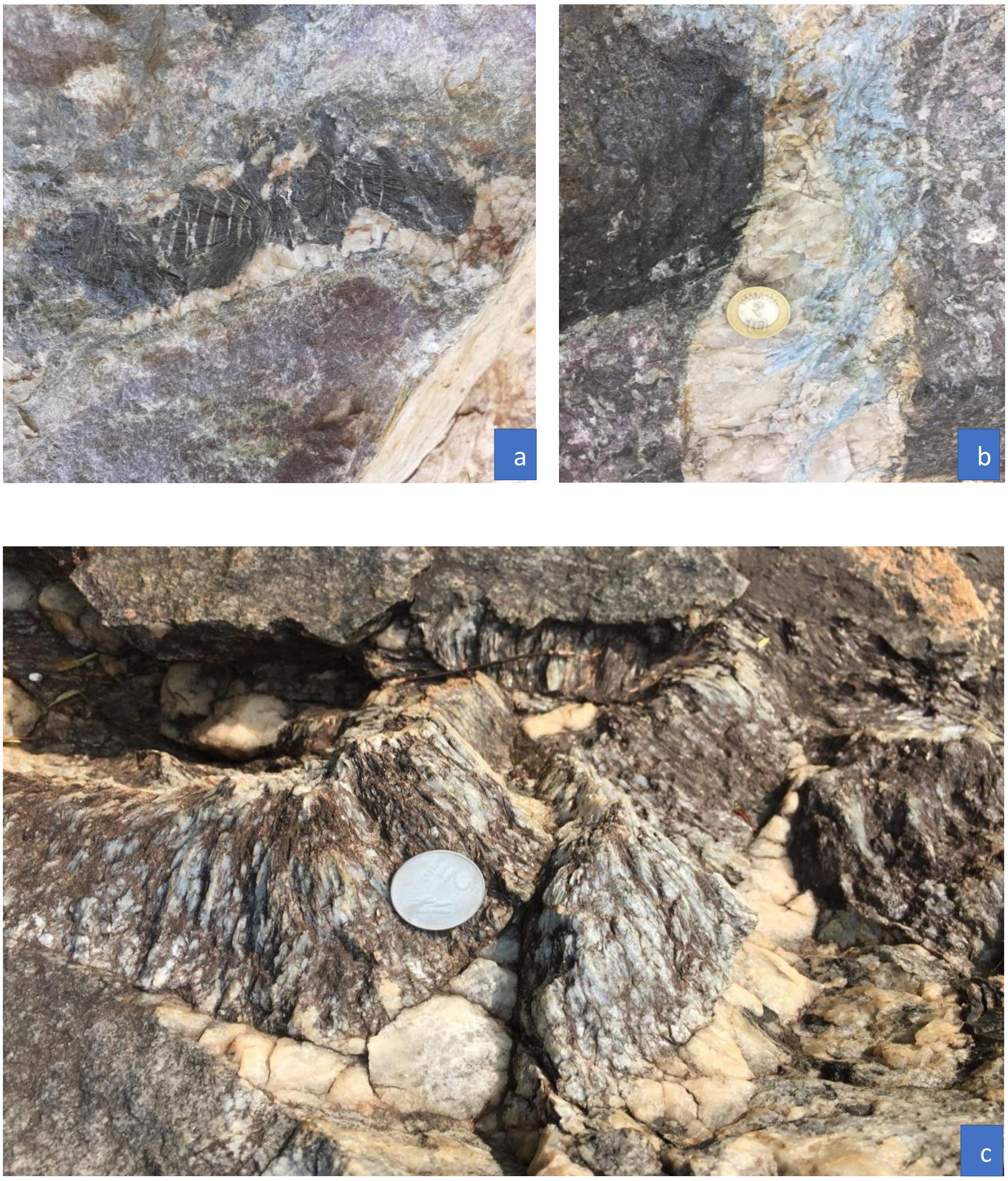

Figure 5.5 Field Photograph showing **(a)** Tremolite and **(b)** Kyanite minerals with in quartz bands intruded in hydrothermally altered purple quartzite, **(c)** exposure of Kyanite quartzite, Panajia, Mayurbhanj dist., Odisha.

At places kyanite and Tremolite mineral found associated with quartz bands (Fig 5.5 (a) & (b)). The kyanite quartzite is traced all along the Panijia hillock (Fig 5.5 (c)). These bands are associated with quartzite. Due to hydrothermal alteration quartzite shows a purple colour, hard and compact nature. Some later quartz bands cross cutting earlier Tremolite bands are also observed. In north western part quartzite becomes hard, whitish and relatively poor in kyanite.

Fig 5.5 The field photograph of **(d)** & **(e)** fuchsite bearing quartzite exposed near Purnapani in the north of Panajia, Mayurbhanj dist., Odisha.

In the north of the Panajia village near Purnapani village there is a beautiful exposure of fuchsite bearing quartzite (Fig 5.5 (d) & (e)). The green colour fuchsite quartzite aligned along N60°E and dipping 50° towards NW. Multiple generations of deformations are observed in quartzite including small scale chevron fold to large scale reclined folds. Biotite-chlorite-sericite-quartz schist shows rotation of strike from N20° to N100°. Main foliation trend is N40° with sub vertical dip (~80°) towards NW. Some joints such as N30° and N300° intersect the foliation plane. In south eastern part, the area is mostly soil covered, a very few outcrops of schistose amphibolite are exposed in the area.

5.2.4 Dumurdiha area

Dumurdiha area is in the southern part of study area and is mostly soil covered except NE-SW and E-W trending small hillocks of quartzite and outcrops of schistose and gabbroic rock. Quartzite in the area composed mainly of fine-grained quartz, micaceous minerals like sericite and fuchsite are observed in the foliation plane. Quartzite is greenish in colour which may be due to presence of fuchsite and some patches are reddish due to ferruginisation. Bands of magnetite and tourmaline are found along the foliation plane as well as along fractures in quartzite (Fig 5.6 (a) & (b)).

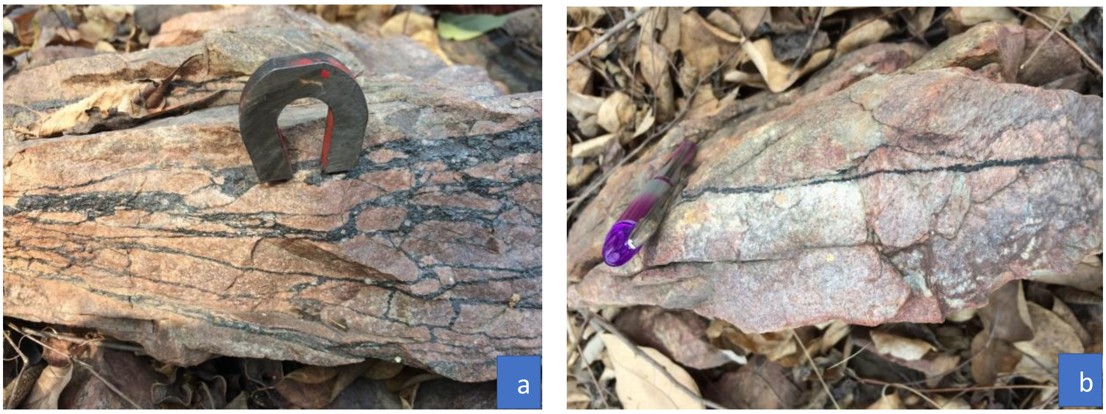

Figure 5.6 The field photograph of ferrugenized quartzite showing **(a)** magnetite, and **(b)** tourmaline bands along fracture planes respectively, Dumurdiha, Mayurbhanj dist., Odisha. (Pen size 14cm; horseshoe magnet length 3cm)

Malachite and sulphide are also observed along the plane. Mainly two sets of foliations are present in quartzite. One set varies from N110° to N140° and dipping at angle of 25° towards NE. Second one varies from N40° to N70° and dipping towards NW at angle of 40°. Along the foliation plane yellow colour secondary uranium mineralization has also been observed along with malachite (Fig 5.6 (c) & (d)). In the area Biotite-chlorite-sericite-quartz schist has also exposed in the northern part of quartzite. It also shows imprints of folding. Foliation trend in schistose rock varies from N50°E to E-W. It is dipping towards NW at angle of ~55°.

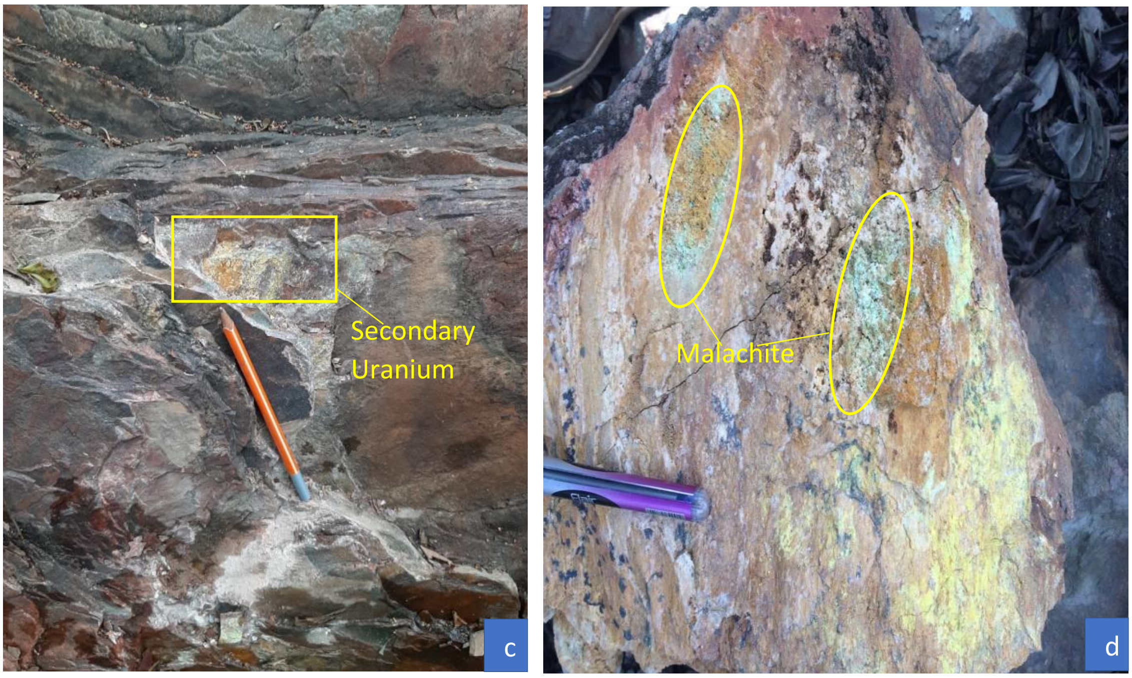

Figure 5.6…(Contd.) the outcrop of ferrugenized quartzite showing **(c)** secondary uranium mineralization along foliation planes, **(d)** malachite stains along with secondary uranium mineralization, Dumurdiha, Mayurbhanj dist., Odisha. (Pencil size 13cm; pen size 14cm).

The area has undergone multiple phase of deformation. Major joints observed in the area show N15° and E-W trend with sub vertical dip. Northerly plunging folds and north easterly plunging asymmetric folds are present in the area. Some small-scale faults were observed along the hinge zones of the folds. Shearing in the area is confined to N40-60° planes represented by foliation planes. Other than those, some sedimentary structures like cross stratification, ripple marks have also observed in the Dumurdiha quartzite (Fig 5.6 (e) & (f)). The thickness of the cross strata varies from ~3 to 6cm. Mazumder, (2005) has indicated these trough cross beds might have formed due to migration of large ripples outside channel. In south of Dumurdiha village the grey color coarse grained foliated Rompahari granite is found in close association with quartzite. The attitude of the granitic foliation is N60°E.

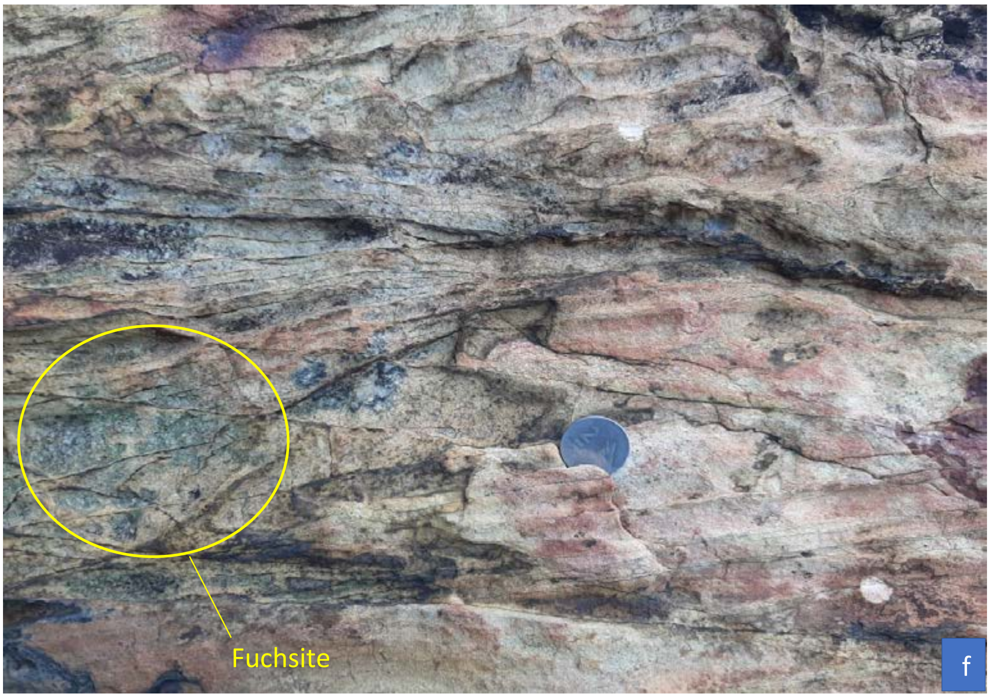

Figure 5.6 (Contd.) the field photograph of ferrugenized quartzite showing **(e)** cross stratification, indicates fluvial origin, and **(f)** presence of fuchsite minerals, Dumurdiha, Mayurbhanj dist., Odisha.

5.3 Distribution of Mafic and Ultramafic Bodies in the Area

Figure 5.7 The field photograph of **(a)** Undeformed gabbroic body in close association with intensely sheared kyanite quartzite, **(b)** outcrop of amphibolite present in south eastern part of the Panajia, Mayurbhanj dist., Odisha.

In the north western part of Dumurdiha quartzite, discordant undeformed younger gabbroic rocks are intruded into biotite-chlorite-sericite-quartz schist and ferruginous quartzite (based on subsurface data). These rocks are medium to coarse grained, comprised mainly of pyroxenes and plagioclase. Other than that, magnetite, sulfides and dendritic growth of manganese minerals are also present with in gabbro. The same gabbroic body is also exposed near Panajia area. Here in Panajia it is in close association with kyanite quartzite. The kyanite quartzite is deformed and crenulations are developed on its surface, whereas the gabbroic body is underformed (Fig 5.3 (a)).

Meta-basaltic rocks of greenschist to amphibolite grade are present in the area. In south eastern part of Panajia village, a very few outcrops of schistose amphibolite are exposed in the area (Fig 5.3 (b)). These amphibolite bodies are also present in the subsurface borehole cores samples collected from Tilogria, Kusumbari and Dumurdiha area.

The metabasaltic bodies of chlorite-biotite schist (greenschist-facies) are also exposed on surface (Fig 5.3 (c)) (near Khesarpur) as well as in the subsurface samples of Panajia and Dumurdiha. Latter the whole area is intersected by the undeformed very fine grained dolerite dykes.

Figure 5.7…(Contd.) The field Photograph shows **(c)** chlorite-biotite schist exposed in Khadiasol village, western part of Kehsarpur, Mayurbhanj dist., Odisha.

5.4 Radioactive anomalies in the Study Area

Uraniferous radioactive lenses of different dimensions are present in NE-SW trending quartzite along a length of 300m. Dimension of radioactivity ranges from spotty to 26m x 0.3-1m. Radioactivity was found along the foliation plane of ferrugenised quartzite. Secondary uranium minerals, sulphides, magnetite and malachite are also associated with radioactive quartzite. Some of the N20°E trending vertical fracture in the Dumurdiha quartzite also shows radioactivity along with high ferruginisation. Radiometric assay results of ferruginous quartzite show % U_3O_8 (β/ɣ) ranges from <0.01 - 0.95 % and %ThO_2 ranges <0.005 - 0.056%. Other than quartzite, spotty radioactivity anomalies are located in biotite-chlorite-sericite-quartz-schist of Dumurdiha area. Few Spotty thoriferous radioactivity anomalies are located in kyanitiferous quartzite of Tilogoria and Panijia areas. Feldspathic veins intruded into Romapahari granite also show activity upto 0.1% eU_3O_8. Other lithounits such as Romapahari granite, metabasalt bodies, gabbro and non-radioactive quartzite and schist shows background radioactivity only.

1. **Dumurdiha anomaly in Quartzite (45Q 468593E 2437101N):** Ferrugenized quartzite has reported anomaly upto 0.95% eU_3O_8 based on β-γ spectrometry. The dimension of the anomaly is 0.5 x 0.5m and it occurs along foliation plane trending towards NE. Despite that, numerous anomalies of low grade are also recorded in the same lithounit.
2. **Dumurdiha anomaly in the Bt-Chl-Ser-Qtz Schist (45Q 468712E 2437329N):** Chlorite-sericite-quartz schist reports radioactivity up to 0.047% eU_3O_8 based on β-γ spectrometry. The dimension of the anomaly is sporty.
3. **Panajia anomaly in the Kyanite quartzite (45Q 467350E 2437702N):** The radioactive anomaly recorded up to 0.019% eU_3O_8 based on β-γ spectrometry. In the similar lithounit thoriferous anomalies have also recorded.
4. **Madanasahi anomaly in the Granite (45Q 467298E 2442277N):** The activity in the area is limited to quartz-feldspathic vein intruded into Granite. Value up to 0.1% eU_3O_8 is reported in the vein.
5. **Kesharpur anomaly in the Granite (45Q 467251E 2444511N):** Similar to Madanashai anomaly, the radioactivity in the Granite is limited to quartz-feldspathic vein. The radioactivity up to 0.10% eU_3O_8 has been reported based on β-γ spectrometry.

5.5 Discussion

The northern part of the area occupied by Romapahari granite, which equivalent of Mayurbhanj granite (Misra, 1999). In the central part, the major lithounits present are hornblende-biotite-chlorite-quartz schist, biotite-chlorite-sericite-quartz schist, and feldspathic schist. The feldspathic schist is not exposed on the surface, based on borehole data its presence has been established. The feldspathic schist in the area also holds low grade uranium mineralization along with sulphides. In the down dip direction i.e. in the southern part of the area there is general transition to Kyanite quartzite, fuchsite quartzite, cross stratified ferruginous quartzite, and metabasalts. Gupta, (1985); Mazumder, (2002), has opine that Dhanjori formation is made up of two members: phyllites, quartzite, and thin conglomerate comprise the lower member, whereas volcaniclastic rocks along with some quartzite and phyllites are important component of the upper member. Mazumder, (2004) further identified trough cross bedding in upper dhanjori sandstones and suggest its fluvial origin. In the present area the lower part of Dhanjori is not observed so far (absence of conglomerate facies), however, fuchsite bearing quartzite, cross stratification, and metabasalts at its base indicates a few components of upper Dhanjori formation.

Many researchers like Dunn, (1937), Dunn and Dey, (1942), Banerjee, (1962), Saha, (1994) have identified large number of detached bodies of feldspathic schist (schistose soda granite) and soda granite all along the Singhbhum shear zone. The genesis of feldspathic schist (Schistose Soda granite) is still controversial, however, there is general opinion that its origin is either post shearing or during shearing. Ghosh, 1972 was in favour that the feldspathic schist is product of granitization of shear zone metasediments.

The metasediments exposed to the north of feldspathic schist belongs to Chaibasa formation as suggested by Misra, (1999) & Misra, unpub. Ph.d thesis, (1993).

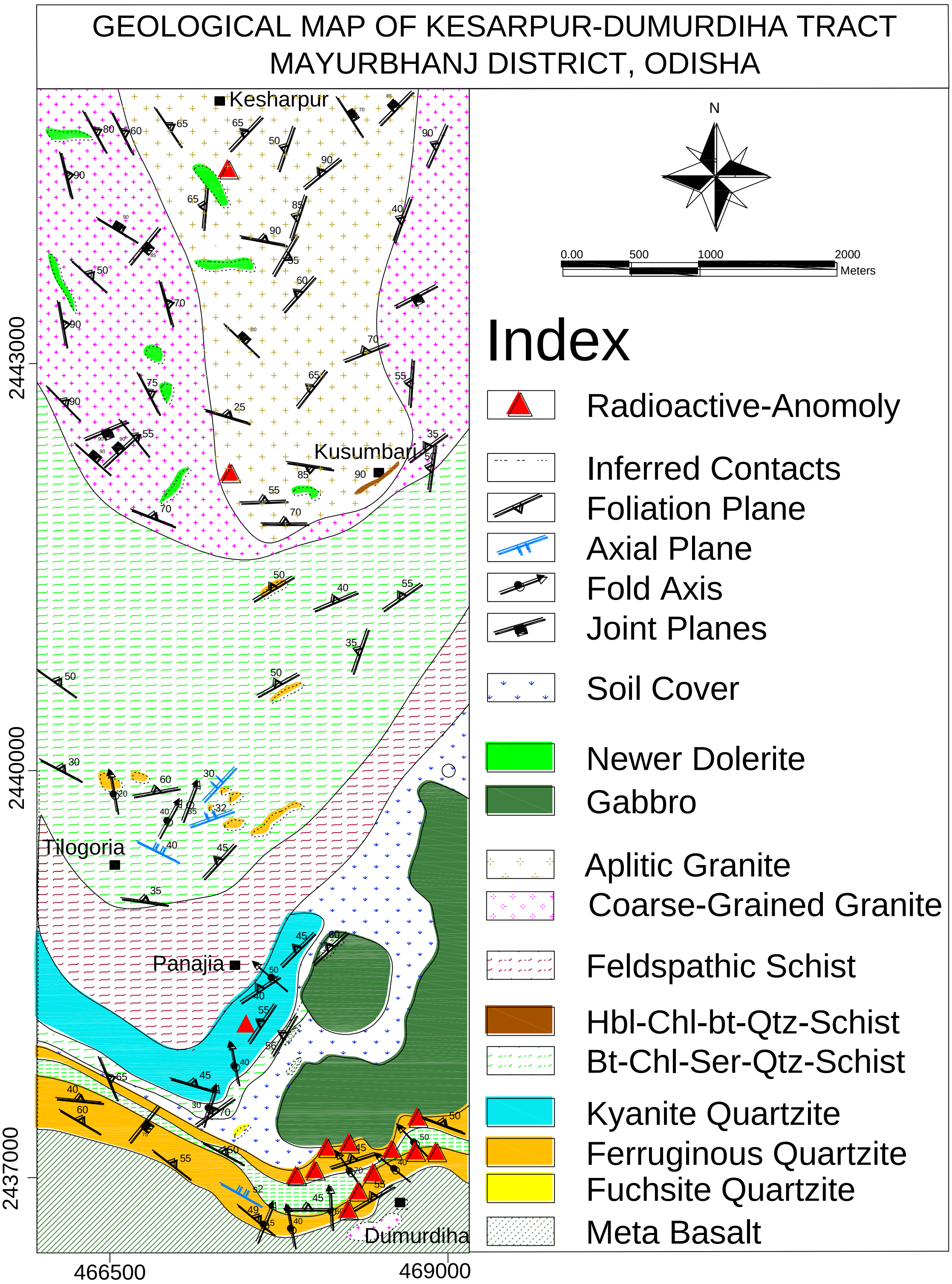

Figure 5.8 Detail Geological (1: 5000 Rf) map of the area.

CHAPTER 6

Structural Interpretation of Study Area

A fairly detailed structural analysis has been carried out along Kesharpur-Kusumbari-Tilogoria-Dumurdiha tract. The rocks shows well developed primary and secondary structures both in mega- and mesoscopic scale. On the megascopic scale the area exposes a large synformal structure plunging towards north. The core of the synform occupied by the Romapahari granite, whereas, the outer part consists of metamorphites of Singhbhum Group. Mesoscopically the rocks consists of planar features defined by dimensional parallelism of mica flakes, quartz grains, and feldspars augens.

6.1 Morphology of the Structural Features of the Romapahari Granite

Two different varieties of the Romapahari Granite have been identified in the area. The western-most part of the area occupied by grey color coarse grained hornblende-biotite granite, whereas the central and the eastern part of the area occupied by pink color fine grained, massive to poorly foliated aplitic granite. The coarse grained variety has significant penetrative structural features and exhibit porphyroclast of feldspars (Fig 6.1 (a)), whereas the fine variety consists of microcline, quartz and plagioclase.

6.1.1 Planar structures of Romapahari Granite

Microscopic observation reveals that foliation plane in the coarse sheared granite is defined by dimensional parallelism of quartz, feldspar, discontinuous streaks of mafic minerals (hornblende + biotite) and feldspar augens. Generally this type of foliation plane is very persistent throughout the body. Megascopically at a few exposures the planar features of coarse granite appears to be sinusoidal shape which may be attributed to overlapping arrangement of the feldspar augens (Fig. 6.1 (b)).

Figure 6.1: Field Photograph of Romapahari Granite showing **(a)** Spherical feldspar porphyroclast with strain fringes aligned along foliation plane of granite, **(b)** sinusoidal appearance of foliation due to overlapping arrangement of feldspar augens , Khardiasol, Mayurbhanj dist., Odisha.

Central and the eastern part of granite is fine grained, massive to poorly foliated, equigranular, allotrimorphic, and consists of microcline, quartz, and plagioclase. It resembles with the aplogranite component of MBG (Misra, 1993). At a few exposures it shows intrusive relationship with the Coarse grained variety of Romapahari Granite.

Other than those, sheared cleavages (Fig 6.1(c)), C-C’ shear bands (Fig 6.1(d)), tension gashes (Fig 6.1(e)), SC-fabric (Fig 6.1(f)), crenulation cleavages (Fig 6.1(g)), and assymetric folds (Fig 6.1(h & k)) have also been observed on the surface of Romapahari Granite. At places the mega shear lenses cross-cutting the quartz veins are also visible (Figure 6.1 (i)). Throughout the area the granite has been cross cut by later appeared joint sets and few of them also shows small displacement along NW direction (Fig 6.1(J)). Overall the sense of shear in the area is dextral.

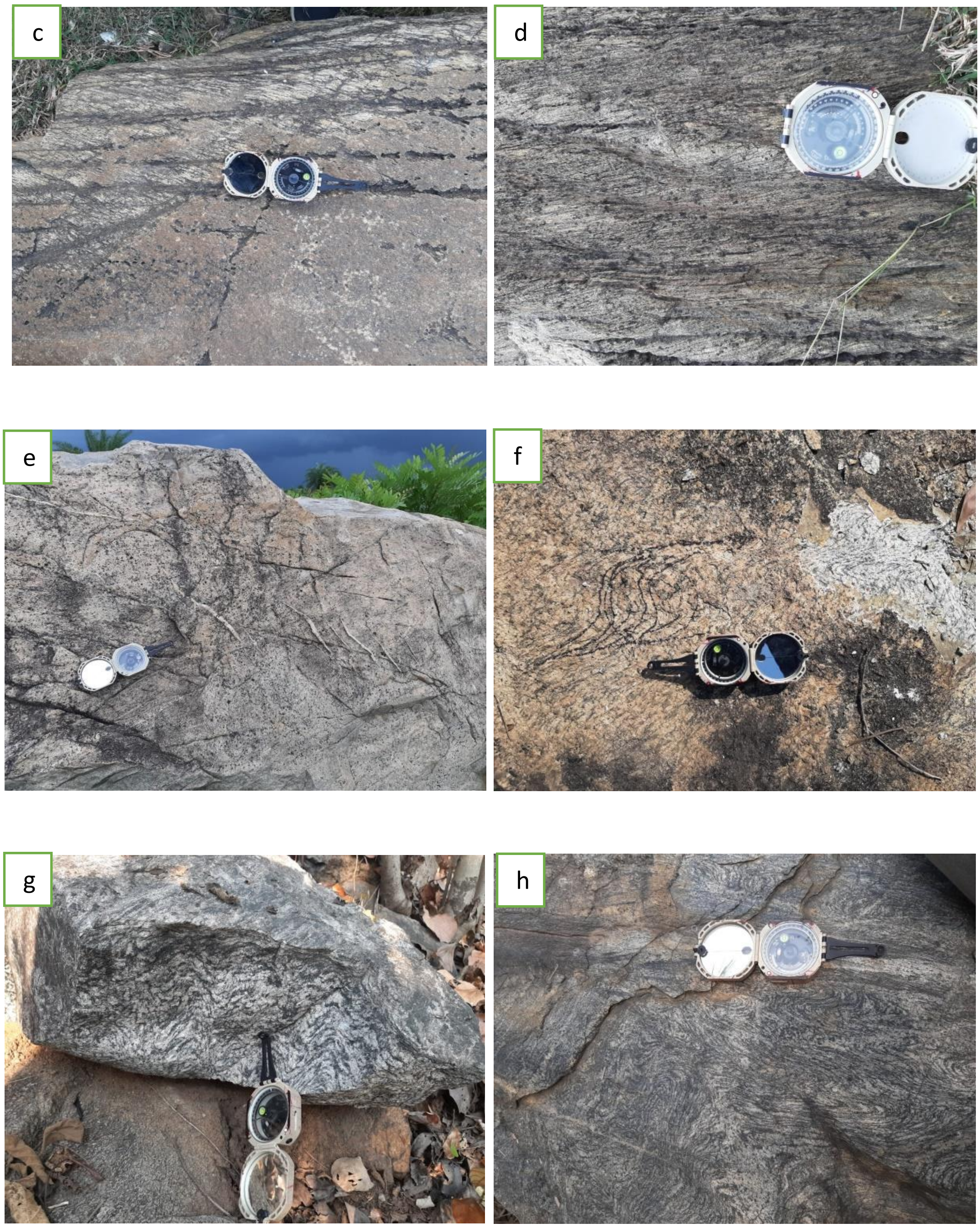

Figure 6.1…(contd.) Field photographs of Romapahari Granite showing **(c)** NW-SE sheared cleavages crosscut by the later shearing along NE –SW direction near Kharidiasol (western part of Kesharpur). **(d)** C-C'-type shear band cleavages (from upper left to lower left)transecting the main foliation near Khardiasol area. **(e)** Tension gashes developed on granitic body near Panasia, dextral sense of shearing along NE-SW direction. **(f)** S-C fabric develops on the surface of Granite, showing dextral sense of shearing. **(g)** Crenulations develop on the surface coarse grained Romapahari Granite. **(h)** Assymetrical folds developed on Coarse grained granite, Kesharpur, Mayurbhanj dist., Odisha.

Figure 6.1… (Contd.) The field photograph of Romapahari Granite showing **(i)** shearing along NE-SW direction, cross-cut the quartz veins, **(J)** small displacement of joint plane in NW-SE direction, **(k)** Asymmetric folds develop on the surface of the Romapahari granite, Kesharpur area, Mayurbhanj dist, Odisha.

6.1.2 Linear Structures of Romapahari Granite

Three types of lineation have been indentified on the Romaphari Granite. They include slicken sides (Fig 6.2 (a)), intersection lineations (Fig 6.2 (b)), and mineral lineation (Fig 6.2 (c)). The intersection lineations defined by the conjunction of foliations plane with latter developed fracture planes, whereas the mineral lineation defined by elongation of quartz and feldspar grains. These are the most common lineations that have been identified on coarse as well as fine variety of the Romapahri granite. Only at a few exposures sub-horizontal slicken sides have been noticed.

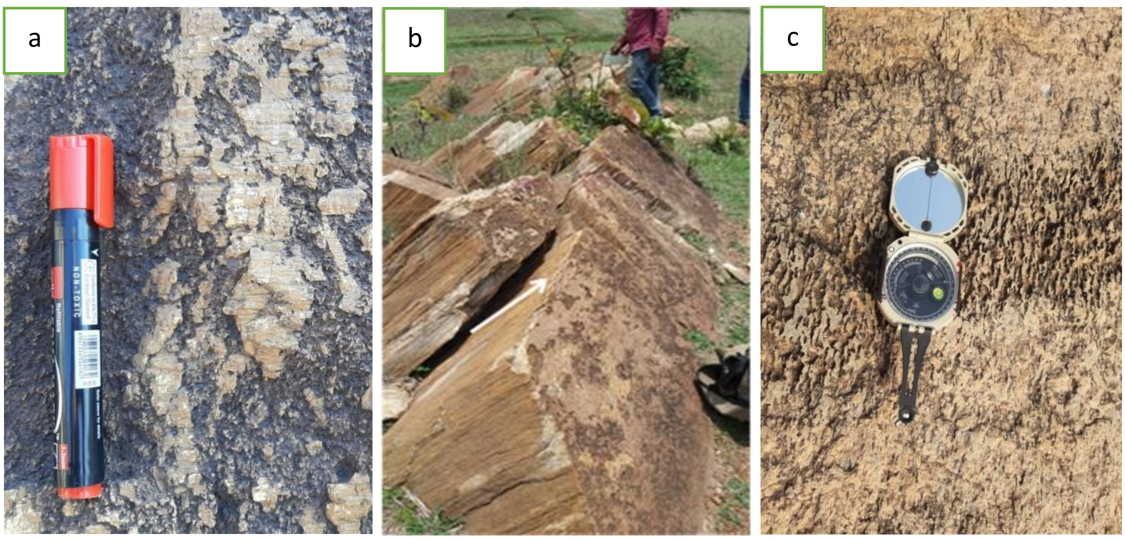

Figure 6.2 The field photograph of Romapahari Granite showing **(a)** Slickensides, **(b)** Intersection lineation, and **(c)** mineral lineations developed on the surface of Romapahari Granite, Mayurbhanj dist, Odisha.(marker size 13 cm)

6.1.3 Microtexural study of Romapahari Granite

Under the microscope many textural modifications have been observed. These microstructural modifications may be in response to different generations of deformations of the area. The textural details correspond to that texture written along with it (Figure 6.3 a-h).

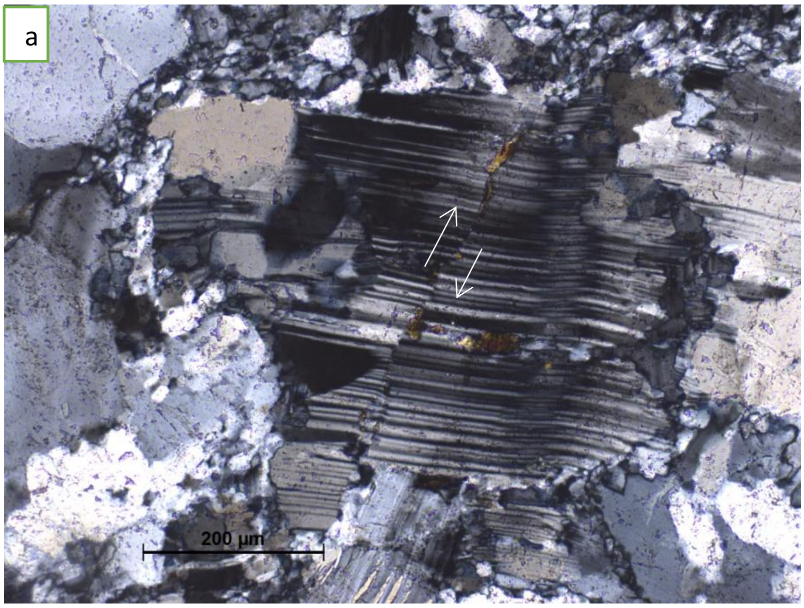

Figure 6.3(a) The photomicrograph of Romapahari Granite showing development of micro fractures with in albite grain of sheared granite, Kesharpur, Mayurbhanj dist. Odisha.

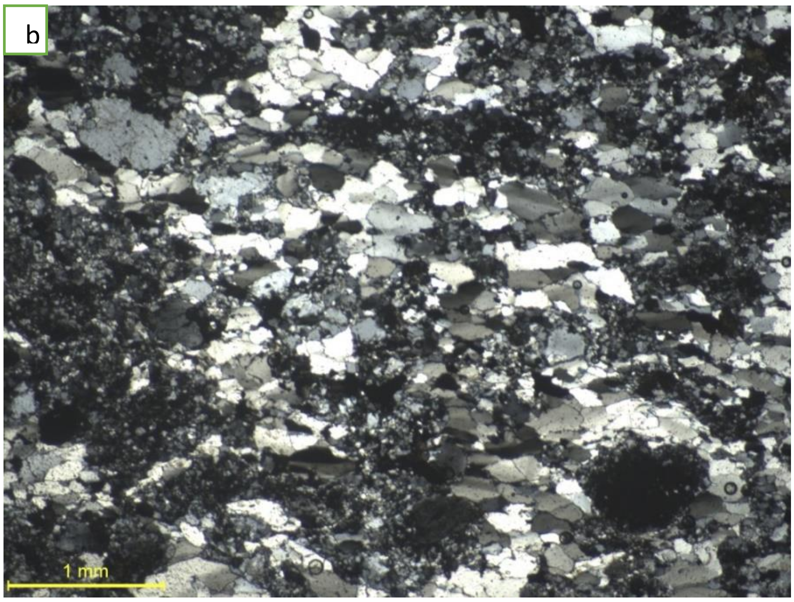

Figure 6.3(b) The photomicrograph of Romapahari Granite showing dynamic recrystallization of quartz grains; old elongated quartz grains with undulose extinction get transformed into smaller grains by recrystallization. Arjundiha, Mayurbhanj, Odisha.

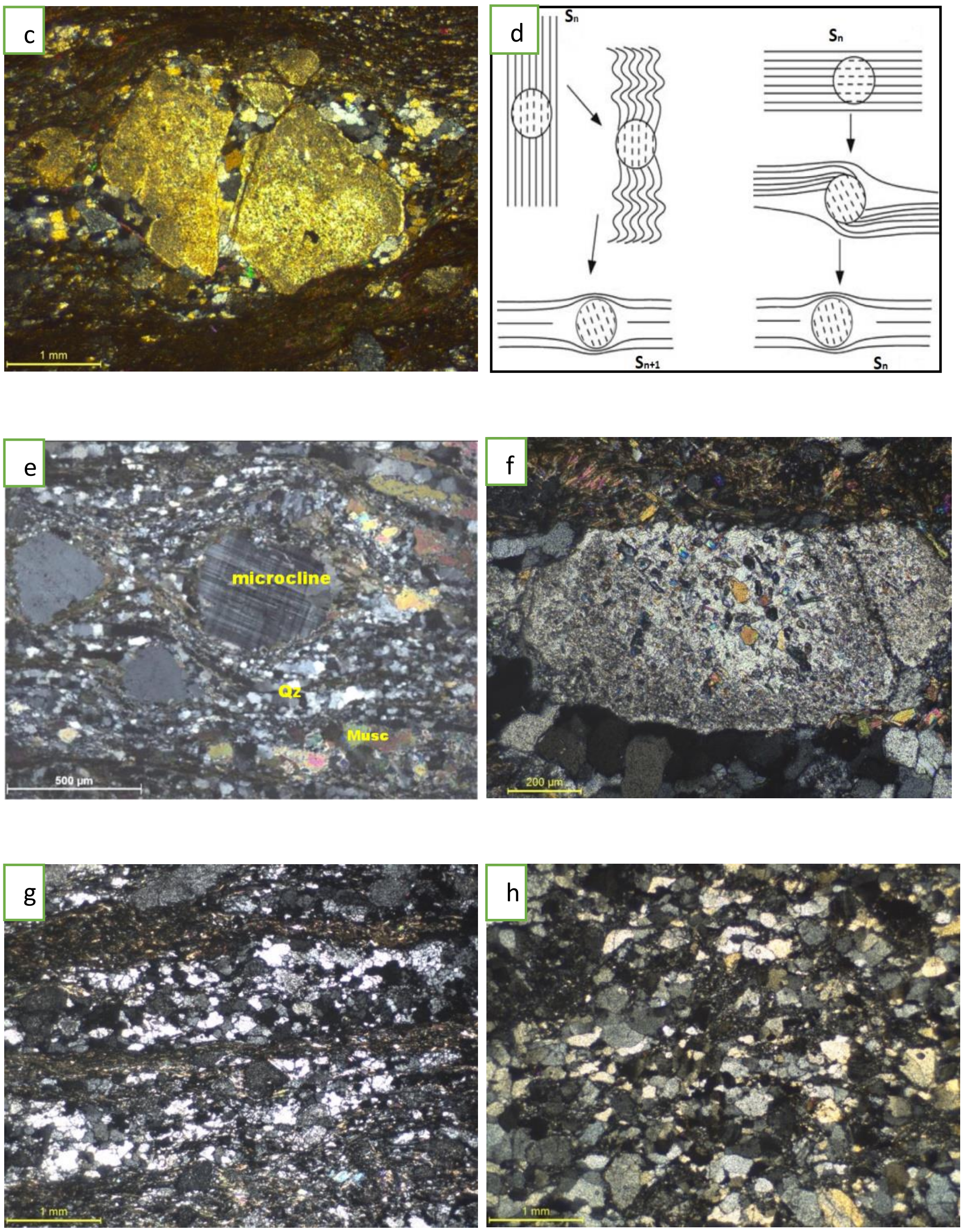

Figure 6.3...(Contd.) The photomicrograph of Romapahari Granite showing **(c)** feldspar porphyroclast bounded by elongated mica flakes. Small micaceous inclusions with in porphyroclast in different orientation w.r.t outer flowage, **(d)** the said texture can be interpreted either as set of two different foliation Sn and Sn+1, or an early and late stage development of a single foliation (right), pressure shadow zone consists of recrystallized quartz and feldspars. **(e)** Porphyroclasts of microcline with mantle of recrystallized feldspar and isolated polycrystalline quartz and mica grains. **(f)** Feldspar porphyroclast bounded by elongated mica flakes also shows small micaceous inclusions with in porphyroclast in different orientation w.r.t outer flowage. Pressure shadow zone consists of recrystallized quartz and feldspars. **(g)** Subparallel orientation of mica-flakes with foliation plane of coarse granite. **(h)** Poorly developed foliation in fine grained granite, near Budhabalang, village, western part of Kesharpur, Mayurbhanj dist., Odisha.

6.1.4 Geometric Analysis of Romapahari Granite

For a detailed geometrical analysis of Romapahari Granite a reasonably good number of structural data has been collected. Attitude of the planar structure (foliations, sheared cleavages, joint plane quartz-veins, sheared-cleavages) and the linear structures (mineral and intersection lineation) have been plotted and contoured on equal area Schmidt net (Fig 6.4). The analysis of the data brings out the followings results.

It has been observe that the poles correspond to foliation of coarse granite fall on great circle indicates large cylindrical fold in the area (Fig 6.4 (a)). The dip of the fold axis is around with an average dip of 50° towards N10°E, whereas the linear fabric of coarse granite such as intersection and mineral lineation forms a cluster around a point plunging north-easterly at angle of 40 degree (Fig 6.4(b)). A small set of lineation with slightly southern rake has also been observed, they shows point concentration along ~ N170° at angle of 60°.

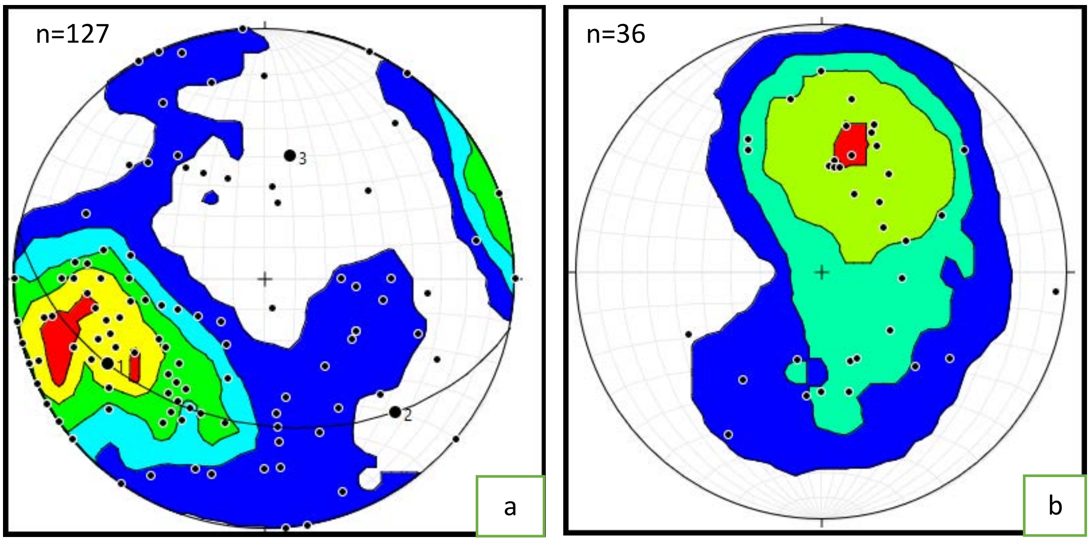

Figure 6.4 (a) Equal area steronet showing poles distribution correspond to foliation, **(b)** and lineation of coarse grained variety of Romapahari Granite.

The poles corresponding to the foliation of fine grained granite shows scattered nature (Fig 6.4 (c)), whereas the majority of the lineations dipping in north-westerly (N329°) direction at angle of 55° (Fig 6.4 (d)). The scattered nature of the poles within fine grained variety may indicate primary origin of foliations (S_g).

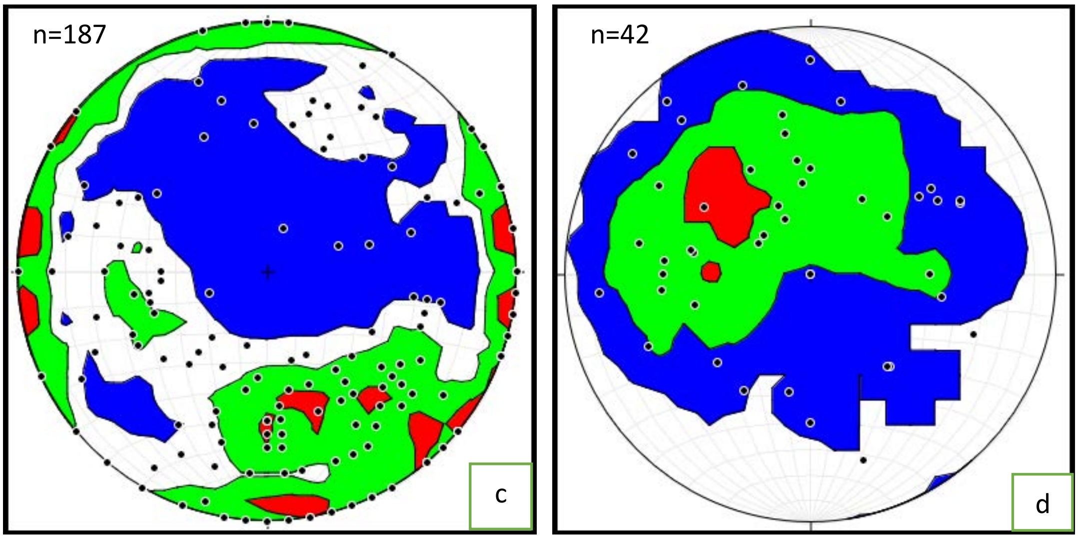

Figure 6.4 (c) Equal area stereonet showing poles distribution correspond to foliation, **(d)** and lineation of fine-grained variety of Romapahari Granite.

Apart from that, few other planar structures have been noticed on the surface of the Romapahari Granite. They include fractured cleavages (Fig 6.1 (c)), joint sets, quartz veins, and shear lenses (Fig 6.1 (d)). The major orientation of quartz-veins, fractured cleavages, and shear lenses seems to be along NW-SE direction (Fig 6.4 (e), (f), (g)). However, the joint planes do not show any specific trend and present in all possible orientations (Fig 6.4 (h)). At a very few exposures set of joints planes exhibiting a small displacement along north to north-west direction has been observed (Fig 6.4 (i)). It has been further notice that a few exposures of Kesharpur, granite exhibit a large shear lenses that cross-cut the quartz veins, and their trend also lying along the NW- SE direction.

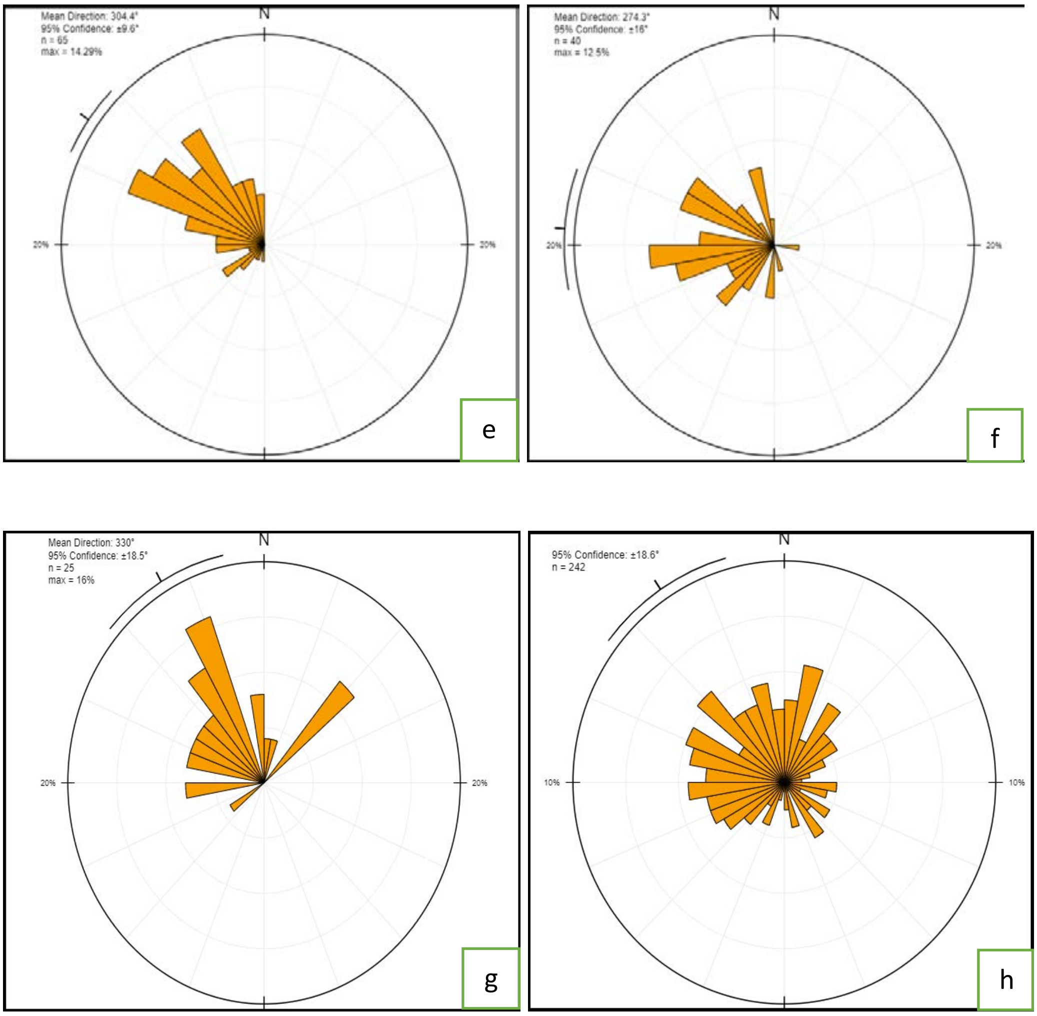

Figure 6.4… (Contd.) Rose diagram showing **(e)** orientation of quartz veins, **(f)** Orientation of fractured cleavages, **(g)** orientation of sheared lenses, **(h)** orientation of joint planes cross-cutting the surface of Romapahari Granite, Mayurbhanj dist., Odisha.

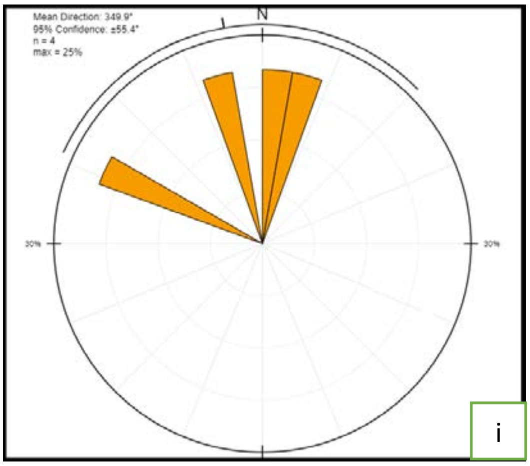

Figure 6.4 (i)..(Contd.) Rose diagram showing trend of joint planes which exhibit small displacement (along NW-SE)

6.2 Morphology of the Structural Features of the Singhbhum Metasediments

As it is evident from field relationships, the Romapahri Granite bears an intrusive relationship with Singhbhum Group of metasediments. The metasediments have been subjected to three phases of deformation (Saha, 1977). These metamorphites belongs to chaibasa and upper dhanjori formation and consists of hbl-biotite-chl-quartz schist, biotite-chl-sericite-quartz schist, muscovite-garnet quartzite, kyanite quartzite, fuchsite quartzite and magnetite bearing sericitic quartzite.

6.2.1 Planar Structures of Singhbhum Metamorphites

In the Singhbhum group of metasediments, different sets of planar structures have been identified. They include mineral foliation defined by dimensional parallelism of mica flakes (sericite, chlorite, and biotite) and mafic minerals (hornblendes), axial planes of fold (fig 6.5(a) & (b)), the crenulation cleavages (fig 6.5(c) & (d)), and the joint set. Despite that, sedimentary structures like cross beds have also seen on the surface of the quartzite exposed near Dumurdiha.

Figure 6.5(a) the field photograph showing development of tight folds within quartzite of Dumurdiha, Mayurbhanj dist., Odisha

Figure 6.5(b) The field photograph of asymmetrical folds developed within quartzite of Dumurdiha, Mayurbhanj dist. Odisha (pensize 14cm)

Figure 6.5(c) The field photograph of crenulation cleavages developed within schist of Tilogoria, Mayurbhanj dist., Odisha (pen size 14cm)

Figure 6.5(d) the field photograph showing Crenulation cleavages developed in biotite-chlorite-sercite-quartz schist, Tilogoria, Mayurbhanj dist. (pen size 14cm)

6.2.2 Linear features of Singhbhum Metasediments

Three set of lineations have been identified on the surface of Singhbhum-metasediments. These linear features include stretching lineations (fig 6.6 (a)), Pebble lineations (fig 6.6 (b)), and intersection lineation. Stretching lineations are mostly associated with quartzite exposed in Tilogria and Dumurdiha area. In most of the exposure they are dipping in direction of north to north-east at angle of 50° to 60° degree. Pebble lineations are observed near the Budhapalang River, Jaganathpur village. These lineations are excellently developed on the surface of quartzite. The pebble are flattened and intensely drawn out to form rods plunging in the N-W direction (N340°) at angle of ~35°. The intersection lineation observes on the Dumurdiha quartzite and they also plunges towards north-east direction at angle of ~50°.

Figure 6.6(a) Stretching and slicken side developed on Ferrugenized quartzite, Tilogoria, Mayurbhanj dist., Odisha.

Figure 6.6(b) Pebble lineation developed within quartzite near Chandani-pahar, Budhabalang Mayurbhanj dist., Odisha. Shear direction NW-SE.

6.2.3 Microtextural study of Singhbhum Metasediments

Similar to the Romapahari granite, with in Singhbhum metasediments, many different textural features have been noticed under microscope. These textural features consists oblique foliations defined by elongated tiny quartz grains, assymetrical folds, crenulations cleavages, and fragmented porphyroclasts construed by mica flakes, σ-type shears sense indicator, and boudins defined by feldspars grains (figure 6.7). The detail of observed texture written along with microphotograph.

a

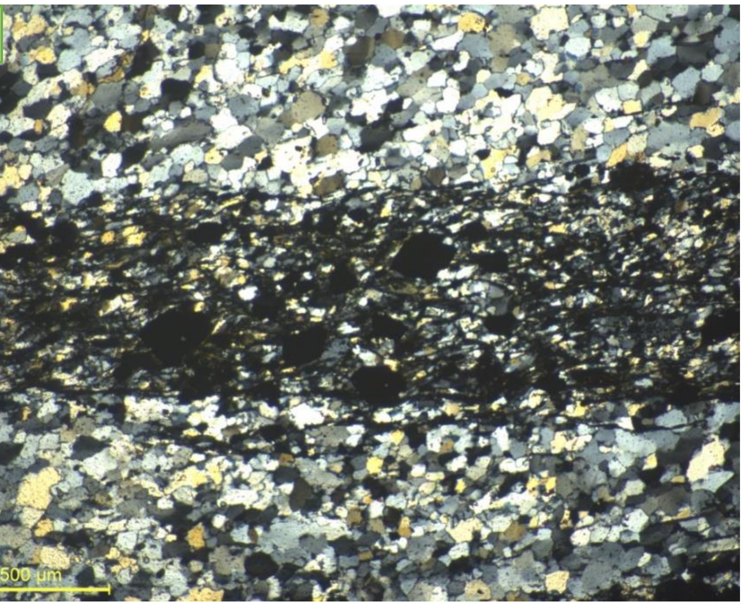

Figure 6.7(a) The photomicrograph showing band of opaque minerals lying along the oblique foliation of Ferrugenized quartzite, Dumurdiha, Mayurbhanj dist., Odisha.

b

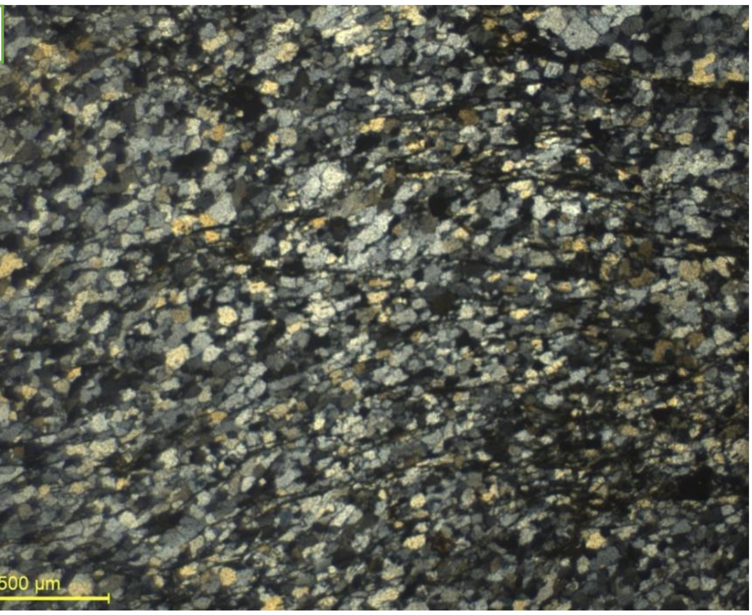

Figure 6.7(b) Oblique foliation defined by tiny quartz grains of Ferrugenized quartzite, Dumurdiha, Mayurbhanj dist., Odisha.

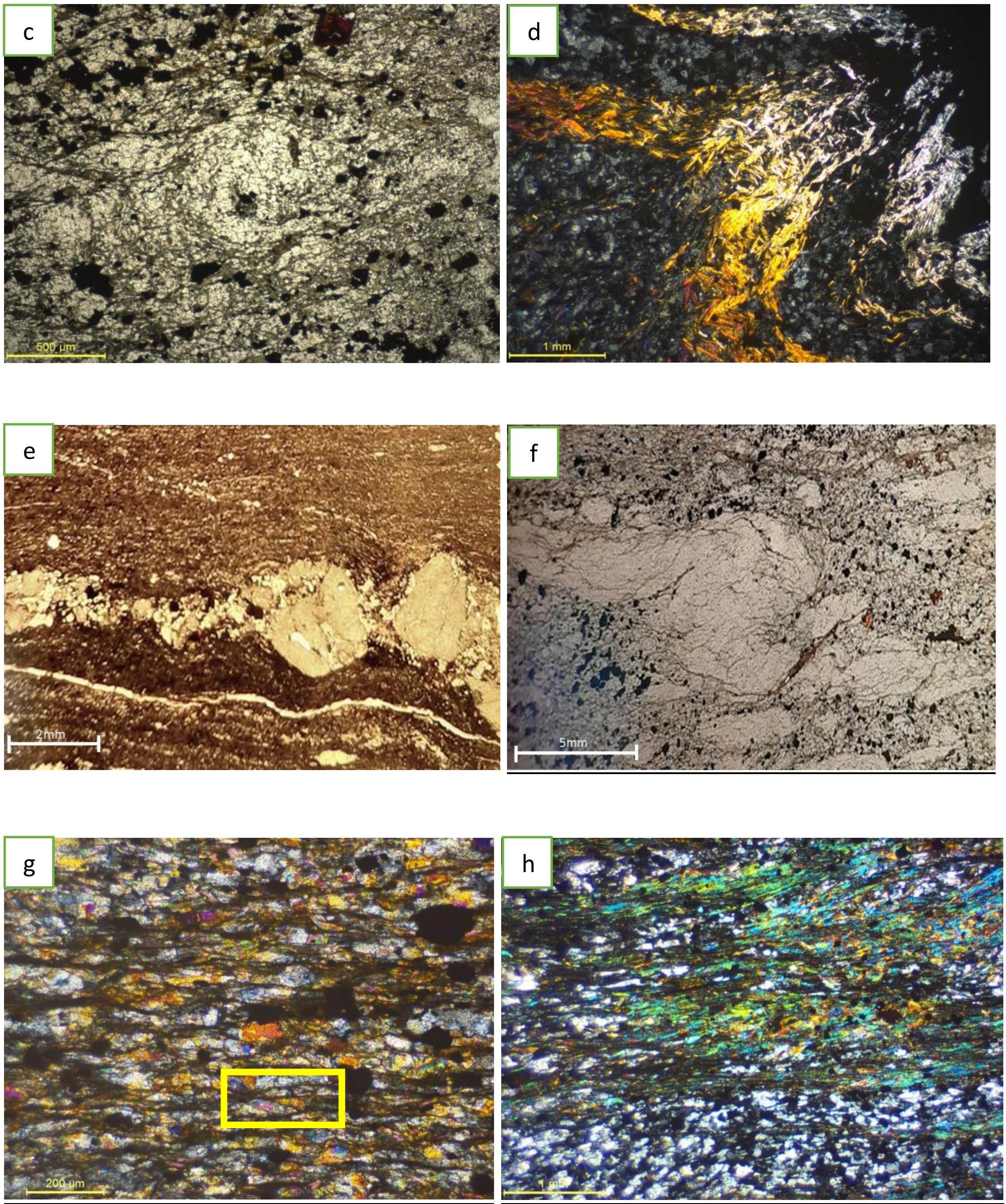

Figure 6.7… (Contd.) the photomicrographs showing **(c)** σ-type porphyroclast developed within Ferrugenized quartzite of Dumrudiha. **(d)** Asymmetric fold developed within bt-chl-ser-quartz schist defined by mica flakes. One limb (left) shows elongation of mica flakes (due to extension) and other shows crenulations. **(e)** The quartz crystal is boudinaged within schist near Budhabalang River. **(f)** σ-type porphyroclast developed within ferrugenized quartzite of Dumurdiha. **(g)** Mica fish arranged between C-type shear bands of mylonitic schist, box bounds the fragmented porphyroclast of mica. **(h)** S-C fabric defined by the mica-flakes within Tilogoria Schist, Mayurbhanj dist., Odisha

6.2.4 Geometrical Analysis of Singhbhum metasediments

Attitude of planar and linear fabric reported from the Singhbhum meta-sediments of the study area has been plotted on equal area Schmidt net and the following observations have been made.

The foliations corresponds to different lithounits (quartzite and schist) when plotted in-conjunction, their poles seem to lie on great circle (Fig 6.8(a)). This indicates the possibility of cylindrical folds with fold axis plunges in north-east direction (~ N007°) at an average angle of ~40°.

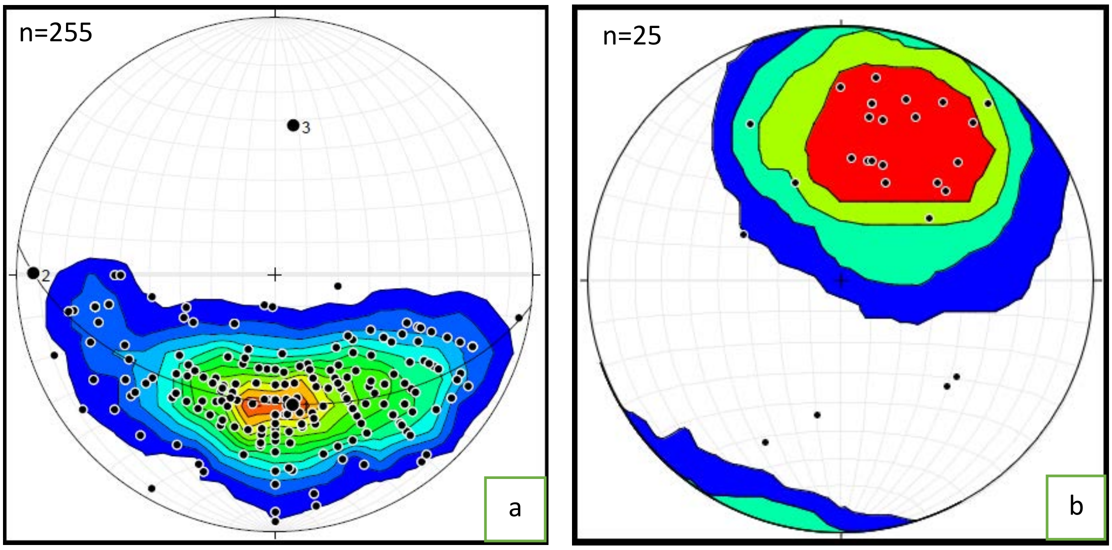

Figure 6.8 Stereonet projection of the **(a)** foliation, and **(b)** lineation developed on the surface of the Singhbhum-metasediments. Poles of the foliation form great circle whereas lineation plunges in north-east direction.

The linear structures such as mineral lineations and intersection lineations consistently plunge in the north-east direction (Fig 6.8 (b)). Whereas, the poles correspond to fold axis, follows a two set different distributions(Fig 6.8 (c)). One set of poles lying in I quadrant (N-E) whereas the other one lying in II quadrant (N-W). This different distribution of poles corresponds to fold-axis can easily be seen in the Rose diagram (Fig 6.8 (d)).

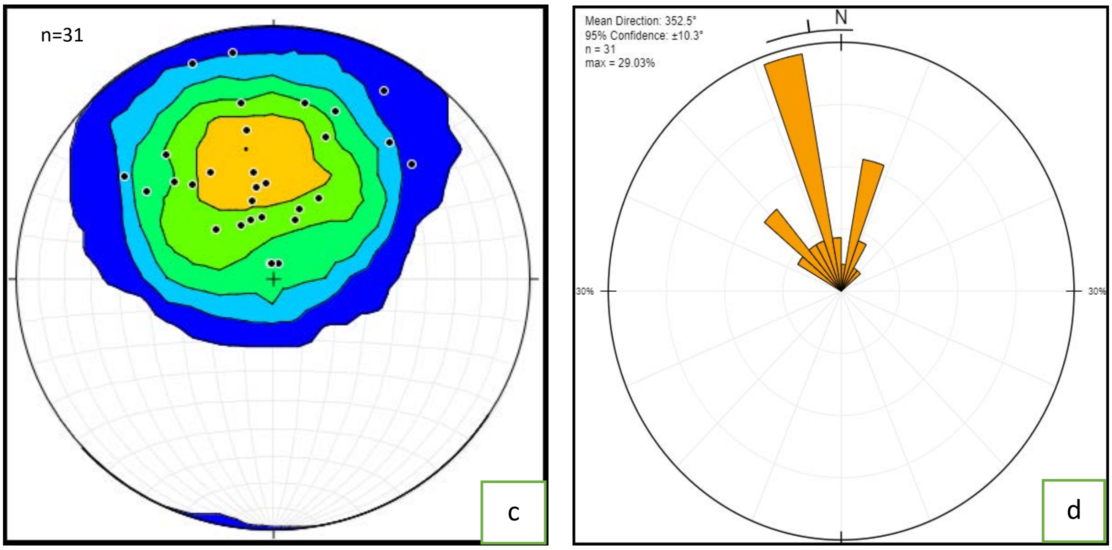

Fig 6.8...(contd). **(c)** Stereonet projection and (d) rose plot representing distribution of poles corresponds to fold-axis in the study area. Bi-drectional distribution of fold axis can easily be visualized in the rose diagram.

6.3 Microtextural study of Feldspathic schist

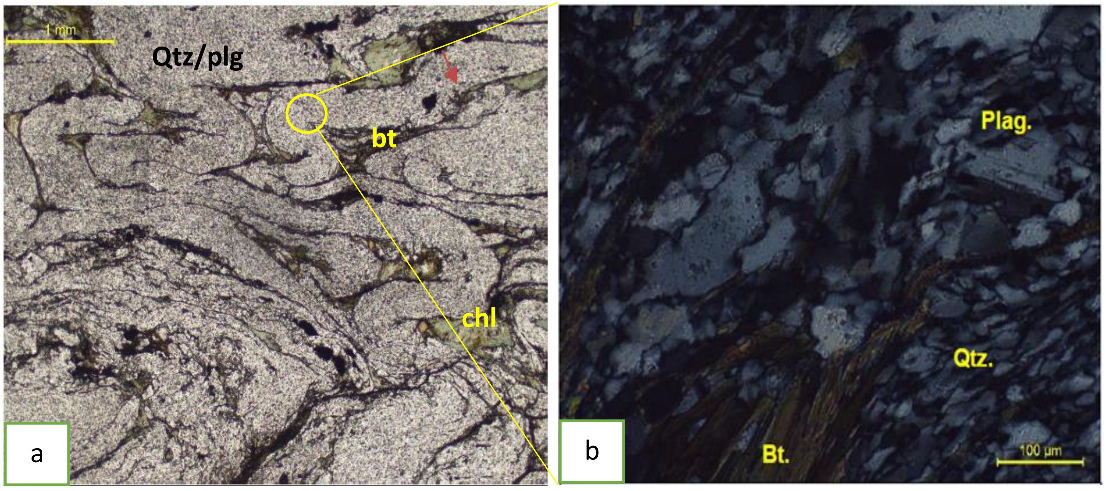

Figure 6.9 The photomicrograph of the Subsurface sample of feldspathic schist showing **(a)** crenulation developed within mylonitic foliations, **(b)** presence of very fine grained quartz and plagioclase crystals with in the mylonitic foliations, Tilogoria, Mayurbhanj, Odisha.

The feldspathic schist is not exposed on the surface, based on subsurface data its presence has been established. The feldspathic schist in the area is highly mylonitised (fig 6.3 (a)). The mylonitic foliations represented by the ribbons of very fine grained higly sheared crystals of quartz and plagioclase. In the area these mylonitic foliations get further folded (fig 6.3(a)). There is still contravery regarding the origin of feldspathic schist. In many literatures it is considered as sheared product of sodagranite.

6.4 Finite strain analysis

The oriented samples of the Romaphari Granite and Singhbum meta-sediments have been collected from the different parts of the study area. They were cut perpendicular to the foliation and parallel to the lineation for the thin sections. Multiple thin sections of each sample were investigated by polarized microscope in order to select strain markers for the strain analysis using the Fry method (Fry, 1979). The Fry method is based on the nearest–neighbour centre–to–centre technique, which uses the relative distance between the centres of each particles or minerals. In two–dimensions, the particles had a roughly random anti-clustered orientation in un-deformed state. When homogeneous deformation affects these particles, the distance between the centres points of the particle are modified. Then the modified particle centres can be used to quantity strain ellipsoid.

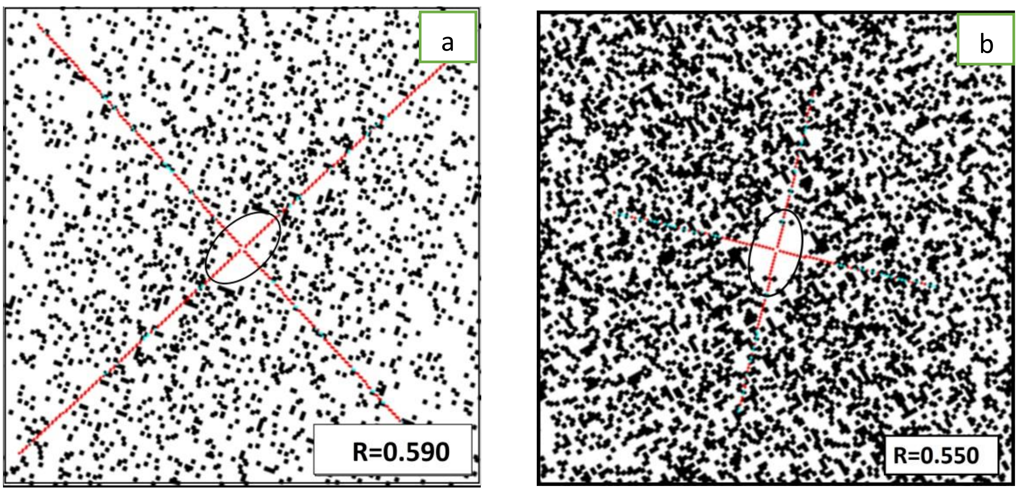

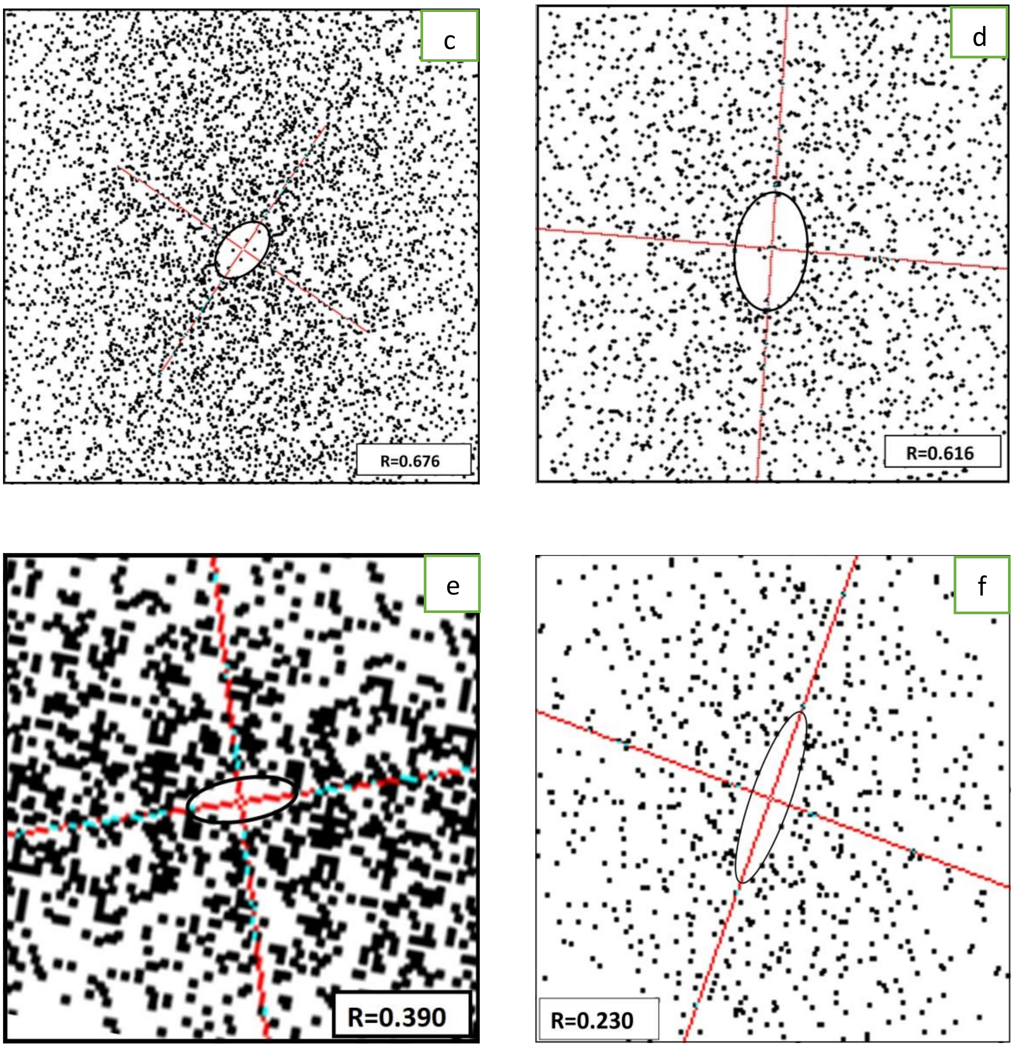

Figure 6.10 (**a**) Finite strain analysis based on the Fry method; strain ellipse of Dumurdiha Schist, **(b)** Dumurdiha granite, **(c)** Dumurdiha quartzite, **(d)** Panajia quartzite, **(e)** Tilogoria Schist , and **(f)** Budhabalang Schist.

The finite strain analysis indicates the rocks in the eastern and western part of the area show dextral sense of shearing which is in sync with field observation. Moreover, the intensity of shearing (based on R value) is higher in schistose rock compared to quartzite and granite. It further indicates as we move from eastern part to the western part the intensity of shearing increases.

6.5 Discussion

In the present area, the Romapahari Granite intrudes into Singhbhum metasediments. Misra, 1999 has observed that the intrusion lacks chilled margin and the metasediments do not show any imprints of metasomatism. A similar observation has also made by Naha, 1960. Therefore they suggested that the granite was not emplaced in a molten condition. Rather the melt mostly crystallized at depth before its emplacement. Now the question arises what should be the possible history of emplacement, whether the emplacement is pre-tectonic or post-tectonic w.r.t folding, and what are the further deformational events that took place before and after the emplacement.

The second phase of Deformation (D_2) was a period of lateral compression which resulted in many mesoscopic and macroscopic folds (Saha et al., 1977). According to Mukhopadhya (1979) the presence of synformal structure in present area can also be attributed to same deformation (D_2). Misra, 1999 has further observed that there is no harmony between the structural data of Romapahari Granite and that of metasediments, therefore, he suggested that the emplacement of granite was post-tectonic w.r.t to folding (D_2) event. However, the present study reveal that there is a certain similarity between the structural data of the coarse-grained variety of Romapahari Granite (Fig 6.4(b)) and that of metasediments (6.8(b)). Therefore the emplacement of a coarse grained Romapahari Granite can be consider either pre-tectonic or syntectonic w.r.t to folding event (D_2). On the other hand the structural data of fine-grained Romapahri granite is highly scattered (Fig 6.4 (c),(d)) and does not show any harmony with metasediments, therefore its emplacement can be considered as post tectonic w.r.t folding event (D_2). The above observations are also consistent with the geophysical data. The scattered nature and small circle near-vertical distribution of poles (Fig 6.4(c)) indicates that the foliations developed within fine-grained granite are of primary nature (Sg) and magma emplacement was near vertical.

Now the second question arises whether the shearing took place in the area is post tectonic or syntectonic w.r.t to folding. According to Saha, (1977), the surface of Romapahari Granite bears some sheared cleavages (Fig 6.1(c)), which heading towards NW-SE direction. These fracture cleavages get further sheared along NE-SW direction (Fig 6.1(c)). The third phase of deformation (D_3) associated with extensive shearing along fracture planes. Therefore these fracture cleavages must be developed before D_3 and get sheared along NE-SW during D_3. Therefore according to Saha, (1977) the shearing (D_3) is post tectonic with respect to folding (D_2). However, the present study reveals that in the north-western part of the area there is strong shearing along NW-SE and in the eastern part the shearing direction is along NE-SW. The second observation is related to presence of mylonitic feldspathic schist (schistose soda granite). In the present area the strong shearing leads to development of mylonitic foliation and they are clearly visible in the feldspathic schist (fig 6.3 (a) & (b)). The subsurface sample of feldspathic schist collected near Tilogoria (close to the hinge of regional fold) shows the mylonitic foliation get further folded. It means after development of mylonitc foliation there must be period of compressional tectonics which results in folding of mylonitic foliation, which indicates there should be possiblilty that shearing is pretectonic with respect to folding. The alternative mechanism to explain bi-directional shearing (NE in western part and NE in Eastern part of the area) in the area is the layer parallel shearing due to regional fold.

The entire study area has been cross-cut by the joint planes and quartzo-feldspathic veins. Since there are no major field evidences suggesting any effect of NE-SW shearing (D_3) on the joint planes, therefore their development can be consider as post tectonic with respect to D_3.

In the north western side of the area (~20km away) NNE-SSW trending highly brittle deformation zone is present. According to Saha, 1977 it represent the extension of Singhbhum shear zone. However, the field observation suggests the said zone represents highly brittle deformation and the shearing that took place in the present area (which is further southward with respect to kendua fault) represents highly ductile deformation. Therefore kendua fault can be considered as relatively younger phenomenon.

6.5.1 Chronology of possible events

1. Emplacement of hornblende-biotite rich coarse grained Romapahari Granite
2. Shearing
3. Folding of Metasediments and coarse granite
4. Emplacement of fine grained aplitic Romapahari Granite
5. Formation of joints planes and intrusion quartzo-feldspathic veins
6. Activation of Kendua-fault

CHAPTER 7

PETROGRAPHY

7.1 Petromineralogical Study

7.1.1 Petromineralogical Study of Romapahari Granite

The samples from coarse grained foliated granite and fine grained massive non foliated granite has been studied under microscope. In the coarse granite the essential mineral identified are, microcline (~45%), quartz (~40%), plagioclase (~5%). The anorthite content in the granite varies from 4.11% (Misra, unpublished Ph.D. thesis, 1993).

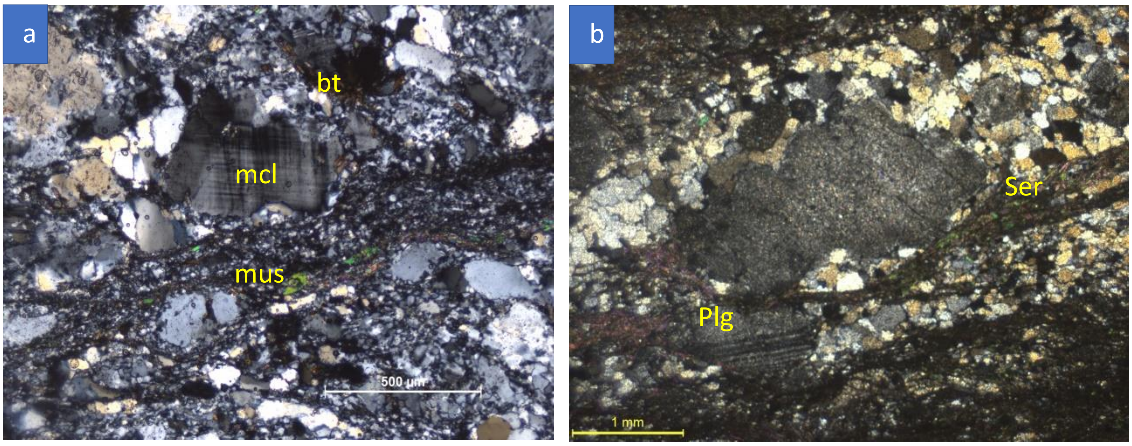

Fig 7.1(a) Photomicrograph of coarse grained sheared granite of Kesharpur showing porphyroclast of microcline with mantle of recrystallized feldspar, polycrystalline quartz, and muscovite (mus). Flakes of biotite (bt) and sericite (Ser) define the foliation planes. **(b)** Porphyroclast of Albite within matrix of polycrystalline quartz and feldspar. Sericite flakes are aligned along planes.

Other minerals identified are chlorite, muscovite, and biotite (fig 7.1(a)). Zircon, epidote, sphene, and hornblende occur as accessory minerals (fig 7.1 (d), (e), (i), & (j)). Plagioclase and microcline are present both as fine anhedral groundmass and coarse-grained subhedral phenocryst (fig 7.1c). In some places the plagioclase shows inclusions of quartz and mica (muscovite). Biotite and sericite flakes with preferred orientation define the schistosity (fig 7.1 (b)). The non-foliated variant of the granite displays hypidomorphic to allotrimorphic granular texture.

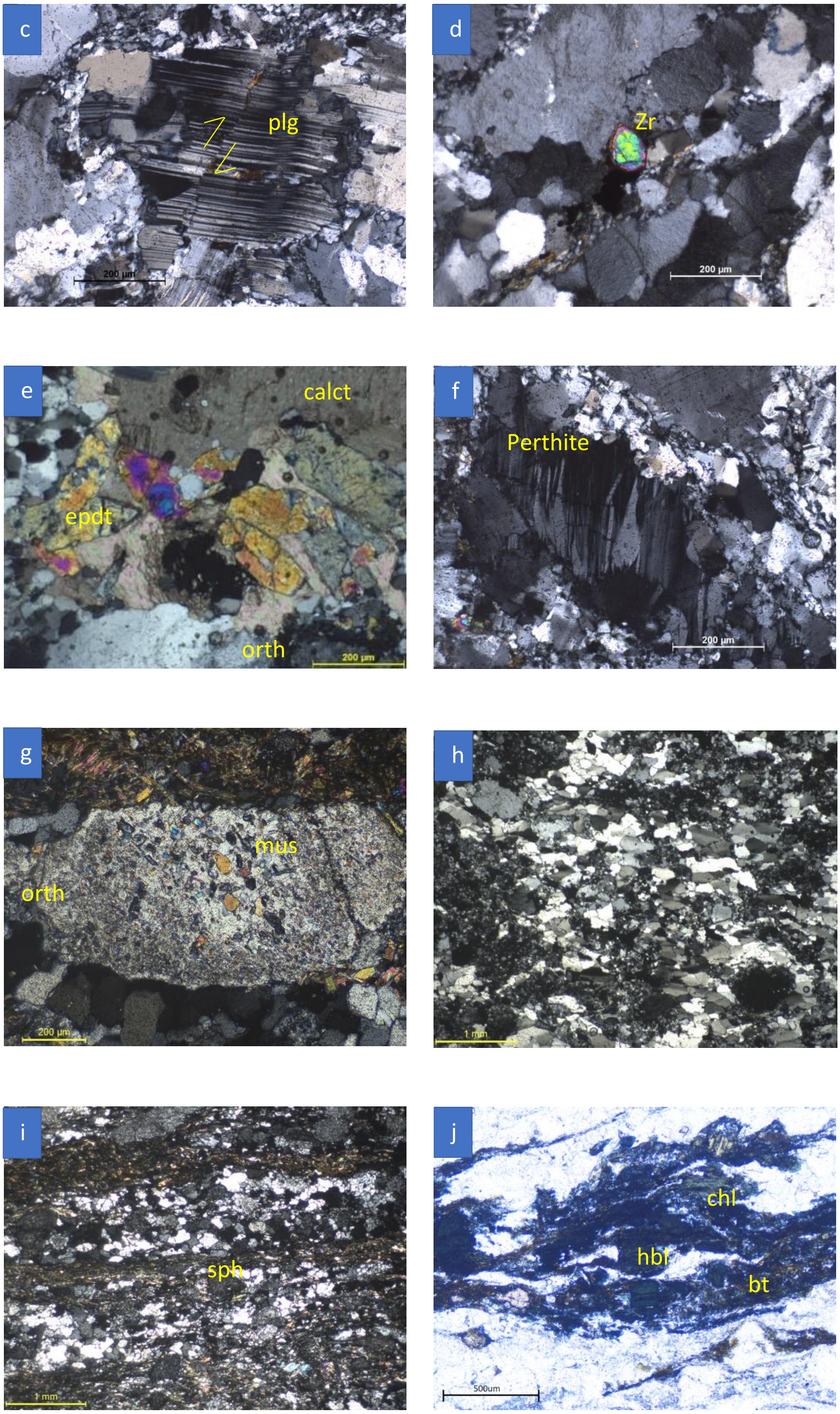

Figure 7.1.. (Contd.) photomicrograph of coarse grained sheared granite showing **(c)** micro-fracture developed in albite grain. **(d)** Small zircon (Zr) grain occurs as accessory. **(e)** Secondary epidote (epdt) and calcite (calct) mineral. **(f)** Perthitic texture. **(g)** Inclusion of mica (musc) and quartz inside orthoclase (orth). **(h)** Undulose extinction shown by a quartz grains. **(i)** Presence of sphene (sph) **(j)** Hornblende (hbl) biotite (bt) and chlorite (chl) minerals along foliation plane.

The similar phases have also been observed in aplogranite (fig 7.1 (k), (l), & (m)), with lesser occurrence of mafic minerals (hornblende + biotite). In addition to that, micro-perthetic textures were also observed in aplitic granite (fig 7.1 (l)) as well as in coarse grained granite (fig 7.1 (f)). At places undulose extinction were also observed within a few quartz grains (fig 7.1 (h)).

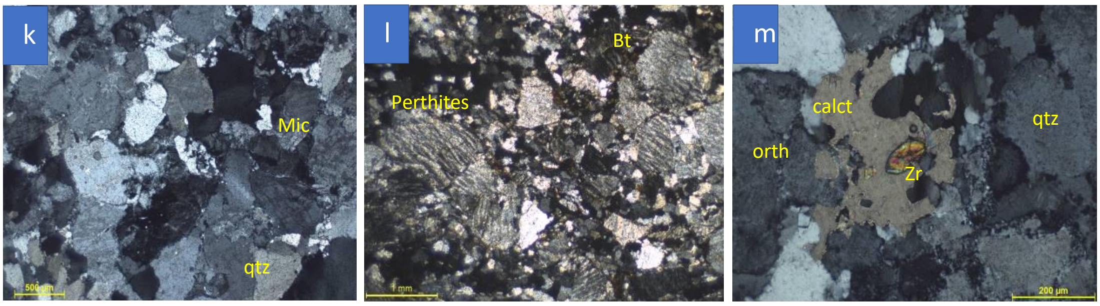

Fig 7.1...(Contd.) **(k)** The photomicrograph showing presence of microcline (Mic) and quartz (qtz) in aplitic granite, **(l)** perthitic texture developed within non-foliated aplitic granite, **(m)** zircon (Zr) enclosed by fracture filling calcite, other mineral phases present are orthoclase (orth) and quartz (qtz).

7.1.2 Ore Mineralogy of the Sheared Variety of Romapahari Granite

The subsurface borehole core samples of sheared granite were studied for the ore minerals. The samples were collected near the Kusumbari area. The oxide ore minerals that are identified includes uraninite (Fig 7.2 (a)), ilmenite, magnetite and hematite. Sulphide minerals present are galena, chalcopyrite, pyrite, pyrrhotite, and bornite (Fig 7.2 (b) & (c)) in descending order of their abundance.

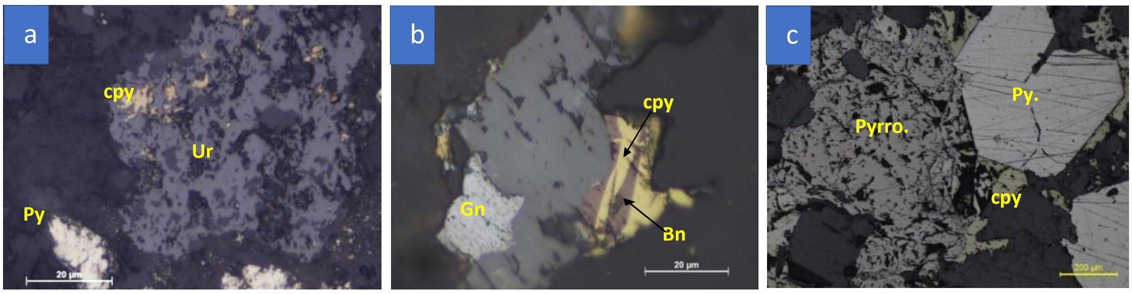

Figure 7.2 Photomicrograph showing **(a)** uraninite (Ur) with inclusion of chalcopyrite (cpy), whereas pyrite (Py) occurs nearby in the neighbourhood of uraninite, **(b)** chalcopyrite, bornite (Bn) and Galena (Gn), **(c)** Pyrrohotite, pyrite and chalcopyrite mineral in sheared granite, Kusumbari, Mayurbhanj, Odisha.

7.1.3 Modal composition of Romapahari Granite

The published data of modal analysis of Romapahari Granite is consistent with the visual estimations. In general both the coarse granied and fine grained granites have very similar composition (Table 7.1). In particular the coarse grained variety of Romapahari granite is relatively enriched in mafic content (biotite+hornblende), whereas the fine grained aplitic granite has higher content of microcline.

Table 7.1 Modal analysis of Romapahari granite based on, Misra unpub phd thesis, (1993), Saha, (1977)

Mineral Type	Coarse granite		Aplitic granite
	Misra, 1993	Saha, 1977	Saha, 1977
Microcline (%)	50.2	47.3	53.5
Quartz (%)	36.9	35.4	30.7
Plagioclase (%)	6.5	9.3	11.6
Mafic (%)	3.9	3.9	1.1
Magnetite (%)	0.8	1.4	0.8
Epidote (%)	1.1	1.6	2

On the QAP diagram (Fig 7.3) both coarse and fine grained granite are closely associated. The coarse granied variety occupies field of both alkali feldspar granite (Misra, unpub ph.d. thesis, 1993) and granite (Saha, 1977), whereas the fine grained variety occupy the field of granite (Saha, 1977).

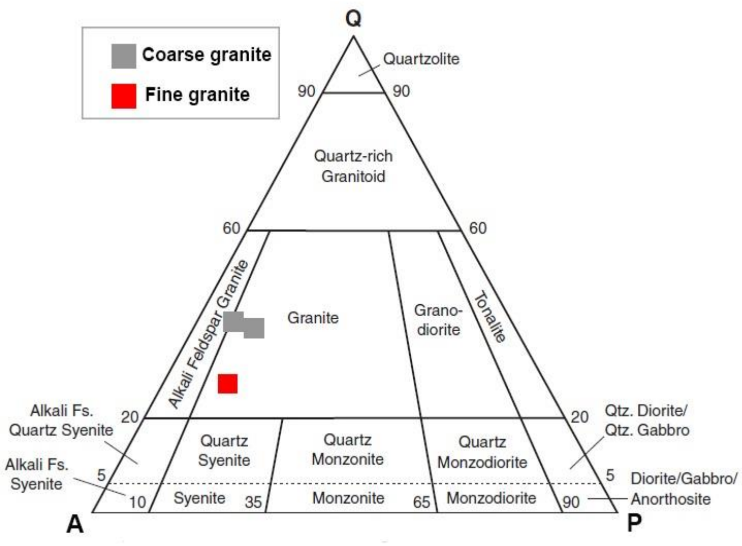

Figure 7.3 Different units of Romapahari Granite (coarse and fine-grained) plotted on QAP diagram, the overall composition of granite lying in the field of granite to alkali feldspar granite. QAP diagram after Le Maitre, (2002).

7.1.4 Petromineralogical Study of Singhbhum Metasediments

7.1.4.1 Kusumbari Area

In the Kusumbari and its adjoining area the major lithounits exposed are hornblende-chlorite-biotite-quartz schist and biotite-chlorite-sericite-quartz schist. The major minerals identified includes sericite, chlorite, biotite, quartz with minor epidote, sphene, hornblende, tourmaline, and other opaques minerals (Fig 7.16, (b), (c), & (d)). *Hornblende-chlorite-biotite-quartz schist* consists of biotite and quartz with minor amount of muscovite and hornblende with sphence as accessory mineral. Monazite occurs as an inclusions in biotite and exhibit pleochroic haloes around the grain (Fig 7.4 (c)). At places apatite is present along the cleavage planes (Fig 7.4 (a)).

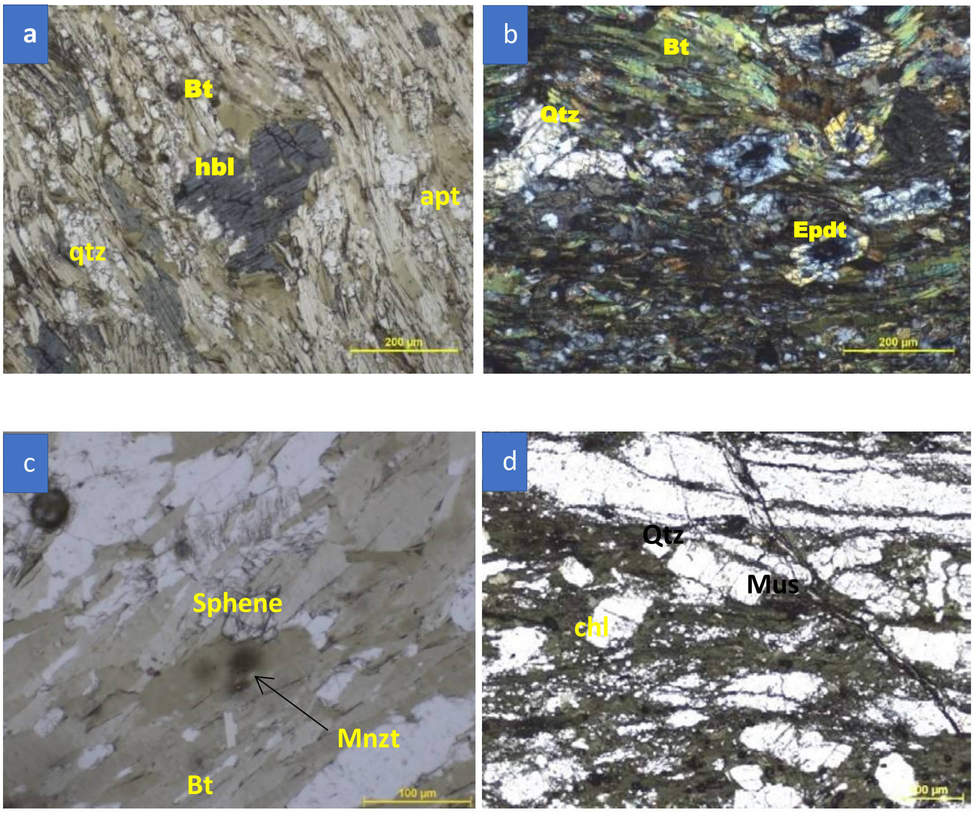

Figure 7.4 Photomicrographs of **(a)** hornblende-biotite-schist of Kusumbari area showing hornblende (hbl) both athwart to and along the foliation planes, and aptatite (apt) occur along foliation plane. **(b)** Zoned euhedral epidote (Epdt) amidst biotite (Bt). **(c)** Late stage well developed sphene crystals, and monazite (Mnzt) inclusion within biotite grains. **(d)** Chlorite - quartz schist flakes Kesarpur area.

In *Biotite-chlorite-sericite-quartz schist* quartz grains show undulose extinction sutured boundaries, moderately high degree of elongation giving rise to lenses of quartz-rich zones with swerving of schistosity around them (Fig 7.4 (e)). Zircon and monazite are present in significant amount. Aggregates of fractured grains of monazite occur in micaceous rich portions causing discoloration in the phyllosilicates and are aligned parallel to the foliation (Fig 7.4 (f)). Zircon also occurs as aggregate in micaceous zone (Fig 7.4 (f)).

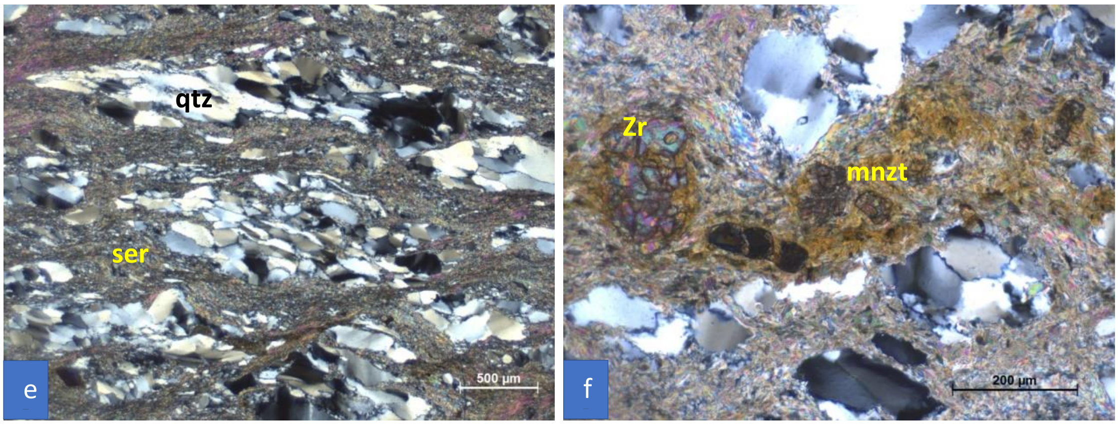

Figure 7.4 Photomicrographs showing **(e)** aggregates of quartz grains displaying undulose extinction and swering of schistosity around the lenses of quartz-rich zones them. **(f)** Fractured zoned zircons (Zr) and monazite (mnzt) in the sericite-rich bands.

7.1.4.2 Ore mineralogy

The oxide phases identified from schistose rocks of Kusmubari area include uraninite and ilmenite (Fig 7.5 (a)). Uraninite is the radioactive phase that occurs as very fine anhedral grains with size ranging from 10 to 20 microns, enclosed within biotite flakes producing characterizing radioactive halos in the latter (Fig 7.5 (d & f)). Sulphide minerals like galena, molybdenite, pyrite, chalcopyrite, pyrrhotite, as fine lamellae of pentlandite within pyrrhotite are observed in these Schistose rocks (Fig 7.5 (e)). At places close association of chalcopyrite and uraninte was also observed ((Fig 7.5 (c)). Molybdenite is mostly seen enclosed by pyrite or pyrrhotite (Fig 7.5 (e)).

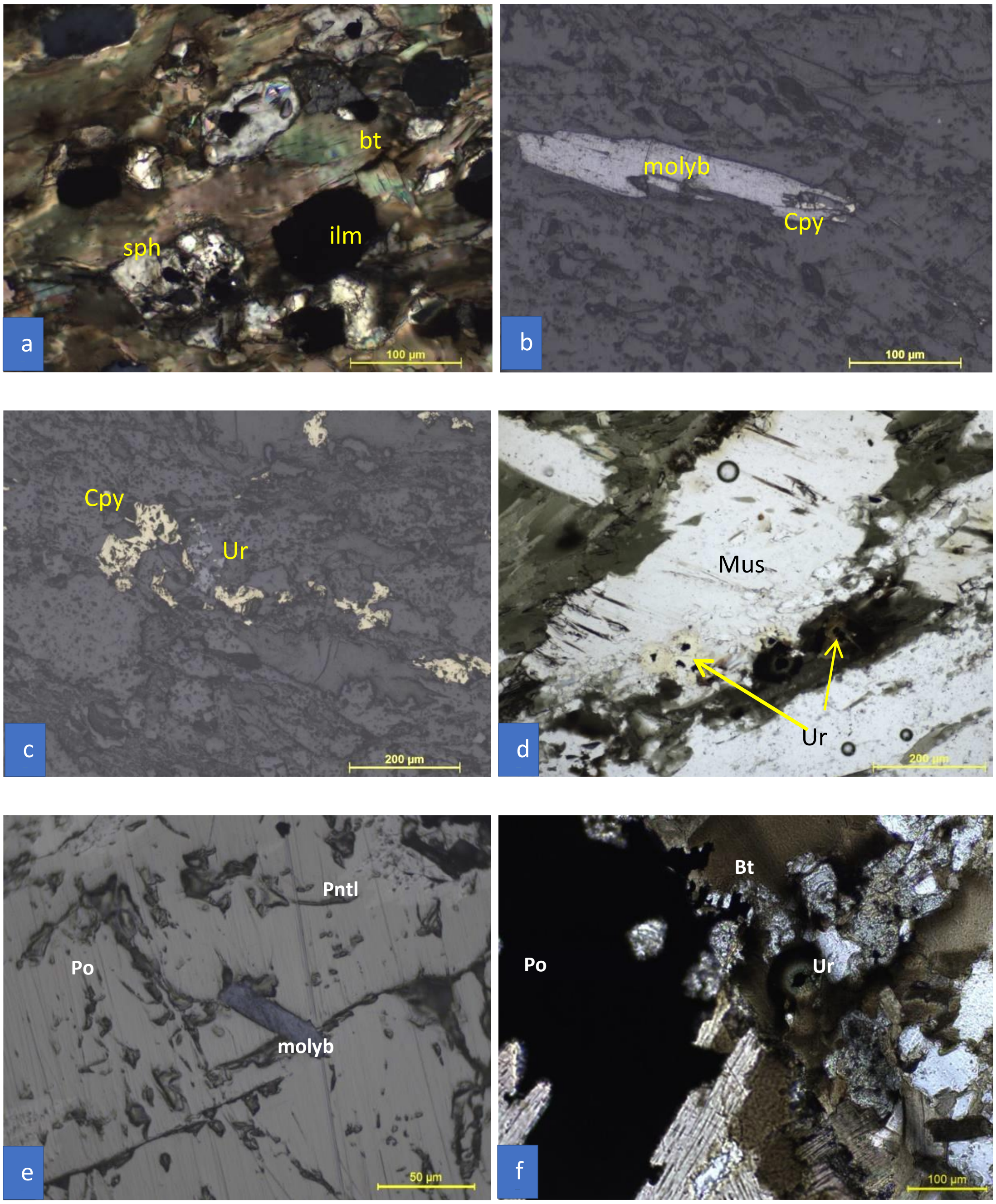

Figure 7.5 Photomicrograph of **(a)** hbl-bt-ch-qtz schist showing occurrence of sphene (sph) with ilmenite (ilm) specks within biotite flakes. Inset shows the same photo under reflected light **(b)** Molybdenite (molyb), uraninite (Ur) and sphene (sph) enclosed within biotite (Bt). **(c)** Chalcopyrite (Cpy) and uraninite (Ur) occurs together. **(d)** Uraninite (Ur) enclosed by biotite (Bt) as well as muscovite flakes that exhibit radiation halos. **(e)** Molybdenite (molyb) enlcosed by pyrrhotite (Po) that latter being replaced peripherally by pentlandite (Pntl). **(f)** Anhedral uraninite (Ur) as an inclusion within biotite.

7.1.4.3 Tilogoria Area

The major lithounits present in the Tilogoria area are Feldspathic schist, biotite-chlorite-sericite-quartz schist, and Ferrugenious quartzite. The subsurface borehole core samples of radioactive feldspathic schist were studied under microscope. Quartz, plagioclase, chlorite, and biotite are the major mineral phases whereas epidote, muscovite and calcite occur as accessory minerals. The rock displays extensive recrystallisation, tight polyclinal foldings and effects of mylonitization (fig 7.6 (a & b)). Plagioclase and quartz underwent grinding process leaving finer sized quartz and relict plagioclase grains (fig 7.6 (c & d)).

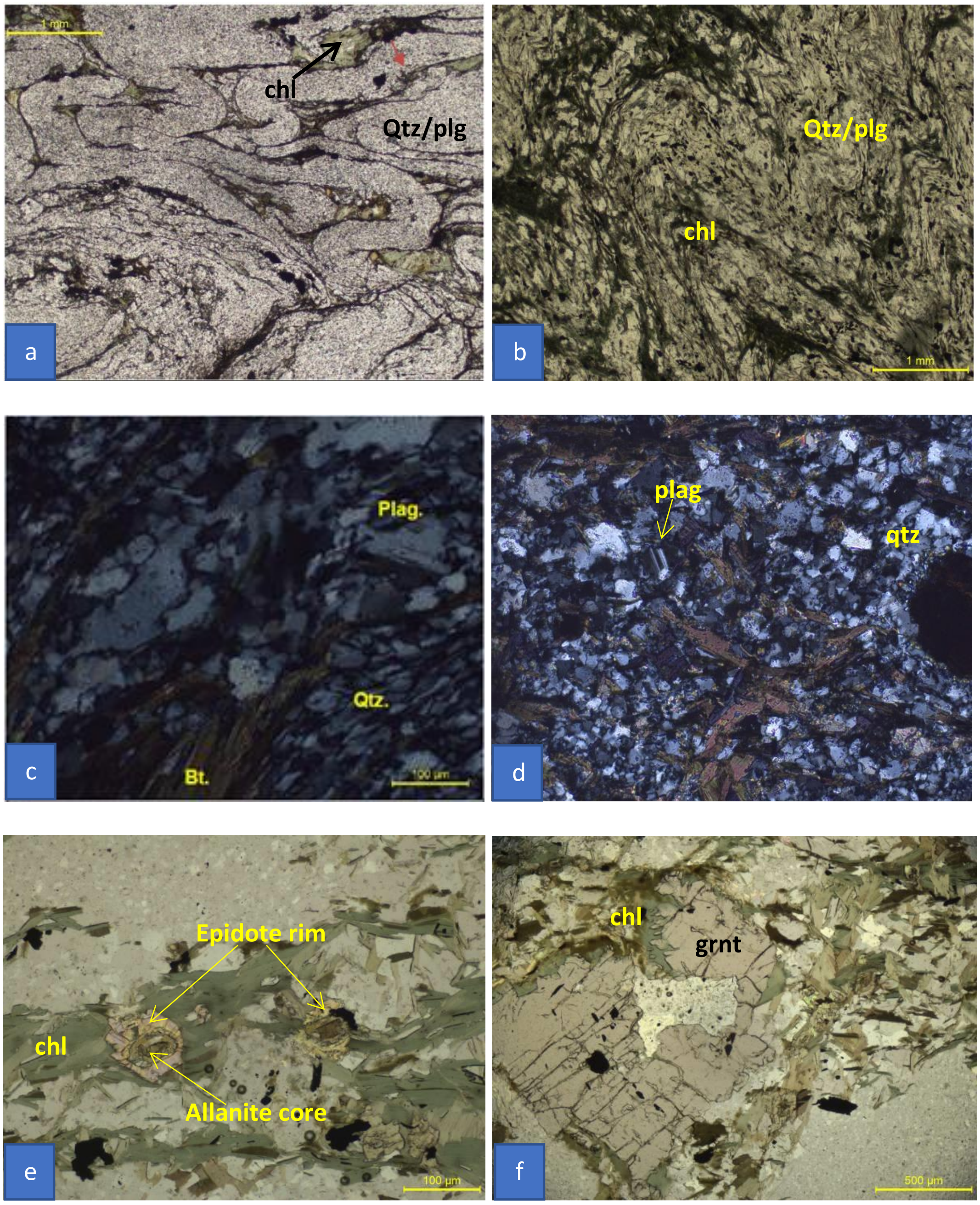

Figure 7.6 (a & b) Photomicrographs of feldspathic schist showing ribbons of highly mylonitised quartz (Qtz) and plagioclase (Plag) grains with latter appearance of chlorite veins. **(c & d)** Relict of plagioclase (Plag) in fine grained matrix of quartz (qtz) and plagioclase. **(e)** Metamict allanite rimmed by epidote. **(f)** Garnet (grnt) shows marginal retro alteration to chlorite (chl).

Biotite-Chlorite-Sericite-Quartz schist is host rock that does not hold any radioactive mineral phase. In hand specimen it is light brown in color, highly crenulated, and sericite-rich. Under microscope the major phases identified are biotite, chlorite, chloritoid, sericite, and quartz (fig 7.6). Unlike the feldspathic schist in biotite-chlorite-sericite schist plagioclase is absent and intensity of deformation is comparatively less. At places, chloritoid mineral occurs along with crenulated foliation has also observe (fig 7.6 (a)).

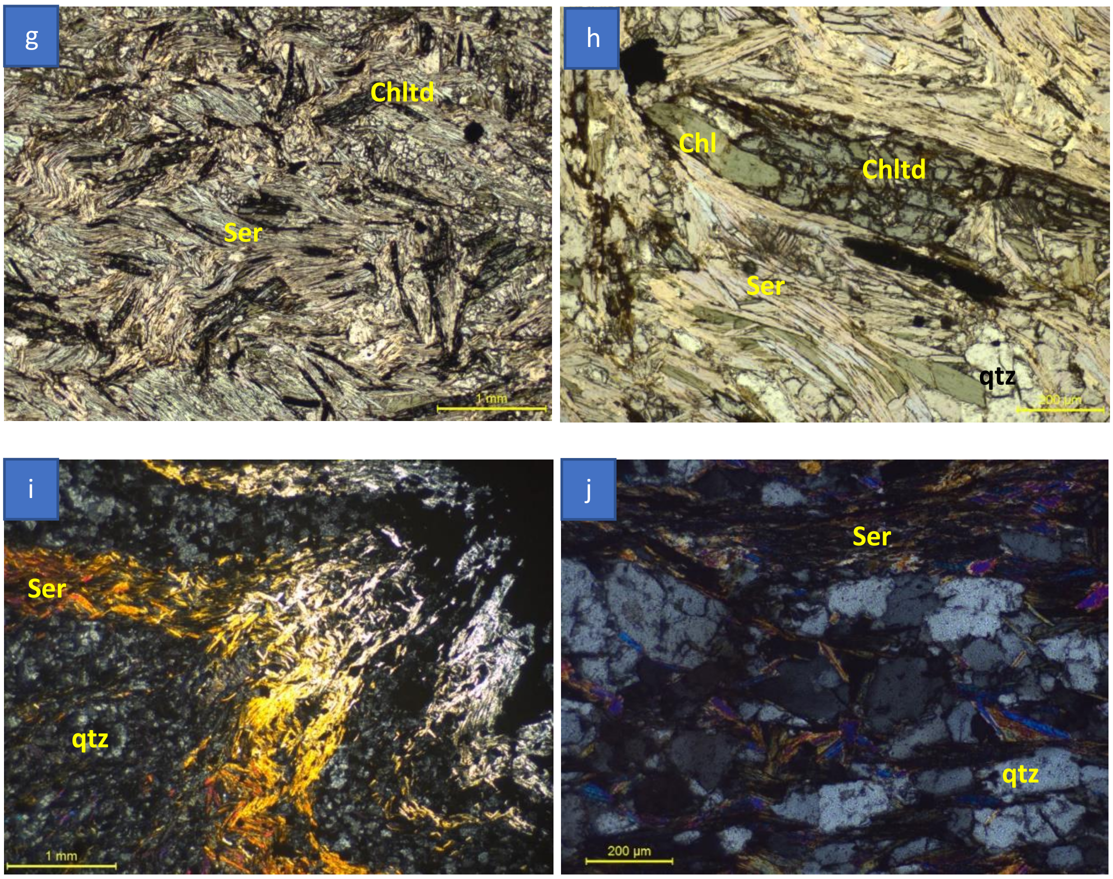

Figure 7.6 photomicrograph of chlorite-sericite-quartz-schist shows **(g)** chloritoid swerving along with crenulated foliation. **(h)** Secondary chlorite forming from alteration of chloritoid. **(i)** Asymmetric fold developed with in schist, one limb (left) shows elongation of mica flakes (due to extension) and other shows crenulations (due to compression). **(j)** Relatively less deformed sericite-quartz-schist.

7.1.4.4 Ore Mineralogy

The ore minerals identified in feldspathic schist from Tilogoria are pyrite, chalcopyrite, magnetite, and ilmenite (fig 7.7 (c) & (e)). At places uraninite shows signatures of rotation, inclusion of fine grains of quartz, sulphide minerals are mostly anhedral and are parallel to the foliation. Uraninite is mostly enclosed in biotite/chlorite flakes (fig 7.7 (c) & (d)) and shows close spatial association with pyrite, magnetite and epidote (fig 7.7 (a) & (b)). There is drastic difference in grain size and shape of uraninite with respect to matrix. Magnetite can remove U(VI) from solution through reduction to U(IV) coupled to oxidation of Fe(II), with precipitation of UO2 on the Magnetite surface (Timothy A. Marshell, 2015).

$$2Fe^{2+} + UO_2^{2+} \text{------>} 2Fe^{3+} + UO_2$$

The above reaction could explain the close association of Fe -bearing phases with Uranium minerals (figure7.7 b& c).

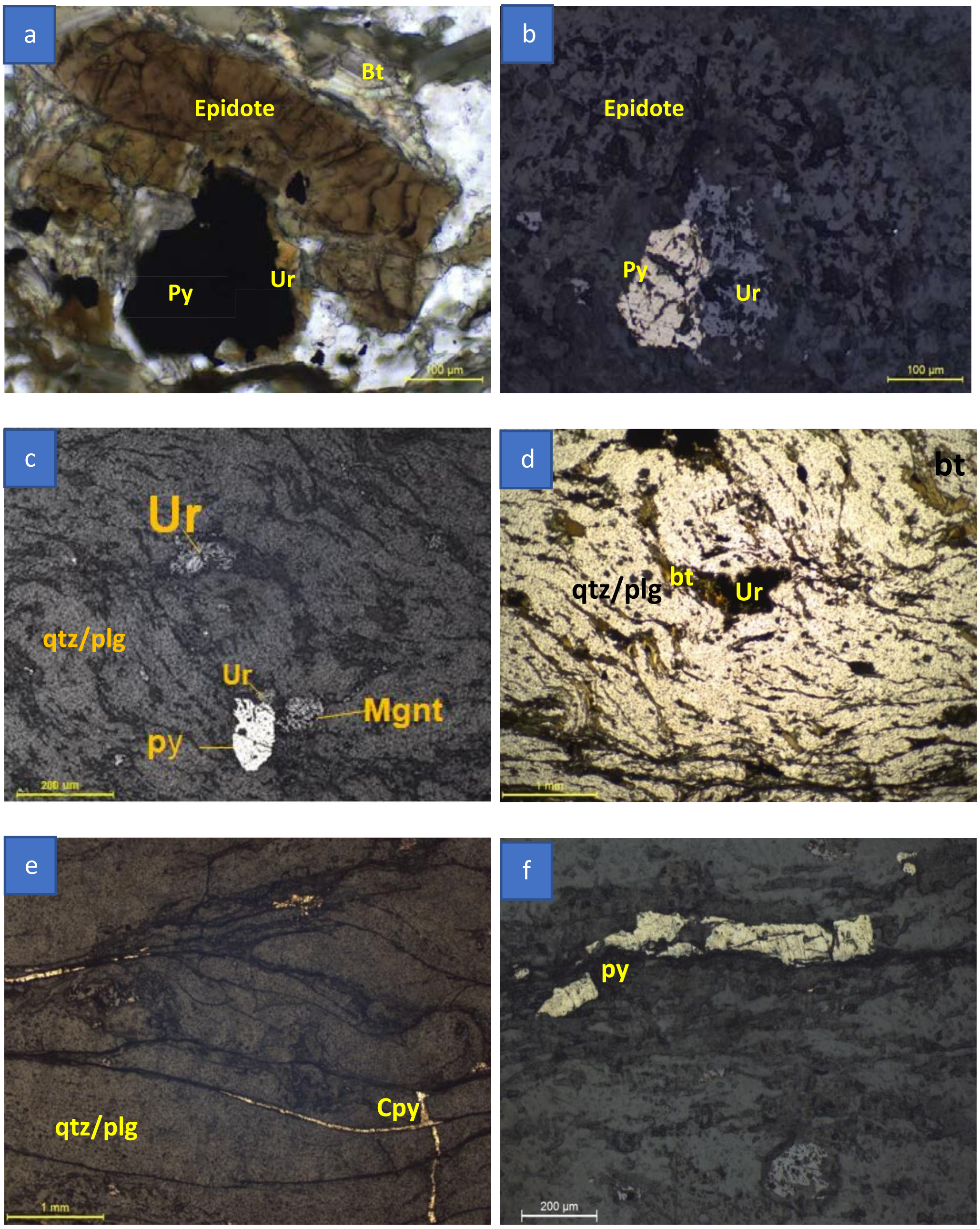

Figure 7.7 Photomicrogrpaht of feldspathic schist shows **(a)** uraninite (Ur) and pyrite (Py) in juxtaposition with each other and get enclosed by epidote in mylonitised quartzo- feldspathic schist. **(b)** Same image in reflected light. **(c)** Uraninite (Ur), shows spatial association with magnetite (Mgnt), and pyrite (Py) and associated with late chlorite (chl) and biotite (bt) veins, **(d)** Same image in PPL. **(e)** Similar to uraninite, chalcopyrite (Cpy) occurs along mylonitic foliation along with chlorite veins**. (f)** The pyrite mineral showing book-shearing texture developed on pyrite (py) grain.

7.1.4.5 Comparison of feldspathic schist with other areas of SSZ

Saha (1994) observed that in feldspathic schist is well cleaved with fine biotite flakes along foliation and feldspar phenocrysts and quartz grains are highly strained. The feldspathic schist in study area also shows the similar feature as described by Saha, (1994). To further confirm it, the feldspathic schist from the study area is compared with the feldspathic schist in the different part of Singhbhum shear zone (figure 7.8). It appears that both texturally and mineralogically they are very similar.

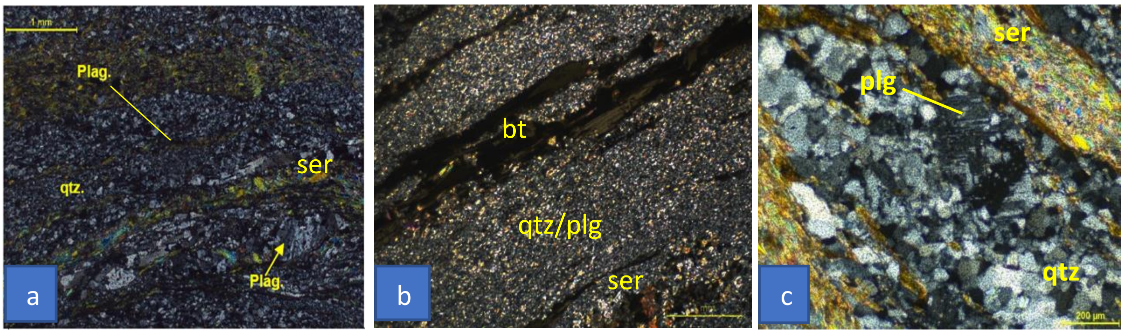

Figure 7.8(a) Feldspathic schist present in Tilogoria, Mayurbhanj, Odisha. **(b)** Feldspathic schist present in Tamajhuri -Pathergora area, East-Singhbhum, Jharkhand. **(c)** Feldspathic schist exposed in Mouldih, Jharkhand (Parvej Alam, unpub M.tech thesis, (2018)).

The feldspathic schist of the study area also host low grade uranium and copper mineralization. The genesis of feldspathic schist is controversial, however, most of the opinions are in favour of its either syntectonic or post-tectonic origin with respect to the shearing event in SSZ. A few researchers further believe that its origin is related to granitization of shear zone metasediments (Ghosh, 1972).

7.1.4.6 Dumurdiha

In the Dumurdiha area the main lithounits exposed are ferruginous quartzite, fuchsite quartzite, kyanite quartzite (Panajia) (figure 7.9 a), biotite-chlorite-sericite-quartz-schist, gabbro and metabasalts. Most of the rocks consist of more than 80% quartz. Other mineral identified are apatite, sericite, chlorite, tourmaline, zircon (figure 7.9 c), and kyanite, The sericite and chlorite defines the schistosity plane (figure 7.9 b & d),. The quartz grains also show the oblique foliations.

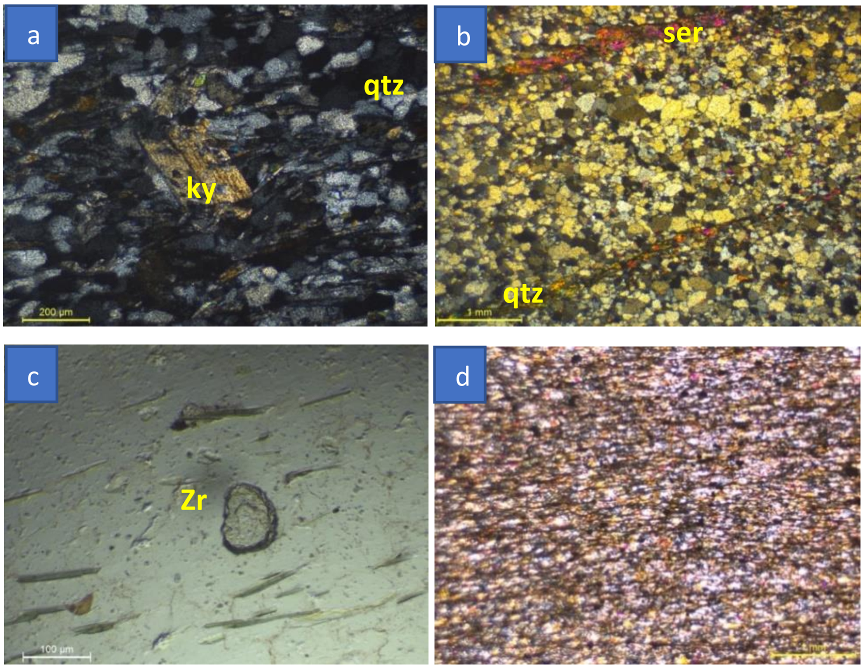

Figure 7.9 Photomicrographs show **(a)** Kyanite quartzite, where kyanite (ky) not aligned along foliation plane indicates post-tectonic origin. **(b)** sericite quartzite, quartz (qtz) aligned along foliation plane, sericite (ser) define the foliation plane.**(c)** zircon (Zr) grain in quartz matrix. **(d)** sericite-chl-quartz-schist, very thin lamella of sericite

The ore mineral identified are uraninite (figure 7.9 (e) & (f)), magnetite, chalcopyrite, and pyrite. On the surface there are two types of uranium occurrence one is yellow color, irregular outlined (anhedral), and highly altered and second is moderately altered, subhedral affected by later hydrothermal veins. The XRD data suggest subhedral variety is uraninite, whereas yellow color anhedral variety is torbernite (figure 7.9 (g)). In subsurface samples uranium mineralization is also identified in quartz-chlorite veins hosted by gabbroic body. The Ore mineral identified are chalcopyrite, pyrite, magnetite, and hematite occurring along quartz-chlorite veins hosted in gabbroic bodies (figure 7.9 (i), (j), & (k)). The uraninite and monazite occur as main radioactive phases (figure 7.9 (k)). The presence of tourmaline (figure 7.9 h) further indicated fluid related mineralization. The ferrous ion may act as reducing agent for uranium rich fluids.

$$\mathbf{(UO_2)^{+2} + Reductant \rightarrow U^{+4} + Oxidized\ reductant}$$

The presence of apatite further interferes while attaining equilibrium in above reaction, where its presence helps in squeezing out U(IV) by ion exchange, resulting in forward shifting of the reaction with increased U(IV) supply (Altschuler Z.S, 1958). The above reaction further explain the close association of apatite bearing minearls with uranium phases (figure 7.9 e & f).

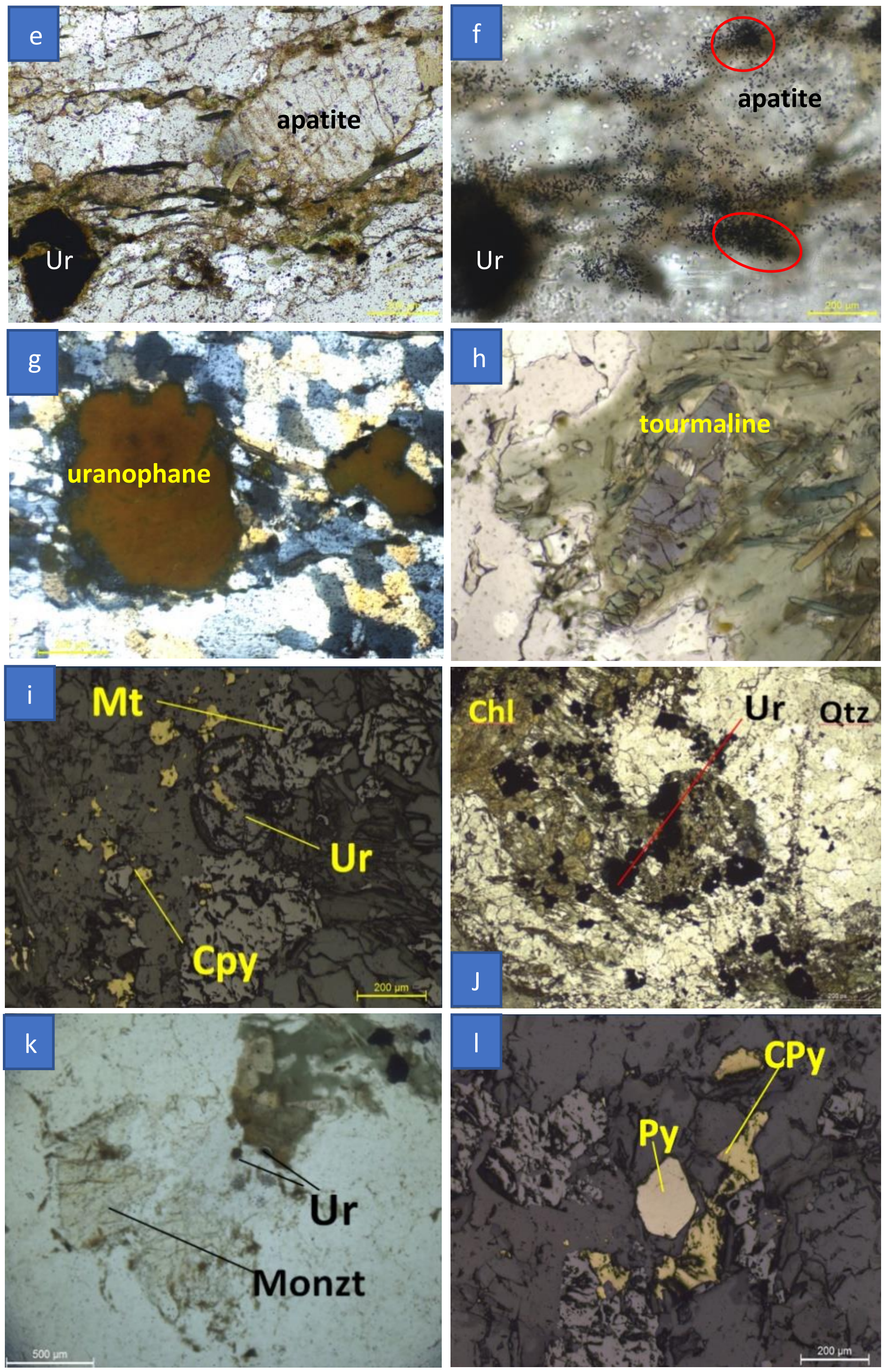

Figure 7.9 (e) surface sample of radioactive quartzite, the uraninite mineral affected by later hydrothermal veins, **(f)** corresponding alpha track of uraninte, indicates apatite control on mineralization, **(g)** surface sample of radioactive quartzite, the secondary uranium mineral uranophane showing irregular boundaries, **(h)** subsurface sample of radioactive chlorite quartz vein, tourmaline crystal enclose by chlorite (chl), **(i) & (j)** subsurface sample, uraninite (Ur), chalcopyrite and magnetite in close association further get surrounded by chlorite minerals **(k)** monazite (Monzt) and dusty uraninite (Ur) in radioactive quartz and chlorite vein **(l)** chalcopyrite (Cpy) and pyrite (Py) in same sample.

7.1.4.7 Petromineralogy of basic rocks in the area

Meta-basaltic rocks of greenschist to amphibolite grade are present in the area. In south eastern part of Panajia village, a very few outcrops of schistose amphibolite are exposed on the surface. These amphibolite bodies are also present in the subsurface borehole cores samples collected from Tilogria, Kusumbari and Dumurdiha area. The major phases that have been identified in the thin section are chlorite, magnetite, hornblende, and quartz in order of their decreasing abundance (Figure 7.10a). The magnetite bands appear to be relatively younger and occur along the foliation plane. The chlorite present in the rock appears to be altered product of amphibole (hornblendes).

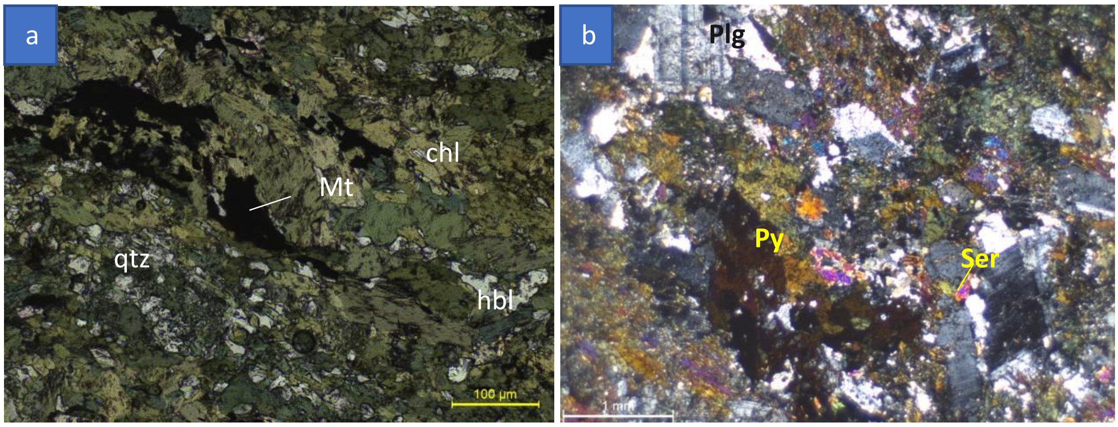

Figure 7.10 photomicrographs of **(a)** amphibolite schist consists of chlorite (chl), magnetite (Mt), quartz (qtz), and hornblende (hbl), **(b)** non-foliated gabbroic rock shows the assemblage of plagioclase (plg) and pyroxenes (Py), and sericite (ser).

In the north western part of Dumurdiha, discordant undeformed younger gabbroic rocks are intruded into biotite-chlorite-sericite-quartz schist and ferruginous quartzite (based on subsurface data). The same gabbroic body is also exposed near Panajia area. The gabbroic bodies are non-foliated, medium to coarse grained, comprised mainly of pyroxenes and plagioclase (Figure 7.10b). The crystals of pyroxenes and plagioclase are randomly oriented. At places the plagioclase get altered to sericite as well.

7.2 X-Ray differaction study of Romapahari Granite, feldspathic schist, and Singhbhum Metasediments.

The extensive use of X-rays for the analysis of atomic structural arrangements is based on the fact that waves undergo diffraction when interacting with systems which are spaced at distances of the same order of magnitude as the wavelength of the particular radiation considered. X-ray diffraction in crystalline solids takes place because the atomic spacing is in the 10^{-10} m range, as are the wavelengths of X-rays.

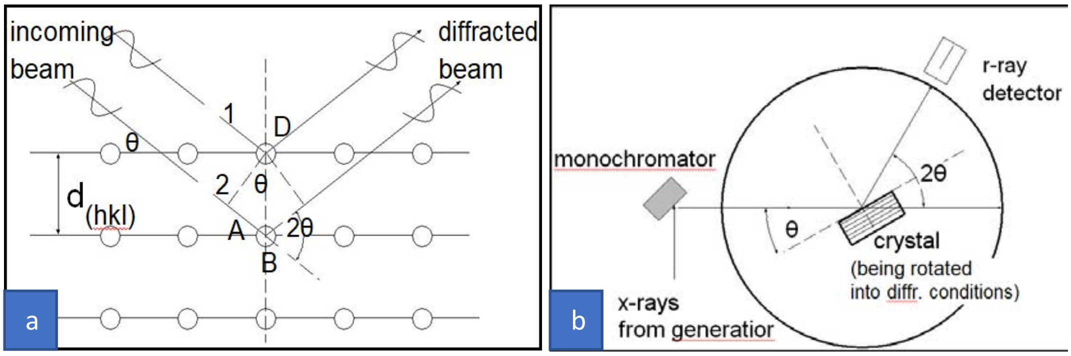

Figure7.11 **(a)** The schematic diagram shows the Bragg's law, assuming the planes of atoms behave as reflecting planes, and **(b)** X-ray Diffractometer setup.

The geometrical conditions which must be satisfied for diffraction to occur in a crystal were first established by Bragg. He considered a monochromatic beam of X-rays with coherent radiation to be incident on a crystal, as shown in figure 7.11a. Moreover, he established that the atoms which constitute the actual scattering centres can be represented by sets of parallel planes which act as mirrors and “reflect” the X-rays. In cubic systems the spacing of these planes, $d_{(hkl)}$ is related to the lattice constant.

For constructive interference of the scattered X-rays (the appearance of a diffraction peak) it is required that the beams, scattered on successive planes, be “in phase” after they leave the surface of the crystal. In terms of the beams labelled 1 and 2 in figure 7.11a this requires that the distance (AB) + (BC) be equal to an integral number of wavelengths (λ) of the incident radiation.

$AB+BC = n\lambda \qquad (n=1,2,3\ldots\ldots)$

$AB = BC; \quad \sin\theta = AB/d_{(hkl)}$

$n\lambda = 2d_{(hkl)}\sin\theta$ ……………………(equation 7.11a)

This relation (equation 7.11a) is referred to as Bragg's Law and describes the angular position of the diffracted beam in terms of λ and $d_{(hkl)}$.

If figure 7.11a consider as representative for a "diffractometer" set-up figure 7.11b, the collimated beam of X-rays impinging on a (100) set of planes and at 2θ to the incident beam a detector which registers the intensity of radiation. For a glancing incident beam (small θ) the detector will register only background radiation. As θ increases to a value for which $2d \sin\theta = \lambda$, the detector will register high intensity radiation ans we have diffraction peak. From the above it is evident that the diffraction angle (θ) increases as the interplanar spacing, $d_{(hkl)}$, decreases.

Bragg condition for particular $d_{(hkl)}$ values can be satisfied by adjusting either one of two experimental variables: (a) λ, the wavelength of the X-ray beam used, or (b) θ, the orientation of the crystal planes relative to the incident X-rays.

In the Debye-Scherrer method (figure7.11c) the sample is ground to a powder and placed (in an ampoule) into the center of a Debye-Scherrer camera. Exposed to monochromatic X-rays, in this way a large number of diffracted cone-shaped beams are generated such that the semi angles of the cones measure 2θ, or twice the Bragg angle for the particular diffracting crystallographic planes. The reason diffracted beams are cone-shaped is that the planes in question (within the multitude of randomly oriented grains) give rise to diffraction for any orientation around the incident beam as long as the incident beam forms the appropriate Bragg angle with these planes – thus there is a rotational symmetry of the diffracted beams about the direction of the incident beam. Those planes with the largest inter-planar spacing have the smallest Bragg angle, θ.

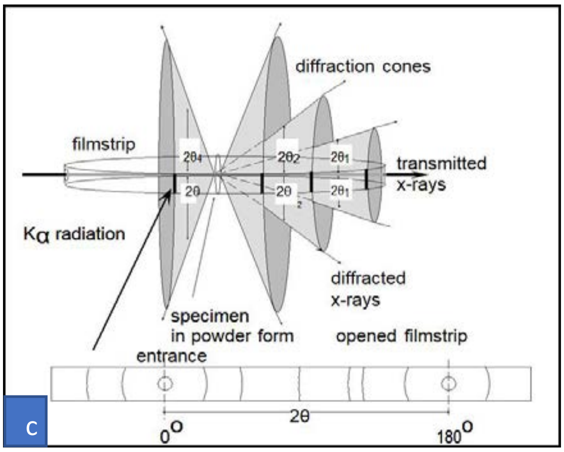

Figure7.11 **(c)** the schematic diagram shows the Debye-Scherrer powder diffraction setup and analysis.

In a Debye–Scherrer arrangement, after exposing a powder of a crystalline material to monochromatic X-rays, the developed film strip will exhibit diffraction patterns such as indicated in figure7.11c. Each diffraction peak on the film strip corresponds to constructive interference at planes of a particular interplanar spacing $d_{(hkl)}$. The problem now consists of "indexing" the individual lines – i.e., determining the Miller indices (hkl) for the diffraction lines holds as follows:

$$\lambda = 2d_{(hkl)} \sin\theta \ \ ; \ d_{(hkl)} = \frac{a}{(h^2 + k^2 + l^2)^{\frac{1}{2}}}$$

$$\lambda^2 = 4d^2_{(hkl)} \sin^2\theta \ \ ; \ d^2_{(hkl)} = \frac{a}{(h^2 + k^2 + l^2)^{\frac{1}{2}}}$$

$$\frac{\sin^2\theta}{(h^2 + k^2 + l^2)} = \frac{\lambda^2}{4a^2} = \text{const.}$$

$$\frac{(\sin^2\theta)_1}{(h^2 + k^2 + l^2)_1} = \frac{(\sin^2\theta)_2}{(h^2 + k^2 + l^2)_2} = \frac{(\sin^2\theta)_3}{(h^2 + k^2 + l^2)_3} = \text{const.}$$

Since the sum $(h^2 + k^2 + l^2)$ is always integral and $\lambda^2/4a^2$ is a constant, the problem of indexing the pattern of a cubic system is one of finding a set of integers $(h^2 + k^2 + l^2)$ which will yield a constant quotient when divided one by one into the observed sin2θ values. (Integers such as 7, 15, 23, etc. are impossible because they cannot be formed by the sum of three squared integers.)

Lines for the corresponding θ values are obtained from the geometric relationship of the unrolled film strip. Between the exit hole of the X-ray beam ($2\theta = 0$) and the entrance hole ($2\theta = 180$) the angular relationship is linear (figure7.11c). The increasing θ values for successive lines are indexed θ_1, θ_2, θ_3 etc., and $\sin^2\theta$ is determined for each. If the system is simple cubic we know that all planes present will lead to diffraction and the successive lines (increasing θ) result from diffraction on planes with decreasing interplanar spacing: (100), (110), (111), (200), (210), (211), (220), etc. From above equation above we recognize:

$$\frac{\sin^2\theta_1}{1} = \frac{\sin^2\theta_2}{2} = \frac{\sin^2\theta_3}{3} = \frac{\sin^2\theta_4}{4} = \frac{\sin^2\theta_5}{5} = \text{const.}$$

If the system is BCC, however, we know from the selection rules that only planes for which (h + k + l) = even will reflect. Thus:

$$\frac{\sin^2\theta_1}{2} = \frac{\sin^2\theta_2}{4} = \frac{\sin^2\theta_3}{6} = \frac{\sin^2\theta_4}{8}\ etc. = \text{const.}$$

SC can be differentiated from BCC through the fact that no sum of three squared integers can yield 7, but 14 can be obtained from planes (321). For FCC systems, the selection rules indicate reflections on planes with unmixed h, k, l indices.

$$\frac{\sin^2\theta_1}{3} = \frac{\sin^2\theta_2}{4} = \frac{\sin^2\theta_3}{8} = const.$$

$$\frac{\sin^2\theta}{(h^2 + k^2 + l^2)} = \ const$$

Lattice constant of the unit cell is obtained, knowing the wavelength of the incident radiation:

$$\frac{\sin^2\theta}{(h^2 + k^2 + l^2)} = \ const. = \frac{\lambda^2}{4a^2}$$

To study the radioactive phase and associated minerals, six numbers of samples have been generated from different localities of the study area. Out of six, four are subsurface samples and two are samples (from Kesharpur and Dumurdiha).

Table 7.2 Mineralogy of different rock type based on XRD analysis

Rock Type	**Locality**	**Atomic Minerals**	**Ore Minerals**	**Rock forming mineral**
Granite	Kesharpur		Ilmenite, Magnetite, Titanite	Albite, Biotite, Microcline, Chlorite
hbl-bt-chl-quartz-schist	Kusumbari	Zircon(traces)	Pyrite, Pyrrhotite, Molybdenite, Anatase(traces), Chalcopyrite, Violarite(Traces), Marcasite(Traces	Biotite, Quartz
Sheared Granite	Kusumbari	Zircon(traces), Rutile(traces)	Pyrite, chalcopyrite,pyrrhotite, molybdenite, Pyrrhotit	Albite, Biotite, Microcline, Chlorite, Epidote(traces)
Sheared Granite	Kusumbari	Uraninite(traces), Zircon(traces), Rutile(traces),Allanite(traces	Pyrite, Chalcopyrite, Molybdenite, Pyrrhotite	Biotite, Microcline, Quartz, Hornblende(traces)
Feldspathic Schist	Tilogoria	Uraninite	Pyrite, chalcopyrite, Ilmenite, Pentlandite(traces), Magnetite	Albite, Biotite, Chlorite
Ferruginous Quartzite	Dumurdiha	Uraninite, Zircon(traces), Uranophane (traces),Meta torbernit	Hematite, magnetite	Chlorite, Quartz,fluorapatite(traces)

In Tilogoria area the uraninite is intimately associated with pyrite, chalcopyrite and pentlandite. It shows an anomalous unit cell parameter value which indicates substitutional solid solution between uraninite and thorianite. The extent of ThO_2 substitution in the lattice is expected to be about 2 to 3 percent. Based on an analysis of atomic scattering factor the extent of stoichiometric deviation of the oxygen content in the formula unit is at very narrow range from $UO_{2.05}$ to $UO_{2.06}$ (Table 7.3). Pentlandite in close association with uraninite indicates a significantly lower oxygen fugacity condition (fO_2) which was modified most likely due to a relatively elevated sulphur fugacity (fS_2) condition during the crystallization of uraninite.

In the Dumurdiha area, the stoichiometric deviation of oxygen content in the formula unit of uraninite by Gronovold method is found to be $UO_{2.03}$. The extent of oxygen non stoichiometry calculated from the approximate atomic scattering factor ratio falls in the range between $UO_{2.08}$ and $UO_{2.09}$.

Table 7.3 unit cell parameter of uraninite from Tilogoria and Dumurdiha area

Rock Type	Locality	a(Ã…)	b(Ã…)	c(Ã…)	A^3	oxygen content
Feldspathic Schist	Tilogoria	5.4784 Â ± 0.00126	5.4784 Â ± 0.00126	5.4784 Â ± 0.00126	164.43	$UO_{2.05}$ to $UO_{2.06.}$
Ferruginous Quartzite	Dumurdiha	5.4669 Â ± 0.0008	5.4669 Â ± 0.0008	5.4669 Â ± 0.0008	163.39	$UO_{2.08}$ to $UO_{2.09.}$

7.2.1 Environment of Uranium mineralization based on unit cell parameter

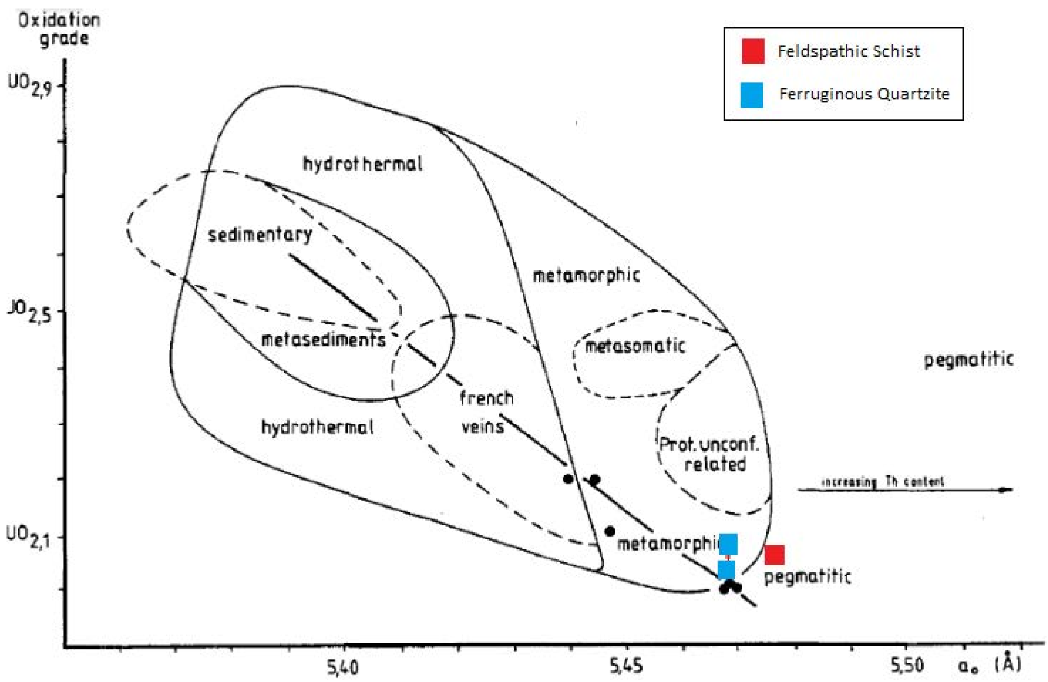

Figure 7.11d Correlation diagram of oxidation degree-lattice constant for uranium oxide phases and their tentative attribution to genetic fields. Xu et al.(1981),Cathelineau et al. (1981), Fritsche et al. (1988)

Physico-chemical characteristics of U-oxides and related crystallographic variations and genetic implications have been researched by a number of geoscientists. Results from some of these authors have been summarized by F.J Dhalkamp, (1993).

1. The unit-cell dimension appears to be a function of formational temperature i.e. the higher the temperature the larger the a_o and the lower the oxidation level.
2. There is a positive correlation exsits between a_o and Pb content which can be only valid if elementary Pb (ionic radius = 1.75 A) is involved. Pb^{4+} has a radius of 0.84 A hence it is smaller than U^{4+} (1.01 A) and almost equals U^{6+} (0.8 A) and can therefore not cause expansion of the U-oxide lattice. Due to this a lattice reduction is postulated if Pb^{4+} replaces U^{4+} with increasing age.
3. Unit-cell dimension vs age: Larger unit-cells related to older U-oxides would imply that the auto-oxidation of U-oxides plays only an insignificant role. On the other hand, a positive correlation of a_o and temperature exists. This would theoretically permit the deduction of a positive correlation of age and temperature that does not appear feasible. For these reasons the correlation of a_o and age can be only fictitious, or of secondary nature respectively.

Based on these above observation the global data from different environment has been complied in form of figure 7.11d. It shows correlation between oxidation degree and lattice constant and their attribution to genetic field of uranium. The results from the present study when plotted on this diagram shows the mineralization has took place in environment that varies from metamorphic (Dumurdiha area) to Pegamatitic regime (Tilogoria area). The uraninite grains in the feldspathic schist (schistose Soda Granite) shows there pegmatitic origin whereas the uraninite grains occur in ferruginous quartzite shows the metamorphic environment, however, the data from both the area lying very close to boundary therefore there is certain ambiguity regarding their origin.

7.3 Electron-Probe Microanalyses (EPMA)

One grab and two subsurface boreholes samples have been generated for the EPMA analysis. The first subsurface borehole sample (B-496) belongs to the radioactive feldspathic schist in Tilogoria area, the second subsurface borehole sample (B-495) belongs to the radioactive quartz-chlorite vein intruded into gabbro, and the third grab sample (B-497) belongs to radioactive ferrugenized sericitic quartzite exposed near Dumurdiha village. The EPMA analysis was performed at 15 / 20 kV accelerating voltage and 20/40 nA beam current. The study involves 10 mineral phases and 99 points with 2410 determinations.

Radioactive phases recognised and analysed are uraninite and zircon in ferrugenized sericitic quartzite, uraninite in feldspathic schist, and uraninite, xenotime and monazite in chlorite quartz vein. Besides, chalcopyrite, pyrite, magnetite, apatite and associated gangue minerals like albite, epidote and chlorite were also analysed in these samples.

7.3.1 EPMA result of ferrugenized sericitic quartzite sample (B-495)

7.3.1.1 Chemical composition of Uraninite

Subhedral grains of uraninite (G=3, n=10, 250, 300 & 350 μm) found to occur in a groundmass of quartz and chlorite. The uraninite grain commonly altered, show rims of magnetite and moderately altered and affected by later hydrothermal veins filled with magnetite (Fig 7.12 (a) & (b)). Magnetite veins also show fragments of uranium bearing minerals. BSE image of such uraninite grains with reduced brightness reveals irregular intragranular fractures. Analyses of 10 points in 3 grains of the studied uraninite grains show very high and variable UO_2 (74.52.85.46 wt%; Avg. 80.68 wt%), highly variable PbO (10.79-20.23 wt%), with very low and variable ThO_2 (<0.01.0.66 wt%), RE_2O_3 (0.6-2.62 wt%), Y_2O_3(<0.01.1.54wt%), and CaO(<0.01.1.47 wt%).

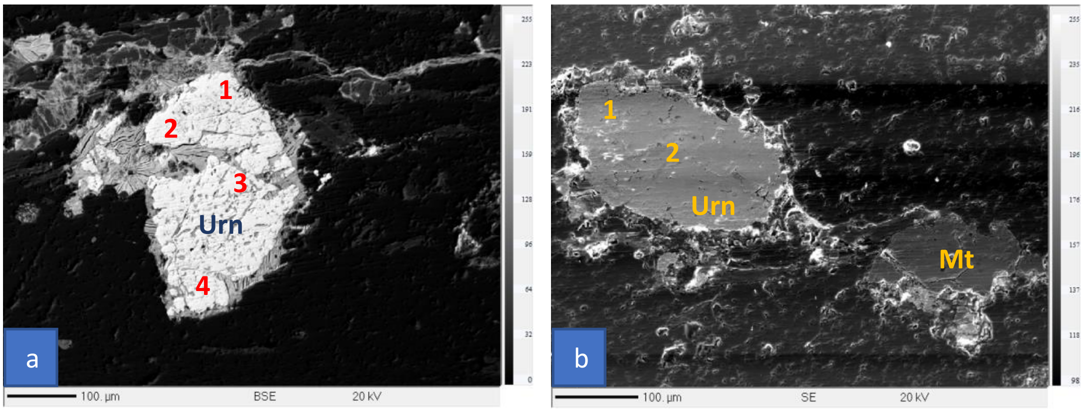

Figure 7.12 (a) BSE image of subhedral uraninite grain (250µm) rimmed by magnetite. Magnetite within fracture of uraninite and prominent fracture observed above the uraninite grain. **(b)** Secondary electron (SE) image of uraninite grain (300µm) in association with magnetite.

7.3.1.2 Chemical composition of Zircon

Single zircon grain was analyzed at three points from core to periphery. Analyses (n=3) of the studied grain shows 32.12. 32.78wt% (32.47 %) SiO_2, 57.75-59.00 wt% (Avg. 58.51 wt%) ZrO_2, 1.20-1.45 wt %, (1.35 %) HfO_2, <0.01.0.02 wt % UO_2, <0.01 wt% ThO_2. Zr/Hf ranges from 34.81.36.37. RE_2O_3 (0.23.0.41wt %) and Y_2O_3 (<0.01) are negligible.

7.3.1.3 Chemical composition of Chlorite

Representative compositions of chlorite grains (n=5) from the study area has been selected for EPMA. Four points analyses in three grains of uranifeorus ferrugenous quartzite show that composition is uniform with MgO: 12.67.13.79 wt.% (Avg. 13.29%), FeO: 25.60-26.84 wt.% (Avg.26.31 wt%), Al_2O_3: 20.84.21.60 wt.% (Avg. 21.34%), SiO_2: 24.05-24.98 wt.% (Avg. 24.51 %) with low analytical total. The studied chlorite show high FeO(t), and comparatively low MgO, chlorite from the study area is Fe rich and has compositions more towards chamosite [$(Fe_5$ Al)(Si_3 Al)$O_{10}(OH)_8$] end member.

7.3.2 EPMA result of feldspathic schist sample (B-496)

7.3.2.1 Chemical composition of Uraninite

Uraninite with irregular boundaries found to occur in muscovite rich bearing groundmass (Fig 7.13 (a)) and also occur in association with magnetite and chalcopyrite in quartz and feldspar-rich ground mass (Fig 7.13 (b)). Analyses of 15 points in 7 grains of uraninite in feldspathic schist sample shows very high and variable UO2 (76.70 - 82.15 wt%; Avg. 80.11 wt%), PbO (12.33.15.68; Avg. 14.03 wt%), very low and variable ThO2 (<0.01.0.26 wt%), moderate to high RE2O3 (2.66 - 5.41 wt%), with very low and variable Y2O3(<0.01.1.54wt%), and CaO(0.15- 0.58 wt%).

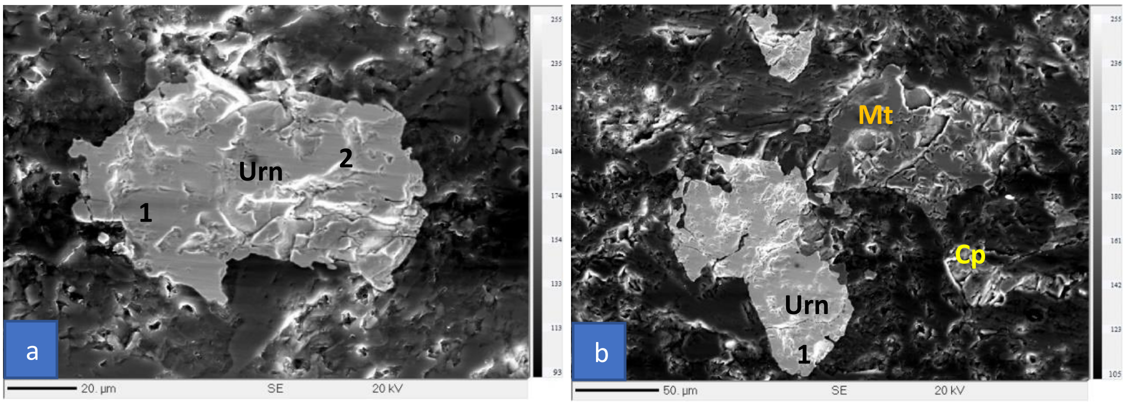

Figure 7.13 (a) SE image of a uraninite grain with irregular grain boundaries (60 µm) in muscovite rich groundmass. **(b)** SE image of uraninite grains with magnetite and chalcopyrite in muscovite rich groundmass.

7.3.2.2 Chemical composition of Chalcopyrite

Eight -point analyses in three subhedral to anhedral chalcopyrite grains (50- 100 um) were done. Such grains found to occur in association with uraninite and magnetite in the studied sample (Fig 7.13 (b)). Mineral chemistry of these grains are given in Table-11.5. The compositional homogeneity, that is in turn, reflected in the data indicates restricted composition of Cu: 30.24. 32.13 wt.% (Avg. 31.00 wt%), Fe: 28.18-29.57(Avg. 28.98 %); S: 31.94.35.58 wt.% (Avg. 33.71 wt%), Mo: 0.43.0.65 wt.% (Avg. 0.59t%), Co: <0.01.0.05 wt%, and Ni : <0.01.0.19 wt% %).

7.3.2.3 Chemical composition of Pyrite

Six point analyses were carried out in two grains of pyrite in the studied sample. EPMA analysis of these grains indicate compositional homogeneity. The analysis show restricted composition of Fe: 44.48- 46.10 wt.% (Avg. 45.34%) and S: 51.93.53.39 wt.% (Avg.52.73%). Analyses also indicated presence of Co: 0.3.0.71 wt.%; Ni: 0.05-0.11 wt.%, and Mo: 0.72.0.89 wt.%.

7.3.2.4 Chemical composition of Apatite

Six point analyses of two fine grains of (40 & 50 µm) apatite were done in the studied sample. Analyses of two such grains indicated 54.48-57.04 wt.% (Avg. 56.32 %) CaO and 41.60-43.66 wt.% (Avg. 42.46%) P_2O_5 suggested restricted compositional variations.

7.3.2.5 Chemical composition of Epidote

Three point analyses of the studied epidote grains show restricted composition of SiO2 [37.76-38.32 wt.% (Avg. 37.95 %)], CaO [21.75-23.49 (Avg. 22.66 %)], FeO [11.14 -11.45 wt.% (Avg. 11.32%)], Al_2O_3[22.61.23.65 wt.% (Avg. 23.16%)], TiO_2 [0.03.0.13 wt%], MgO [<0.01.0.26 wt.%] and MnO [0.28-0.88 wt%].

7.3.2.6 Chemical composition of Albite

Seven point analysis in seven albite grains show very high Na2O [9.04.11.10 wt%], Al2O3 [19.27.22.04 wt%] and SiO2 [64.60-69.33wt%] with low to moderate [0.30-2.64 wt%] CaO. Such grains contain 0.09-0.80 wt% FeO.

7.3.3 EPMA result of radioactive chlorite-quartz vein in Gabbro (B-497)

7.3.3.1 Chemical composition of Uraninite

Uraninite with irregular boundaries found to occur in clusters in association with magnetite in the ground mass of quartz and feldspar. Analyses of 13 points in 6 grains of uraninite in the studied sample shows highly and variable UO_2: 74.37.87.18 wt.% PbO: 9.81.19.16% wt.%, ThO_2: <0.01. 0.70 wt%, RE_2O_3: 1.52.3.10 wt.% ; Y_2O_3: <0.01.1.77 wt%, SiO_2: <0.01.1.20 wt%; CaO: <0.01.0.47 wt% and FeO: 0.01.0.50 wt%. The data shows restricted and very high UO2, variable RE2O3, negligible ThO2, negligible to very low SiO2 with highly variable and high PbO.

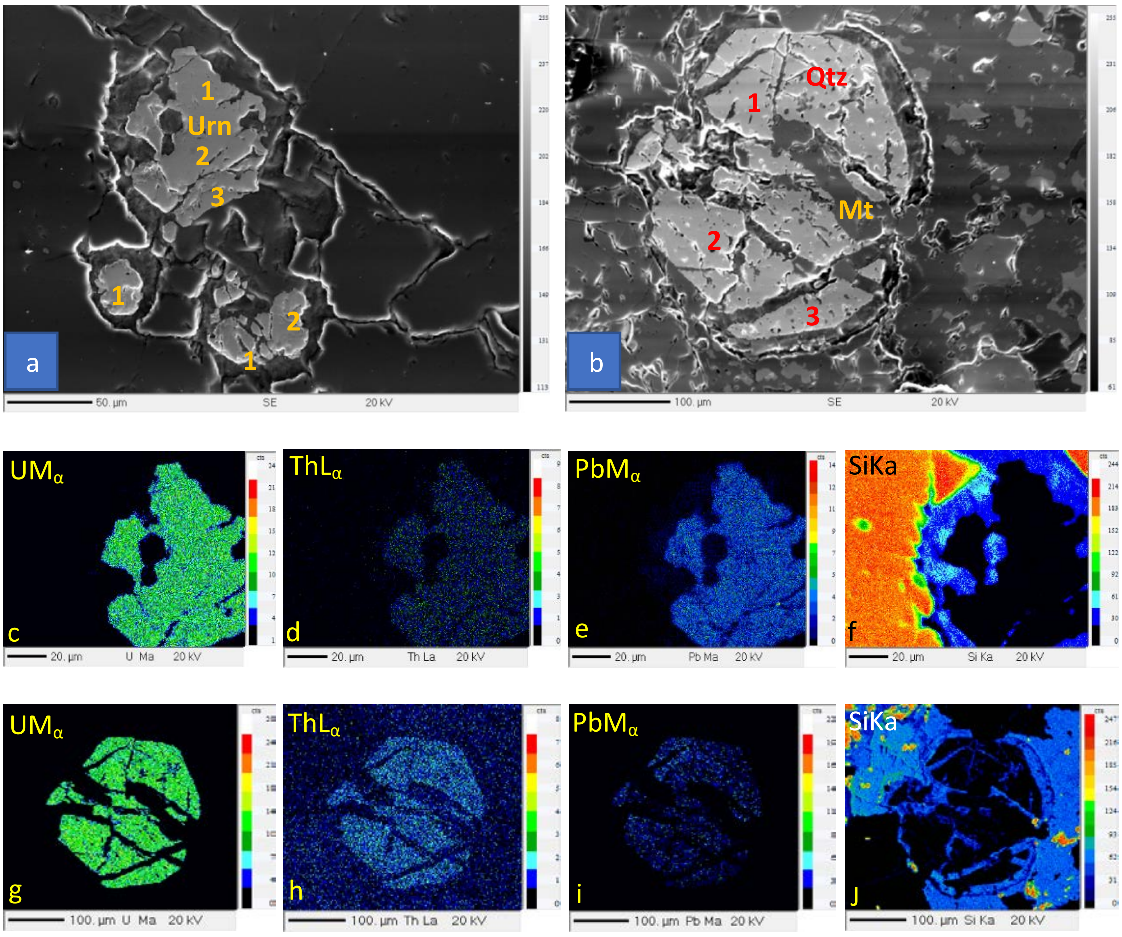

Figure 7.14 (a) SE image of a low Th bearing uraninite (Urn) grain (110 µm) in quartz rich groundmass. **(b)** SE image of a fractured uraninite (Urn) grain (300 µm) in quartz rich groundmass. Magnetite (Mt) and quartz(Qtz) occurring as fracture fillings within uraninite. **(c-f)** X-ray elemental map of uraninite with respect to U, Th, Pb and Si. Scanning of the grain shows enrichment of U, Pb and depleteion of Si and Th**. (g-J)** X-ray elemental mapping of uraninite grain with respect to U, Th, Pb and Si.

7.3.3.2 Chemical composition of Xenotime and Monazite

Aggregate of xenotime grains (Fig 7.15 (a)) (100-1100 micron) occur within quartz rich ground mass of the studied sample. Nine point analyses show very high content of Y_2O_3: 41.85-46.21 wt.%, P_2O_5: 32.31.33.78 wt% and RE_2O_3(t): 17.11.20.64 wt%. HREE (17.11.19.10 wt%) predominates over LREE (0.51.2.01 wt%). Such grains found to contain 0.24 -1.32 wt% UO_2, <0.01.0.64 wt% ThO_2 and 0.32.0.72 wt.% PbO.

The monazite grains are found to occur in association with apatite (Fig 7.15 (b)) in the studied sample. The grain size of monazite ranges from 110-180 μm. EPMA analyses shows restricted and high RE2O3 (67.96-69.46 wt%; avg. 69.97 wt%) and P2O5 (30.55-31.70 wt%; avg. 31.28 wt%). The data shows that LREE content (64.58 - 66.38wt%) predominates over HREE (3.07.3.38 (Avg. 3.18 wt%) with negligible ThO2 (<0.01.0.19%). Amongst the LREE, Ce_2O_3 content in the studied monazite grains is very high and ranges from 30.21 to 32.02 wt%) with an average of 31.42 wt%. Amongst the other LREE, the studied grains are found to contain 15.49-16.90 wt% La_2O_3, 3.87.4.12 wt% Pr_2O_3 and 11.35-12.38 wt% Nd_2O_3 and 2.05-2.47 wt% Sm_2O_3. Further monazite grains show 0.41.1.30 wt% UO_2, <0.01.0.23 wt% Y_2O_3, <0.01.0.23 wt% CaO and <0.01.0.0.07 wt% PbO.

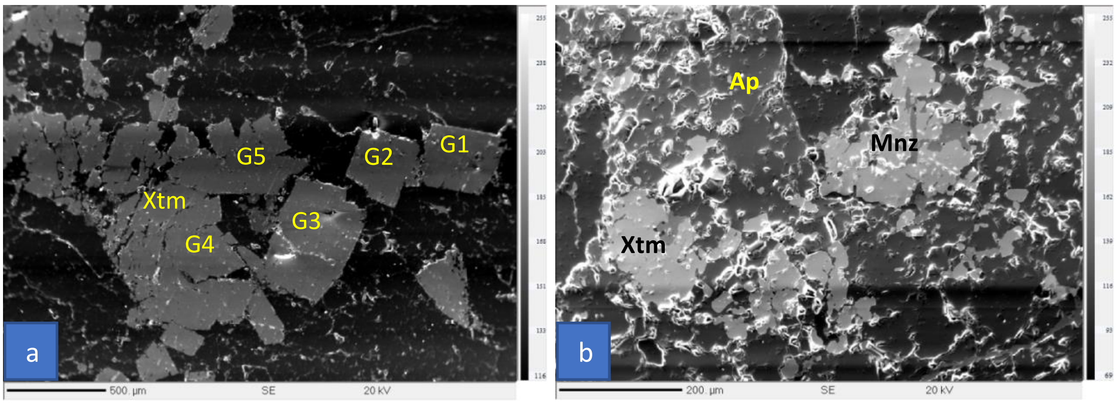

Figure 7.15 (a) SE image showing aggregate of xenotime (Xtm) grains within quartz rich groundmass. **(b)** SE image showing monazite (Mnz) grains within quartz rich groundmass in association with apatite (Ap).

7.3.3.2 Chemical composition of Apatite

The apatite grain occurs as inclusion within monazite. Six point analyses of such apatite grains of apatite were carried out in the studied sample. The compositional homogeneity, that is in turn, reflected in the data indicating restricted composition of CaO: 57.83. 59.51 wt.% (Avg. 58.42 wt%), P_2O_5: 41.88-42.98 wt% (Avg. 42.34 %). Apatite grains show good analytical total.

7.3.4 Chemical ages of Uranium mineralization

The most common isotope of U is ^{238}U, which accounts for 99.27% of the U present today and this decays with a half-life of 4468 Ma (decay constant λ_{U238} 1.55125 $\times 10^{-10}$, Jaffey et al., 1971) to produce ^{206}Pb. The other two isotopes of U have shorter half-lives, ^{234}U being an intermediate stage in the decay of ^{238}U. Some 0.7204% of present day U occurs as ^{235}U that decays to produce ^{207}Pb with a half-life of 703.8 Ma (decay constant λ_{U235} 9.8485 $\times 10^{-10}$, Jaffey et al., 1971). Th occurs only as the single isotope ^{232}Th and decays to produce ^{208}Pb with a half-life of 14,008 Ma (decay constant λ_{Th} 4.9475 $\times 10^{-11}$, LeRoux & Glendenin, 1963). Thus the amount of Pb produced is the sum of the Pb from ^{238}U, ^{235}U, and ^{232}Th (equation 7.3.4). The equation 7.3.5 can be used to calculate the t in case the Th content is very less compared to uranium content.

$$\mathbf{Pb= {}^{238}U\,(e^{\lambda U238t} - 1) + {}^{235}U\,(e^{\lambda U235t} - 1) + Th\,(e^{\lambda U238t} - 1) \ldots\ldots\ldots (7.3.4)}$$

$$\mathbf{t = ln\,(Pb / {}^{238}U) + 1)/ \lambda_{U238} \ldots\ldots\ldots (7.3.5)}$$

Unfortunately it is not possible to change the equation 7.3.4 algebraically into the form '**t**' = some function. Therefore Bowles J.F, (2015) has suggested to estimate the age '**t**' and calculate the amount of Pb produced from the measured amounts of U and Th. This will not match the actual amount of Pb as analyzed so '**t**' can be changed in diminishing increments (by iteration) until the amount of Pb calculated corresponds to the amount measured. The ages calculated by this method shown in table 7.4, 7.5, and 7.6. The major limitation of this method is that Pb loss or initial non-radiogenic Pb may cause erratic chemical ages.

Table 7.4: Chemical Age of uraninite from Ferrugenized-Sericitic Quartzite, Mayurbhanj, Odisha.

Rock Type	Area	Sample Type	Sample ID	Grain	Point	UO2 (wt%)	ThO2 (wt%)	PbO (wt%)	Age (Ma)
Ferrugenized Sericitic Quartzite	Dumurdiha	Grab	B-495	G1(250µm)	P1	82.22	0.66	10.79	**992.074**
					P2	84.38	0.37	12.08	
					P3	85.46	0.08	11.07	
					P4	84.35	0.22	11.62	
				G2(300µm)	P1	80.53	0.13	16.78	**1454.537**
					P2	80.19	0.14	16.69	
					P3	80.16	0.18	17.03	
				G3(450µm)	P1	78.57	<0.01	20.23	**1618.717**
					P2	76.46	0.03	16.09	
					P3	74.52	0.06	18.35	

Table 7.5: Chemical Age of uraninite from Feldspathic schist, Mayurbhanj, Odisha.

Rock Type	Area	Sample Type	Sample ID	Grain	Point	UO2 (wt%)	ThO2 (wt%)	PbO (wt%)	Age (Ma)
Feldspathic Schist	Tilogoria	Core	B-496	G1(60µm)	P1	81.22	<0.01	12.9	**1196.119**
					P2	81.32	<0.01	14.24	
				G2(200µm)	P1	79.68	0.26	15.21	**1255.664**
					P2	81.23	0.03	13.21	
				G3(50µm)	P1	80.16	<0.01	12.33	**1112.765**
				G4(80µm)	P1	80.93	<0.01	13.59	**1202.086**
				G5(120µm)	P1	76.7	<0.01	15.15	**1324.548**
					P2	80.45	<0.01	14.36	
				G6(800µm)	P1	79.84	<0.01	14.29	**1242.544**
					P2	78.93	0.06	15.68	
					P3	79.26	<0.01	12.98	
					P4	78.84	<0.01	12.59	
					P5	82.15	<0.01	14.06	
				G7(300µm)	P1	80.19	<0.01	14.7	**1310.044**
					P2	80.71	<0.01	15.13	

Table 7.6: Chemical Age of uraninite from Radioactive quartz-chlorite vein intruded into gabbro.

Rock Type	Area	Sample Type	Sample ID	Grain	Point	UO2 (wt%)	ThO2 (wt%)	PbO (wt%)	Age (Ma)
Chl-quartz-vein intruded into undeformed gabbro	Dumurdiha	Core	B-497	G1(110μm)	P1	76.07	0.61	16.5	**1539.821**
					P2	75.99	0.12	17.08	
					P3	74.37	0.35	17.26	
				G2(50μm)	P1	74.48	0.39	15.59	**1451.522**
				G3(40μm)	P1	77.81	0.07	15.74	**1411.434**
				G5(40μm)	P1	76.28	0.7	17.21	**1573.958**
					P2	77.89	0.14	17.3	
					P3	75.99	0.18	18.54	
				G6(300μm)	P1	87.18	0.19	11.22	**958.550**
					P2	85.94	0.07	12.28	
					P3	82.43	0.69	9.81	
				G7(150μm)	P1	76.89	0.13	19.16	**1674.051**
					P2	76.04	0.07	18.79	

7.4 Genesis of Sulphide phases

The cobalt content of Pyrite mineral for low temperature, medium temperature, and high temperature environment varies from <100ppm, 100-1000ppm, and >1000ppm, respectively (Mei, J.M, 2000). In the present area the cobalt content of pyrite in feldspathic schist in Tilogoria area varies from 3700-7100ppm points towards high temperature environment. The larger value of the Co/Ni ratio (14.2 to 3.81) implies the higher temperature of pyrite formation (Liu Z, (2018); Li, J.L, (2017)) (Figure 7.16). Pyrites in the area are depleted in Ni, As, Pb, which are different from synsedimentry pyrite (Leng, C.B, 2017), and exhibit characteristic of high temperature magmatic-hydrothermal deposit (Liu Z, (2018). Low Zn, Cd and Bi contents in pyrite further suggest lack of sedimentary source in the formation of pyrite (Keith, M, 2016).

According to Leng, C.B, (2017), the ratio of Fe/(S+As) shows good correlation with depth of formation of pyrite, the ratio of shallow depth environment, medium depth environment, and deep-seated environment of formation are 0.926, 0.863, and 0.846 respectively. The Fe/(S+As) ratio of pyrite in the area varies from 0.849 to 0.868

indicating possible shallower depth of formation of pyrite. The shallow depth and high temperature pyrite formation further indicates the extensional setting. Misra, 1999 has also shows that after the compressional tectonics in the present study area (during D_2 deformation), there exists extensional tectonics during emplacement of Mayurbhanj Granite. Therefore sulphide metallogeny in the present area can be speculated as syn- to post tectonic w.r.t to emplacement of fine grained Mayurbhanj Granite.

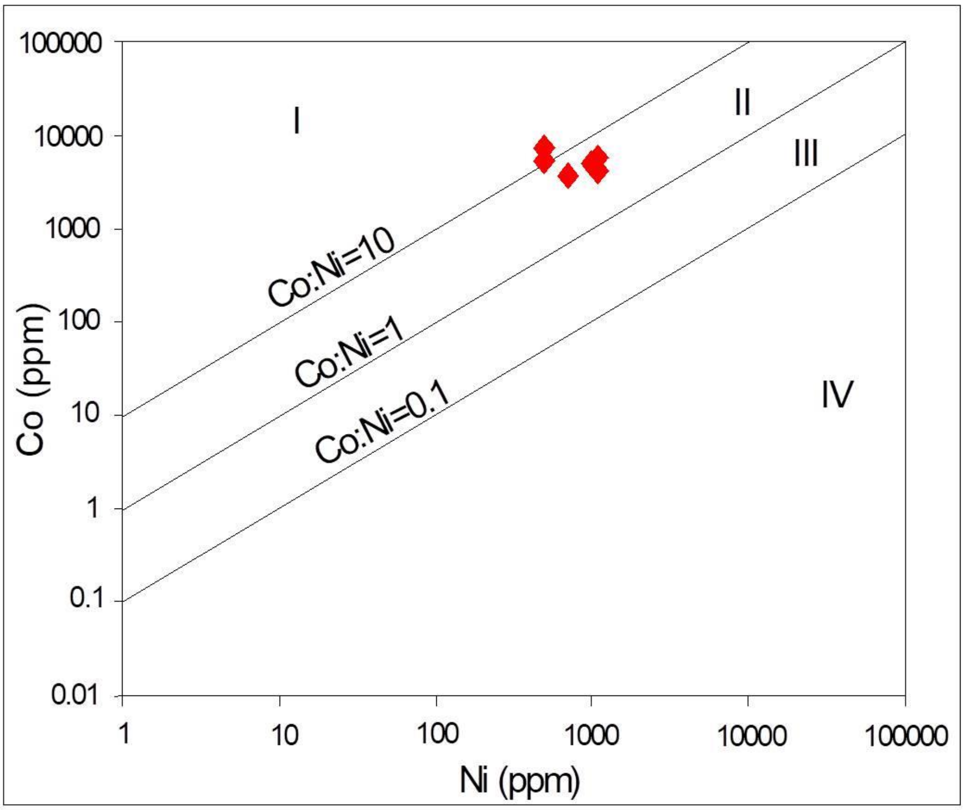

Figure 7.16 Ni vs Co diagram for pyrite associated with feldspathic schist, Tilogoria, Mayurbhanj, Odisha; I, II mineralization related to hydrothermal-magmatic deposit; III, IV sedimentary and sedimentary-reformed field (Liu Z, 2018).

7.5 Genesis of Uranium mineralization

In the present study area the uranium mineralization occurs in continuous thin lenses (Kusumbari and Tilogoria area) to erratically scattered patches (Dumurdiha area). The mineralization is prevailing in medium (lower amphibolite) to lowgrade (greenschist) facies. The host rocks in Kusumbari area is biotite-chlorite-quartz schist and sheared granite, in Tilogoria area it is feldspathic schist, and in Dumurdiha the host rock is ferruginous quartzite. Other than those at a very few exposures the radioactive quartz-chlorite veins also intruded into the different lithounits. The principal uranium mineral is uraninite. It occurs in disseminated form with rock constituents such as apatite, biotite and chlorite. A few secondary minerals of uranium such as torbernite and uranophane also occur in Dumurdiha area, which at places are associated with zircon, monazite, apatite and magnetite. Locally uraninte is associated with Ni, Mo, Cu, Fe and Zn-sulfides and Fe-oxides.

In eightfold coordination system the ionic radius of U^{4+} (1.00 Å) is similar to Th^{4+} (1.05 Å) and Y^{4+} (1.019 Å) (Shannon R.D, 1976), therefore they can be easily incorporated into uraninite structure. Studies showed that incorporation of Th into the uraninite is function of temperature and element availability, thus U/Th ratio provide estimate of temperature of crystallization (M.K Ozha, (2017); Depine, M, (2013); Balboni, E, (2016)). Earlier studies indicates uraninite with U/Th ratio greater than 10^3 is mostly formed by diagenetic or hydrothermal fluids, while uraninite with U/Th ratio less than 10^2 generally crystallize from magmatic fluids or magma (R.M Hazen, (2009); H.E Frimmel, (2014); F Yuan, (2019)). In the present study area the U/Th ratio in feldspathic schist ranges from 1200.4 to 106.54, with average value 514.7, indicating moderate to high temperature origin (figure 7.17 a).

Similar to thorium, Y content in uraninite also is a function of temperature and incorporates into uraninte at high temperature (Hetherington, 2013). In the present area, uraninite shows high Y_2O_3 content (0.47 to 1.77 wt.%, average 1.31wt.%) and suggests uraninite crystallization at relatively high temperature similar to sulphide phases.

REEs with similar ionic radius (especially Tb, Dy, Ho, Er) as that of Y and U^{4+} can easily incorporate into uraninite at high temperature, therefore Mercadier, (2011) has proposed a temperature threshold of approximately 350^{o}C for REE content greater than 1 wt%. In the present area most of the samples shows very high REE content and stay above the threshold limit of 350°C (figure 7.17 a & b).

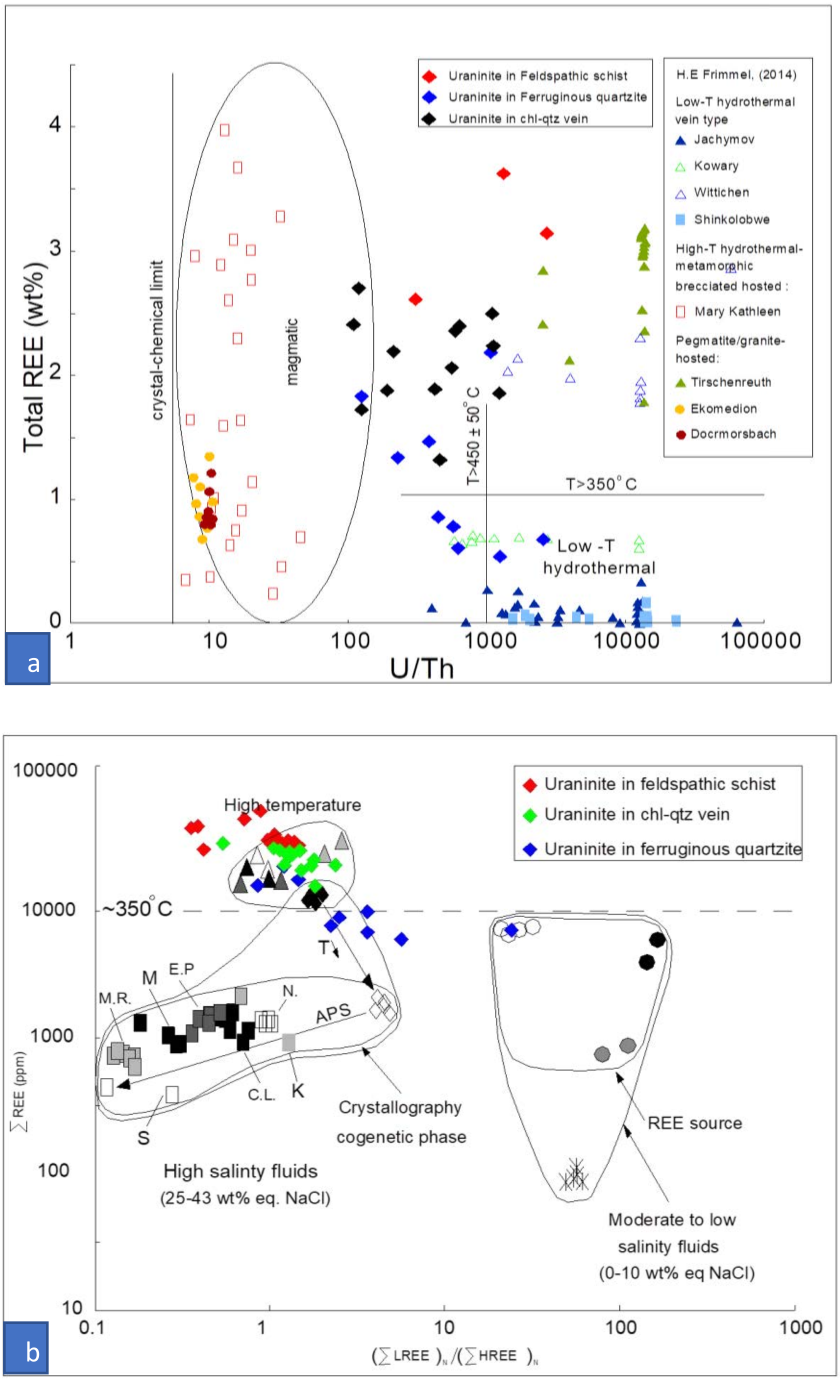

Figure 7.17 (a) The present study data of uraninite superposed over ∑REE versus Th/U diagram taken from H.E Frimmel et al. 2015. The diagram distinguish Low –temperature hydrothermal vein-type uraninite from higher temperature metamorphic-hydrothermal and magmatic urainite by U/Th>10^3. (b) The present study data of uraninite superposed over ∑REE versus (∑LREE/ ∑HREE)$_N$ diagram taken from Meracdier et al. (2011). The diagram shows temperature limit of ~350°C for threshold limit of 1wt% ∑REE.

In the present area the uranium content in uraninite is insensitive to total LREE and HREE content (figure 7.18 a & b), which further suggests the REE incorporation in the uraninite must took place at higher temperature, without any preference.

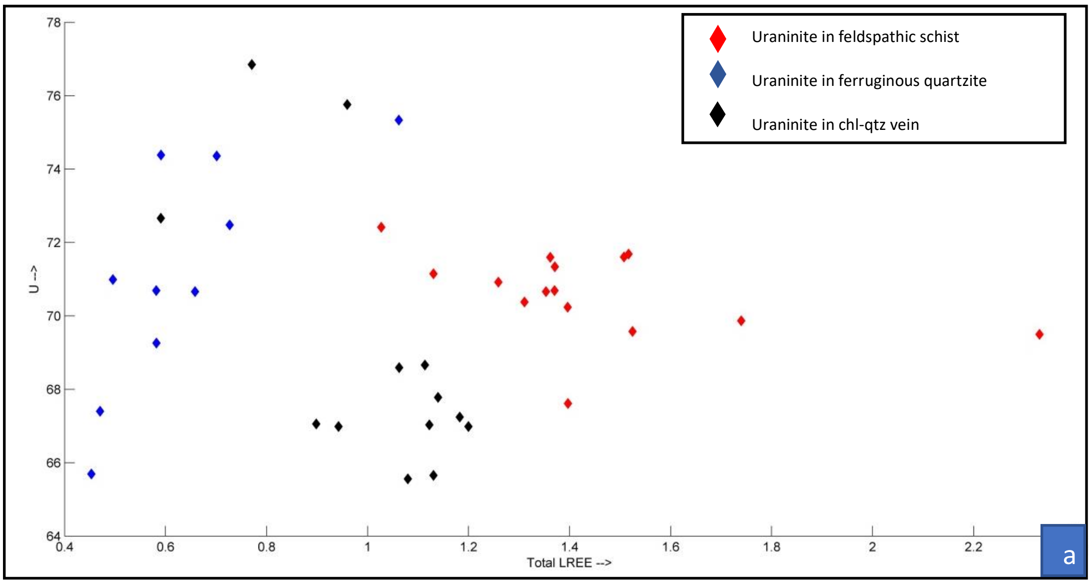

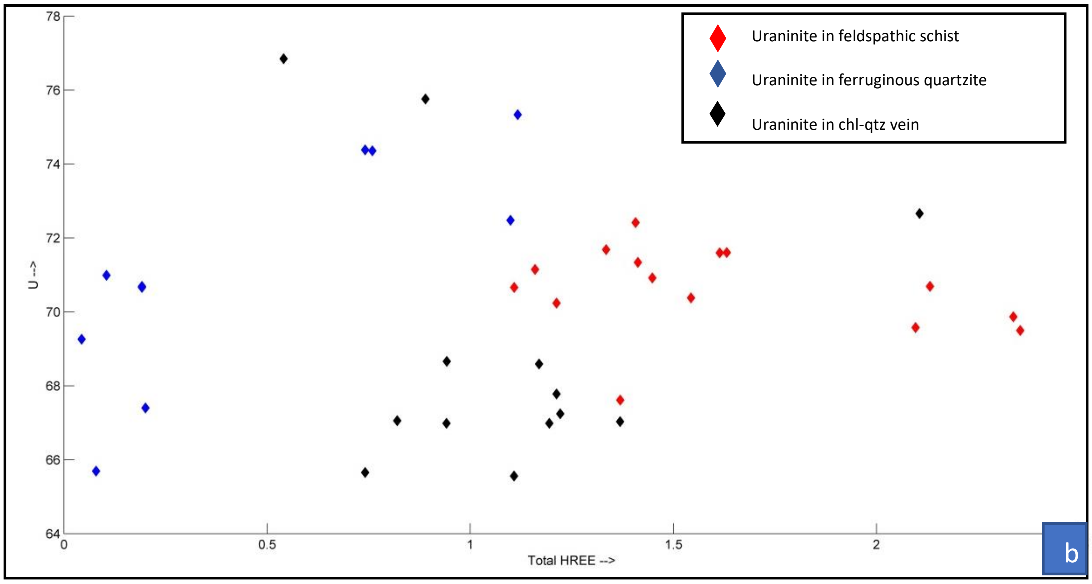

Figure 7.18 (a) U versus ∑LREE and (b) U versus ∑HREE diagrams. Both of the diagrams shows no correlation between U vs ∑LREE, and U vs ∑HREE, which indicates uranium REE incorporation into uraninite must took place at higher temperature without any preference.

The REE fractionation pattern is useful discriminator between different genetic types. Magmatic/Pegmatitic uraninite is characterized by only little fractionation and relatively flat chondrite-normalized REE patterns, whereas, in case of hydrothermal realm, the REE pattern is dependent on overall availability of REE in mineralizing fluids, the co-precipitating REE-incorporating minerals (APS), and the redox state, thus shows significant REE fractionation pattern (Mercadier et al. 2011). In the present area uraninte shows very little REE fractionation which points towards high temperature magmatic/pegmatitc origin. The negative europium anomaly further indicates the early fractionation of plagioclase in the silicate melt (Frimmel, 2015).

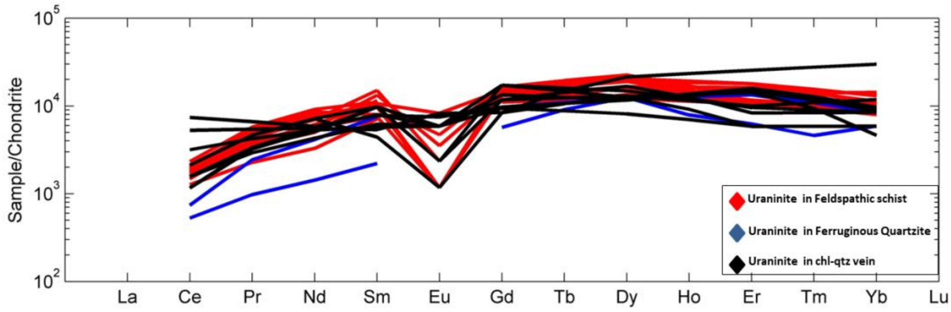

Figure 7.19 The diagram shows the chondrite normalized REE pattern for the uraninite grains occur in feldspathic schist, radioactive chl-qtz vein, and ferrugenious quartzite. The REE pattern is almost flat with small europium anomaly indicates magmatic/ pegmatitic origin (H.E Frimmel et al. 2015).

The unit cell parameter obtained from the XRD analysis also point towards high temperature pegmatitc origin. The highly scattered nature of chemical ages points that uranium mineralization overprinted by events of metamorphism in post mineralization phase.

CHAPTER 8

GEOCHEMISTRY OF ROMAPAHARI GRANITE AND SINGHBHUM METASEDIMENTS

Major, and trace element composition of samples obtained from WD-XRFS and ICP-OES have been used to classify the rock and ascertain its tectonic setting. For the WD-XRF analysis 150-200gm sample has been taken and powdered to 74 µm sizes. The representative ~1 gm powder of each sample was uniformly spread over 20 gm boric acid powder beds and then pelletized to 41 mm diameter by applying pressure 20,000 kg/cm^2. For the quantitative analyses of major oxides, the pellets were subjected to 30 kV accelerating potential and 100 mA beam current, whereas for the trace elements 60 kV accelerating potential and 40-60 mA beam current has been used.

For refractory elements like REEs, Mo, V, Zr, Hf, Nb, Ta etc., ICP-OES technique has been used. It measures the intensity of atomic/ionic emission lines emanating from plasma when the sample solution is introduced to it. The intensity of emission line is directly proportional to the concentration of the element present in sample solution. Operational frequency of generator is 40.68 Mhz, the plasma gas flow and Nebulizer gas flow rate is 12L/min and 0.8L/min respectively, injector tube diameter is 1.8mm.

8.1.1 Chemical Composition of Romapahari Granite

According to the QAPF classification (Streckeisen, 1974) of plutonic rocks most of the samples cluster in the field of alkali feldspar granite and syeno-granite (Fig 8.1a). In the SiO_2 vs (Na_2O+K_2O) diagram by Cox et al. (1979) (Fig. 8.1b), most of the granite plot are falling in the field of granite and granodiorite in the acidic regime. In the A/NK vs A/CNK diagram (Shand, 1943) (Fig. 8.1c), A/CNK values for the granites ranges from 0.8 to 1.6, reveals that they are metaluminous to peraluminous in nature.

In $R_{1.}R_2$ plot by De La Roche et al. (1980) (Fig. 8.1d), where R_1=6Ca+2Mg+Al and R_2=4Si+11(Na+K)-2(Fe+Ti), most of the analysed samples plots lying in the granite field while a few of them deviate into granodiorite, alkali granite, and quartz syenite.

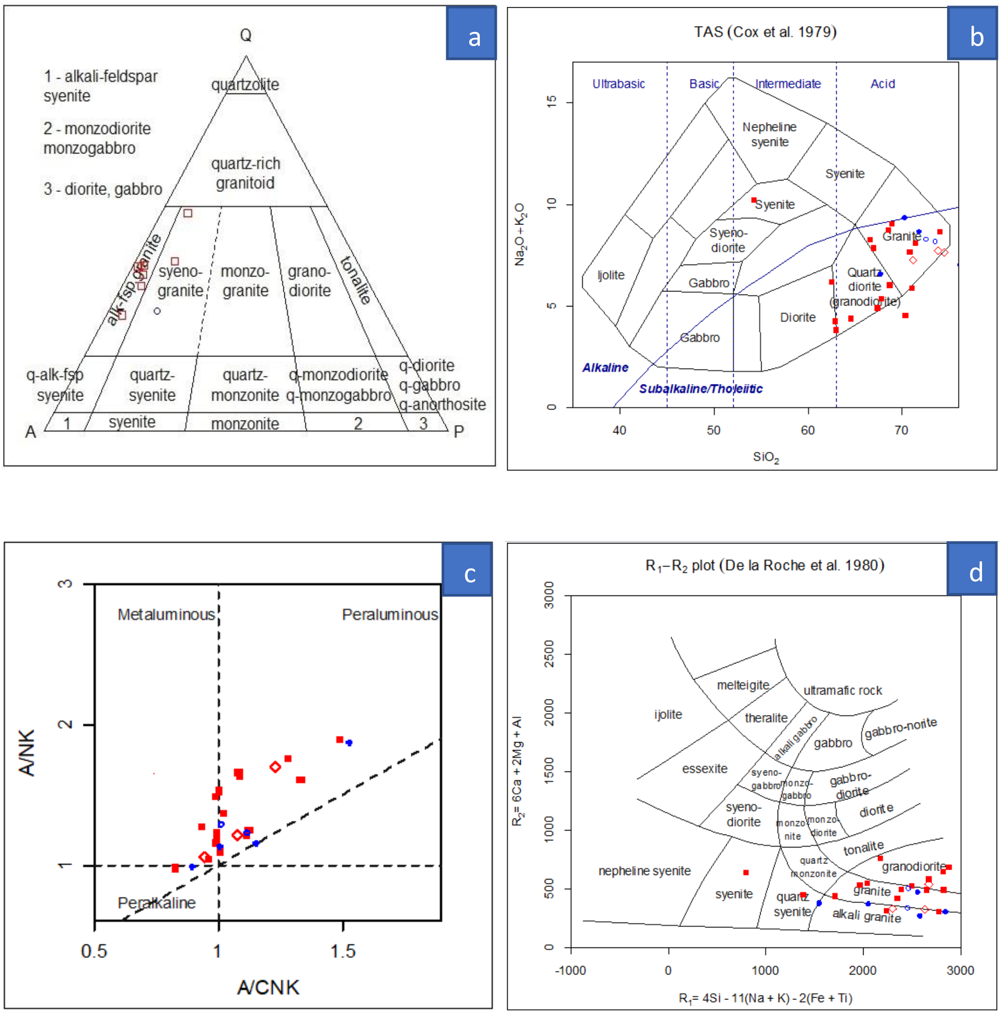

Figure 8.1 Classification of Romapahari Granite based on **(a)** QAP diagram (Streckeisen, 1974), **(b)** The plots of the analysed rock samples are falling into the field of granite, granodiorite in TAS diagram, (cox et al., 1979), **(c)** A/NK vs A/CNK diagram (Shand, 1943), **(d)** $R_{1.}R_2$ plot for analysed samples are classified as granite and granodiorite (De La Roche et al.,1980); Solid red square aplitic granite, solid blue circle coarse granite, open red square published data of aplitic granite (Misra, (2002), Saha, (1977)), open blue circle published data of coarse granite (Misra, 2002).

8.1.2 Tectonic Setting of Romapahari Granite

Based on the Rb vs. (Y+Nb) and Nb vs. Y diagram (Pearce et al., 1984) (Fig. 8.2a), most of the granitic rocks analysed were classified as within plate granite (Batchelor and Bowden, 1985) (Fig. 8.2b).

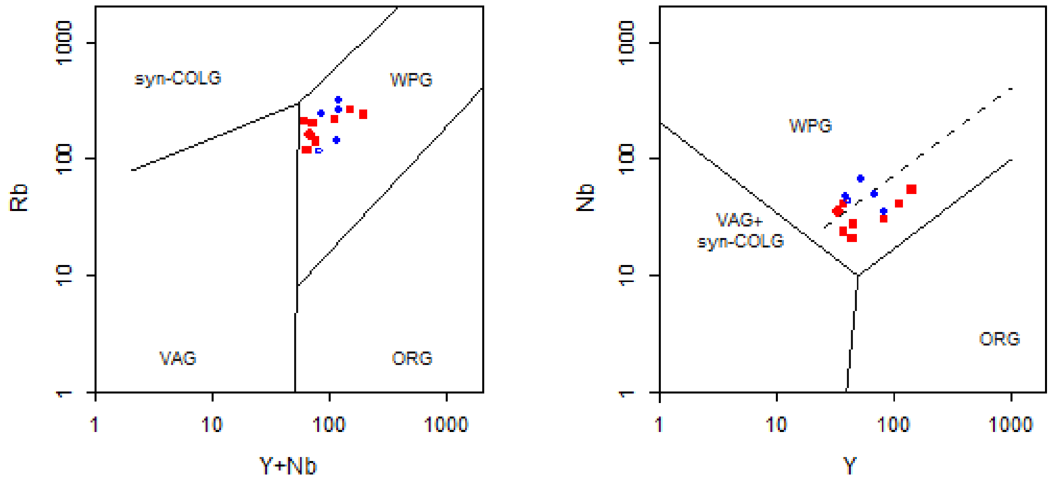

Figure 8.2 (a) log Rb vs. log (Y+Nb) and **(b)** log Y vs. log Nb diagrams (after Pearce et al. 1984) for Romapahari granite; VAG: volcanic arc granite, WPG: within plate granite, syn-COLG: syn-collision granite, ORG: ocean ridge granite.

Based on plots given by Whalen et al. in 1987 to distinguish A-type granites from I- and S-type (Fig. 8.2c), most of the granites are classified as A-type granites. Classification of A-type granite includes both tectonic setting and chemical composition. These granites are within plate granites (non-orogenic) and the magma seem to have exploded in an extensional setting.

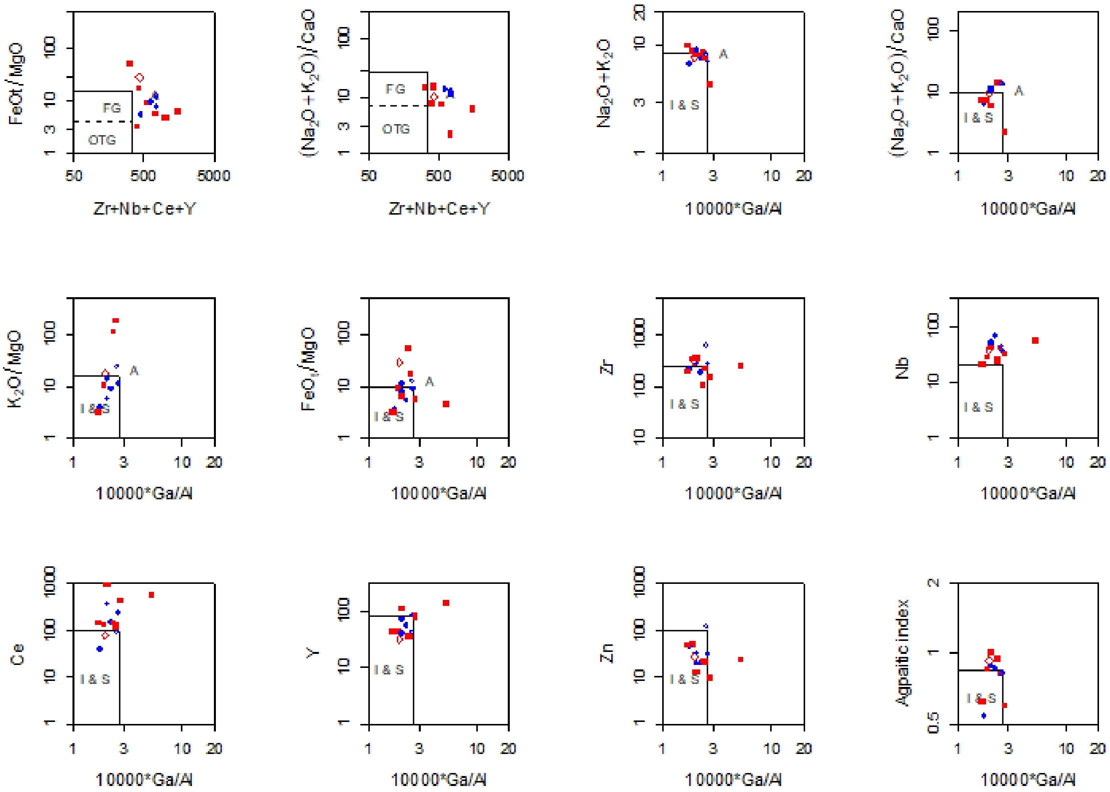

Figure 8.2 (c) Data from Romapahari granite samples (n=32) of different localities plotted on the diagrams given by Whalen et al., (1987) to distinguish A-type granites.

The following characteristics of the collected granite rocks favours that it is an A-type granite.

1. These granites are mostly peraluminous to marginally metaluminous.
2. High total alkali (Na_2O+K_2O) and lower CaO; (Na_2O+K_2O)/CaO ranges from 7.56 to 13.40 for coarse granite and 1.06 to 5.20 for aplitic granite.
3. High FeO_T/MgO; ranges from ~1.87 to 167.30 for coarse granite and 22.23 to 183.57 for aplitic granite.
4. High SiO_2 (~60 to 80%) and Na_2O (~0.5 to 8%).
5. Low Ca and Sr (~13 to 70 ppm).

8.1.3 Harker Variation Diagram

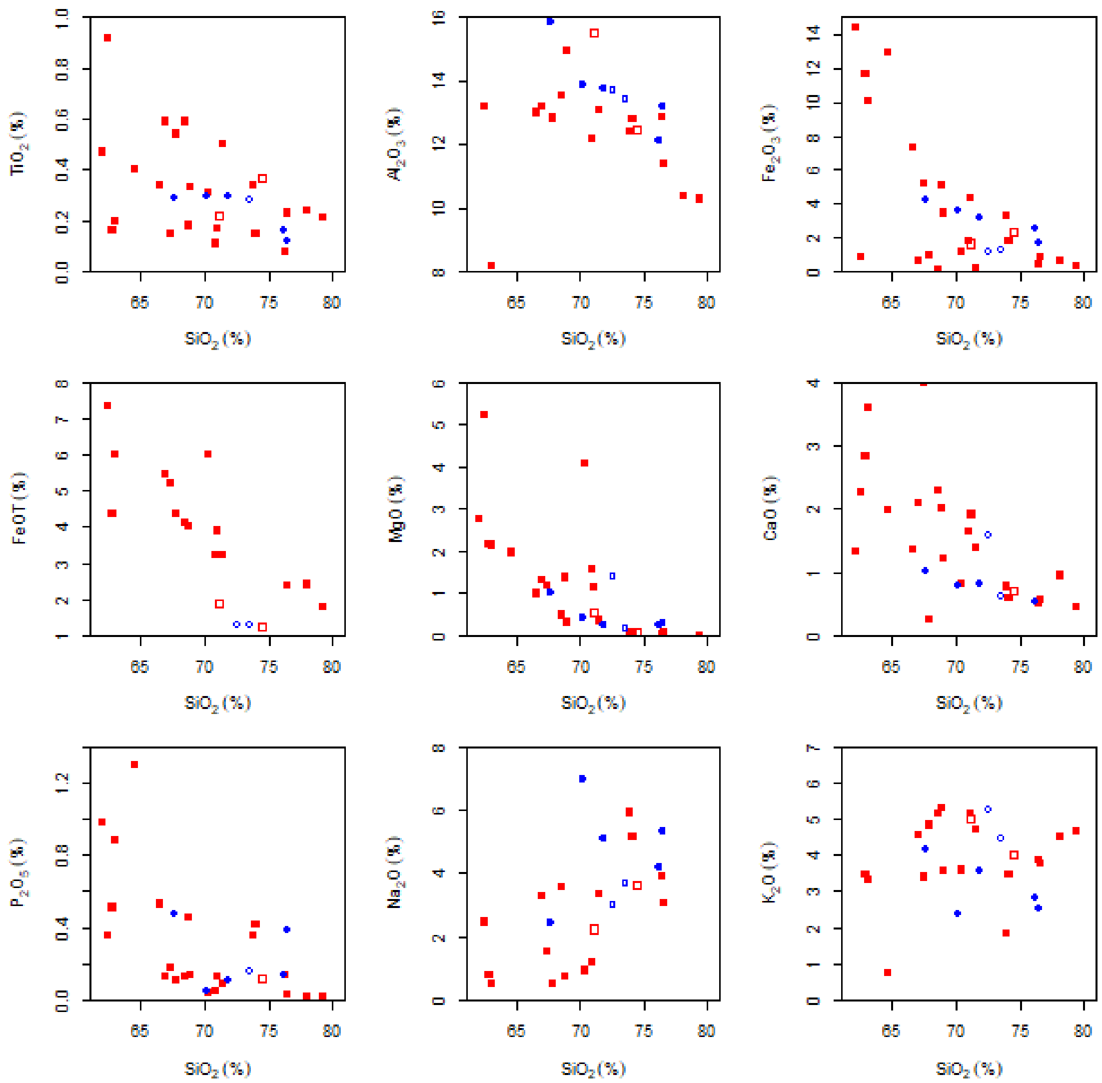

Figure 8.3 Harker variation diagram (SiO_2 vs major oxides) for samples collected from various localities in Singhbhum Shear Zone. Solid red square aplitic granite, solid blue circle coarse granite, open red square publish data of aplitic granite (Misra, (2002), Saha, (1977)), open blue circle publish data of coarse granite (Misra, 2002).

Harker (1909) proposed that SiO_2 increased steadily with magmatic evolution, and he thus used it as the abscissa to indicate the extent of evolution. The magma with the lowest silica content is thus accepted as the parental magma. It may be impossible, however, to demonstrate conclusively that it is a true primary magma because it may also have evolved during ascent (Winter, 2014). In the present study TiO_2, Fe_2O_3, FeO_t, MgO, CaO, Al_2O_3 and P_2O_5 are showing decreasing trend with increase in SiO_2. (Fig 8.3). Slightly positive trend is visible for K_2O and Na_2O.

The decrease in MgO, FeO, Al_2O_3 and CaO as SiO2 increases is consistent with the removal of early-forming minerals from the cooling liquid. MgO, FeO, Al_2O_3 and CaO are incorporated into the typically early-forming mafic minerals and a calcic plagioclase. The elements like K2O and Na2O shows a weak positive trend with SiO_2.

8.1.4 REE Patterns of Romapahari Granite

The samples from coarse granite shows enrichment of LREE (LREE/HREE ~3 to 57), fractionated LREE (Ce_N /Sm_N ~ 2.94 to 4.88), flat HREE (Tb_N /Yb_N ~ 1.62) and strong negative Eu-anomaly (Eu/Eu^* ~0.14 to 0.4). The fine apltic phase is very similar to that of coarse granite in respect of other paramters, i.e. LREE/HREE (~12.84 to 33.78), LREE and HREE pattern (Ce_N /Sm_N ~ 4.64, Tb_N /Yb_N ~ 1.25) (appendix 11.8), however, the total REE content of aplitic phase is less than coarse granite (Fig 8.4). Comparitively high LREE/HREE ratio for the aplitic phase reflectes more fractionated REE. The negative Eu anomaly signifies that the granite derived from fractional crystallisation of plagioclase from granitic magma under reducing conditions, where Eu^{2+} remains stable. The granite which is derived from the magma generated from the partial melting of the already fractionated source, however, shows no pronounced Eu anomaly. Enrichment of LREE over HREE in both the fractions of the Romapahari Granite suggests that they have been derived by the high degree of partial melting of the source rock.

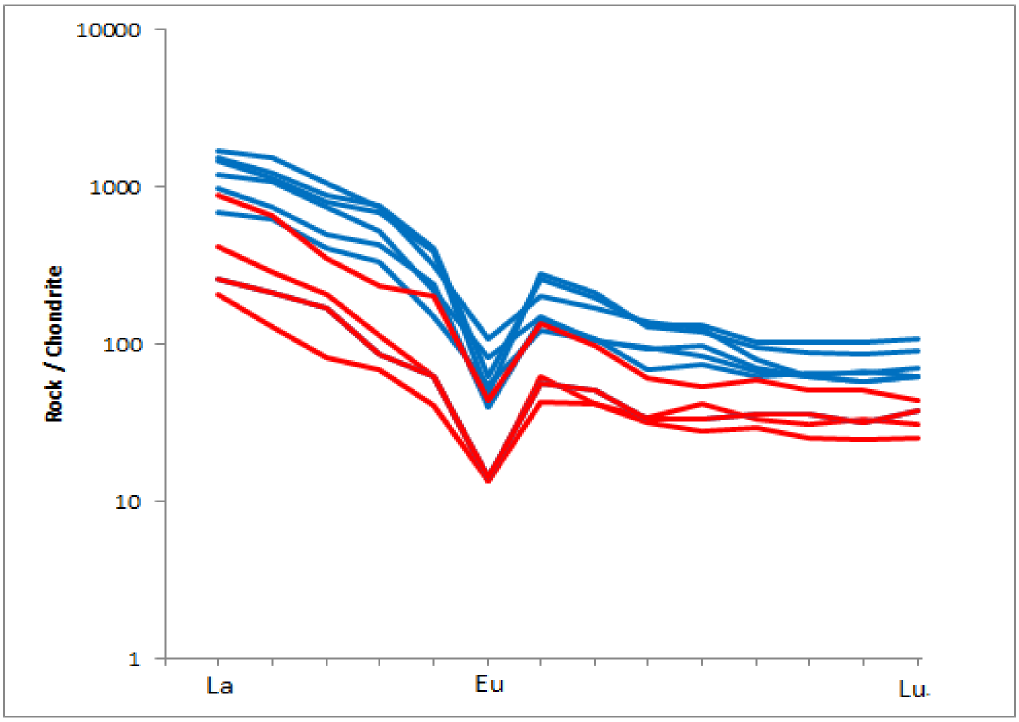

Figure 8.4 Chondrite-normalised REE diagram for the analyses of Romapahari Granite (n=9); Red line represents fine aplitic granite and blue line represents coarse granite.

8.1.5 Spider Diagram

The elements in Spider diagram by Pearce, (1983) arranged in such way so that the LIL elements are on the left side of the diagram, and the HFS elements are on the right. Each set is arranged in order of increasing incompatibility away from the margins, so that the most incompatible elements are just left of the centre of the diagram. In the present study the Spider diagram reveals that Granites are slightly more enriched in LIL as compared to HFS (Fig. 8.5) which gives us clue about the partial melting of its sialic source. Strong Ti trough further reflects influence of Titanite, rutile and ilmenite minerals (Winter, 2014).

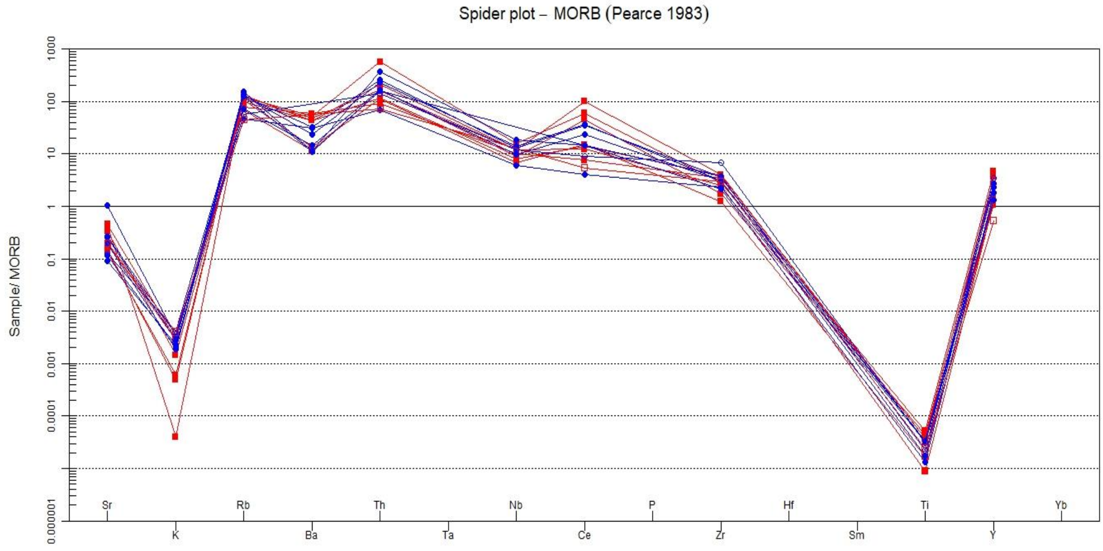

Figure 8.5 MORB-normalised incompatible elemental spider diagrams (Pearce, 1983) for the analyses of Romapahari Granite. Red line represents fine aplitic granite and blue line represents coarse granite.

8.1.6 Discussion on Romapahari Granite

The coarse and fine aplitic granite are similar in major modal composition, as well as in their SiO_2, Al_2O_3, Na_2O, K_2O and CaO chemistry. They are also found to have overlapping FeO and MgO contents. In all the field and discrimination diagrams these two variants show broad overlapping plotting giving rise to a practically single cluster of data. Both of them are A-type within plate granite. The A/CKN values for the fine aplitic granite are restricted to 0.8 to 1.5, whereas the coarse granite field lies in 1 to 1.6. In the spider plot both the variants of Romapahari Granite are enriched in LILE, indicating partial melting of sialic source. In the REE plot the REE pattern for both of the granites is very similar with the more fractionated overall REE pattern for the apltic phase, however, the total REE content is higher in coarse granite compared to that of the fine granite. The low REE chemistry of the aplitic phase depicts the progressive residual nature of source during partial melting, when the magma of the coarse granite phase, relatively enriched in REEs, had already been removed from the source region.

8.2.1 Geochemsitry of Ferrugenized Quartzite in Dumurdiha Area

To understand the controlling factors of mineralization, radioactive as well as non-radioactive surface samples of ferrugenized quartzite were collected. The following observations can be made from field, petrology, XRF, and XRD data.

1. In the field, uranium mineral encrustations occur along the foliation plane and most of the time very high activity is limited to only small patches instead of continuous bands. The XRD data helped in identifying uraninite as primary mineral and torbernite and uranophane as secondary minerals.
2. Major Oxide data indicate high concentration SiO_2 and Fe_2O_3 in active as well as non-active samples. Good concentration of CaO and P_2O_5 has been reflected only in active samples suggesting their close spatial association with apatite mineralisation (table 8.2). Petro-mineralogical study reveals quartz as major phase, and apatite, magnetite and hematite as accessories.
3. The active samples are showing significant positive correlation of U with Cu, Zr and Sr (table 8.1), and significantly higher values of Y and Ce (despite of small negative correlation) (table 8.2).

Table 8.1 Pearson correlation matrix for trace elements present in ferruginous quartzite, Dumurdiha area, Mayurbhanj district, Odisha.

	Cr	Ni	Cu	Sr	Y	Zr	Ce	Pb
Ni	-0.221							
Cu	0.403	0.076						
Sr	-0.099	0.073	0.684					
Y	-0.593	0.046	0.093	0.772				
Zr	0.417	0.560	0.638	0.564	0.038			
Ce	-0.458	0.522	-0.110	-0.159	0.037	-0.216		
Pb	0.554	-0.006	0.957	0.392	-0.235	0.584	-0.193	
U	0.564	0.047	0.957	0.416	-0.217	0.659	-0.201	0.990

Table 8.2: Major and trace element data of active and non-active grab samples of ferruginous quartzite, Dumurdiha area, Mayurbhanj district, Odisha.

	Radioactive (n=5)			Non-Radioactive (n=3)		
	Mean	**Max**	**Min**	**Mean**	**Max**	**Min**
U (ppm)	3202.4	10000.0	796.0	41.3	69.0	20.0
(wt. %)						
SiO_2	84.15	89.34	76.37	92.60	98.77	87.61
TiO_2	0.09	0.16	0.02	0.11	0.23	0.04
Al_2O_3	1.86	3.33	0.69	1.78	2.73	1.00
Fe_2O_3 (t)	8.42	23.10	3.74	3.49	5.32	2.16
MgO	0.99	2.13	0.35	0.61	1.01	0.08
MnO	<0.01	<0.01	<0.01	0.01	0.01	0.01
CaO	3.21	4.20	0.61	0.19	0.20	<0.01
Na_2O	0.09	0.09	0.09	<0.01	<0.01	<0.01
K_2O	<0.01	<0.01	<0.01	<0.01	<0.01	<0.01
P_2O_5	2.66	4.70	0.33	0.20	0.22	0.18
(ppm)						
Cr	256.4	407.0	117.0	264.7	408.0	153.0
Ni	148.2	210.0	98.0	139.0	190.0	92.0
Cu	502.2	1309.0	180.0	33.0	55.0	11.0
Zn	14.0	16.0	12.0	16.7	19.0	14.0
Ga	12.0	16.0	10.0	<10	<10	<10
Rb	<10	<10	<10	11.0	11.0	11.0
Sr	20.4	36.0	10.0	<10	<10	<10
Y	290.2	1002.0	11.0	<10	<10	<10
Zr	124.4	205.0	59.0	126.7	162.0	81.0
Nb	21.0	21.0	21.0	13.0	13.0	13.0
Ba	29.3	30.0	29.0	12.0	12.0	12.0
Ce	164.2	443.0	27.0	51.3	68.0	43.0
Pb	403.8	1031.0	126.0	33.0	62.0	18.0
Th	23.3	27.0	21.0	15.0	15.0	15.0

The higher concentration of tetravalent uranium in minerals like apatite has been investigated thoroughly, this be attributed to the fact that uranous ion and divalent calcium have similar ionic radii (0.99Å & 0.97Å respectively), as a result, replacement between uranous ion and divalent calcium is quite obviuos (Altschuler Z.S, 1958). A similar phenomenon might have happened in the present scenario, where the presence of apatite in the active samples were analysed by XRF technique as well as thin section study. Higher concentration of immobile elements like Y and Zr in active samples can be explained based on the model proposed by René (2008) which explains anomolus concentration of immobile elements like Y and Zr in uranium deposits of Okrouhla´ Radoun and the Rozna´uranium deposits occur in Czech Republic. According to the model, hydrothermal fluids rich in alkalies and CO2, while circulating in source rock, dissolve important minerals of monazite, xenotime and zircon, and became enriched in U, HREEs (Y) and Zr complexes. Later on, these fluids enriched in U and HREE complexes migrate towards meta-sediments and mobilize the uranium and HREEs (Y and Zr) into higher concentration. A Similar process might happened in the present study area where medium to high temperature fluids, rich in U, Cu and REE complexes invaded metasediments (Dumurdiha quartzite) where these complexes came in contact with reducing agents like ferrous ion (indicated by high Fe2O3), they get reduced and precipitate (equation 9.2.2, *Altschuler Z.S, 1958*)

$$(UO_2)^{+2} + \text{Reductant} \rightarrow \underset{\downarrow}{U^{+4}} + \text{Oxidized reductant} \quad \ldots\ldots.. (9.2.2)$$

The presence of apatite further interferes while attaining equilibrium in above reaction, where its presence helps in squeezing out U(IV) by ion exchange, resulting in forward shifting of the reaction with increased U(IV) supply (equation 9.2.2). The process is also known as regenerative capture (Altschuler Z.S, 1958). Regenerative capture along with accessory nature of apatite possibly explains the patchy nature of uranium mineralisation in the study area.

8.3.1 Geochemistry of Feldspathic Schist in Tilogoria area

Both radioactive and non-radioactive sub-surface samples of feldspathic schist have been selected for the study. The highest value of uranium concentration in the radioactive samples is around ~276ppm. To understand the control of uranium mineralization in feldspathic schist, the correlation of uranium with other major and trace element were carried out.

Table 8.3 Major and trace element data of active and non-active subsurface samples of Feldspathic schist, Tilogoria area.

	Radioactive Sample n=10 (=>100 ppm)			Non-Radioactive Sample n=9 (<10 ppm)		
	Max	Min	Mean	Max	Min	Average
U (ppm)	276	100	139.1	<10	<10	<10
(wt. %)						
SiO2	58.76	50.04	52.01	55.51	47.83	51.06
TiO2	0.99	0.76	0.86	1.56	0.83	1.06
Al2O3	17.92	15.96	16.94	17.62	14.11	15.90
Fe2O3(t)	14.22	6.63	11.35	15.30	7.76	12.66
MgO	7.55	3.7	6.34	8.75	4.33	6.62
MnO	0.31	0.11	0.19	0.27	0.15	0.20
CaO	2.92	2.04	2.36	3.90	1.90	2.94
Na2O	9.72	4.37	6.55	8.50	3.54	5.93
K2O	2.67	1.16	1.79	2.95	0.86	1.75
P2O5	0.66	0.21	0.39	1.08	0.12	0.56
Total	100.13	98.01	98.82	99.98	97.99	98.70
(ppm)						
Cr	210	112	176.8	230.0	131.0	181.78
Ni	1420	97	488.3	1935.0	258.0	771.78
Cu	301	31	142.1	458.0	56.0	259.33
Zn	126	43	105.8	121.0	82.0	104.67
Ga	28	24	25.7	27.0	21.0	23.78
Rb	124	58	86.2	110.0	36.0	69.22
Sr	209	44	107.7	130.0	54.0	88.33
Y	71	21	44.3	48.0	26.0	35.56
Zr	220	118	163	181.0	115.0	129.89
Nb	83	13	54.8	50.0	12.0	27.67
Ba	665	221	404.4	871.0	311.0	533.67
Ce	1427	151	783.2	1076.0	424.0	689.67
Pb	63	32	47.7	44.0	18.0	27.33
Th	88	5	22.9	91.0	5.00	17.89

Positive correlation exists between U and Al_2O_3 , Na_2O can be seen in U-Na_2O diagram and U- Al_2O_3 diagram (Fig. 8.6 (a) & (b)). While slight negative correlation between U-CaO and no correlation between U-K_2O exists (Table 8.4). Hence, U content in rocks is somehow related to soda activity. Positive linear relationship between U and Pb is due to the fact that radiogenic lead is an end product of radioactive decay of uranium. Although, there is no correlation between uranium and copper concentration, copper sulphides are spatially associated with uranium

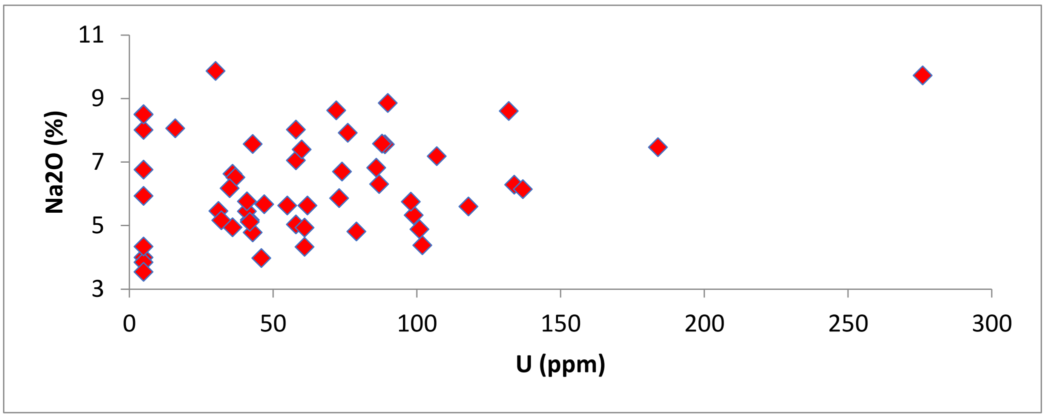

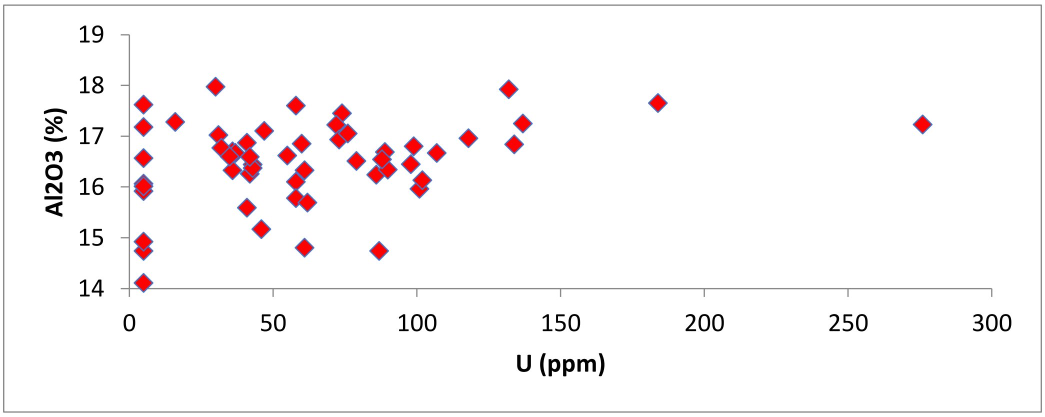

Figure 8.6 (a) Variation diagram U-Na_2O, and **(b)** U-Al_2O_3

Table 8.4 The Correlation matrix of Major and trace element data for the feldspathic schist, Tilogoria area.

	SiO2	TiO2	Al2O3	Fe2O3(t)	MgO	MnO	CaO	Na2O	K2O	P2O5	Cr	Ni	Cu	Zn	Ga	Rb	Sr	Y	Zr	Nb	Ba	Ce	Pb	Th
TiO2	-0.435																							
Al2O3	-0.241	-0.198																						
Fe2O3(t)	-0.692	0.408	-0.304																					
MgO	-0.89	0.355	0.205	0.614																				
MnO	-0.394	0.186	-0.21	0.683	0.357																			
CaO	-0.401	0.461	-0.286	0.317	0.305	0.168																		
Na2O	-0.126	-0.241	0.608	-0.441	-0.006	-0.196	-0.221																	
K2O	-0.088	0.102	0.155	-0.266	0.198	-0.589	-0.023	0.003																
P2O5	-0.482	0.181	-0.073	0.252	0.456	-0.024	0.56	-0.042	0.081															
Cr	-0.412	0.194	0.023	0.507	0.311	0.587	-0.003	-0.015	-0.552	0.079														
Ni	-0.3	0.065	-0.236	0.485	0.161	0.498	0.088	0.069	-0.53	-0.035	0.598													
Cu	-0.29	0.113	-0.252	0.336	0.128	0.209	0.273	0.08	-0.324	0.262	0.35	0.711												
Zn	-0.494	0.175	-0.001	0.556	0.63	0.327	0.131	-0.326	-0.141	0.314	0.522	0.258	0.23											
Ga	0.219	-0.337	0.474	-0.404	-0.049	-0.229	-0.413	0.112	-0.026	-0.061	0.114	-0.266	-0.242	0.294										
Rb	0.221	-0.167	0.193	-0.484	0.001	-0.625	-0.245	-0.029	0.676	-0.068	-0.281	-0.482	-0.276	0.177	0.513									
Sr	-0.097	0.092	0.208	-0.043	0.185	-0.302	0.14	-0.179	0.145	0.165	0.17	-0.066	0.037	0.625	0.443	0.538								
Y	-0.207	0.134	0.167	0.128	0.223	-0.125	-0.019	-0.173	0.121	0.28	0.269	-0.053	0.179	0.577	0.431	0.395	0.573							
Zr	0.675	-0.423	0.099	-0.579	-0.503	-0.267	-0.562	0.053	-0.124	-0.369	0.025	-0.209	-0.233	0.034	0.627	0.507	0.262	0.108						
Nb	-0.074	-0.152	0.219	0.102	0.184	0.035	-0.237	-0.138	-0.157	-0.024	0.42	0.077	0.145	0.635	0.618	0.378	0.638	0.611	0.431					
Ba	-0.504	0.346	0.099	0.176	0.598	-0.283	0.334	-0.108	0.765	0.369	-0.231	-0.261	-0.103	0.233	-0.099	0.418	0.315	0.243	-0.472	-0.042				
Ce	-0.344	-0.053	-0.168	0.526	0.285	0.385	0.148	-0.2	-0.393	0.275	0.597	0.524	0.567	0.572	0.036	-0.159	0.277	0.513	-0.085	0.481	-0.107			
Pb	-0.028	-0.22	0.27	-0.013	0.133	0.036	-0.223	-0.003	-0.186	-0.052	0.438	0.119	0.088	0.627	0.665	0.409	0.658	0.577	0.457	0.896	-0.084	0.403		
Th	0.459	-0.008	0.233	-0.557	-0.497	-0.269	-0.429	0.309	-0.057	-0.315	-0.125	-0.156	-0.226	-0.483	0.363	-0.008	-0.181	-0.043	0.346	-0.132	-0.343	-0.35	-0.117	
U	0.111	-0.305	0.316	-0.253	-0.102	-0.098	-0.203	0.294	-0.023	-0.142	-0.055	-0.113	-0.129	-0.033	0.266	0.19	0.075	0.093	0.274	0.236	-0.247	-0.075	0.384	0.11

The samples from mineralized as well as non-mineralized portion shows similar REE pattern with enrichment of LREE, depletion of HREE and prominent negative Eu anomaly. The total REE content is higher in radioactive samples as compared to non-radioactive samples (Fig 8.6 c).

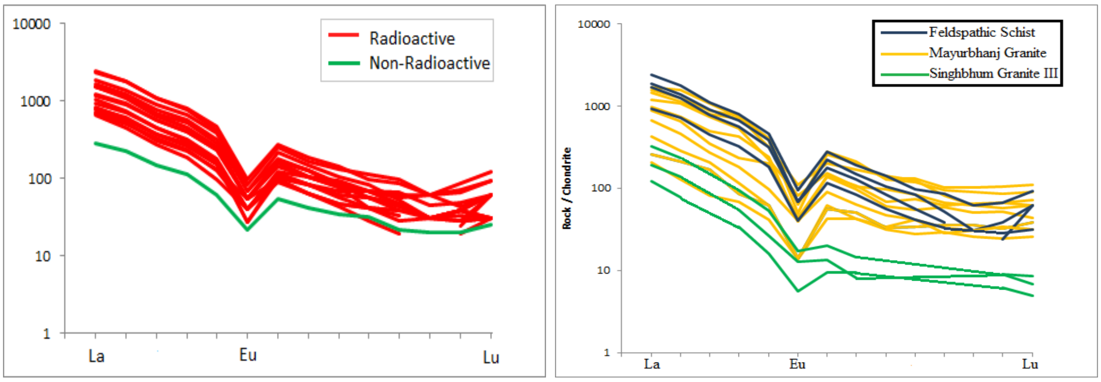

Figure 8.6 (c) The image shows the chondrite normalized REE pattern for radioactive and non-radioactive samples from Feldspathic schist, **(d)** chondrite normalized REE pattern for radiactive feldspathic schist, Mayurbhanj Granite, and Singhbhum granite phase III.

The REE data of a few samples from the radioactive feldspathic schist has been compared with the REE data of Mayurbhanj Granite (Romapahari Granite) and

Singhbhum Granite phase III (Fig 8.6 (d)). The overall REE pattern of Feldspathic schist is similar to that of Mayurbhanj Granite and Singhbhum Granite, however, the total REE content is comparatively higher in the feldspathic schist and Mayurbhanj Granite.

The uranium mineralization in the area appears to be related to Na-Metasomatism. The subsurface borehole data shows gradational contacts of unaltered chlorite-biotite-sericite-quartz schist, partially feldspathised sheared biotite-chlorite-sericite-quartz schist, and sensu stricto feldspathized schist. The above observation suggests that the feldspathic schist in the area is the products of progressive alteration of pre-existing schists within the shear zone by fluids highly rich in soda. The high temperature sodic fluids might have invaded along the schistosity planes within the biotite-chlorite-sericite-quartz schists of the shear zone.

To explain the origin of high temperature sodic fluids for large scale feldspathization along entire shear zone Banerjee and Talapatra, (1966) has suggested if Singhbhum granite (14.3% perthitic orthoclase, 50.7% plagioclase, 29% quartz) is subjected to the melting the first fluid generated will be enriched in albite. They further suggest during the shearing the partial melting of basement Singhbhum Granite has took place which generates sodic fluid. These sodic fluids because of higher mobility compared to potassic fluids came up along shear planes and replaced the rock lying in the upper tectonic levels. The similarity in REE pattern of Singhbhum Granite Phase-III, Mayurbhanj Granite (which also evolved from SBG-III; Misra, 2002) and feldspathic schist (figure 8.6(d)) further supports the above interpretation. The relative enrichment of trace elements U, Cr, Ni etc in feldspathized zone could be explained based on fact that ascending high temperature sodic fluids in course of their passage through shear zone might have collected these elements from shear zone rocks such as sheared metabasalts and sheared metasediments of Chaibasa and Dhanjori.

Slight positive correlation of uranium with Na, and negative correlation with Ca can be explained based on experiments performed by Bindeman and Davis, 2000. They analysed uranium in plagioclases and found a correlation between D_U (partition coeffeicent of Uranium) and X_{An} (molar anorthite content).

$$RT \ln (D_U) = - (484 \pm 195)\ An\% - (7452 \pm 12552) \quad \text{………} (8.3.2)$$

The above equation 8.3.2 indicates as the anorthite content decreases and the composition becomes more albitic, partition coefficient for U^{4+} increases. As a composition shifts towards albite, the size of M-site increases and U^{4+} (1.01Å) starts substituting in the crystal replacing Na (1.18 Å) and Ca (1.12 Å). Therefore it might be possible, Na rich hydrothermal fluids laden with uranium complexes migrate near the surface and during the crystallization the uranium preferentially substitute into soda feldspar.

8.4.1 Geochemistry of chlorite-biotite-quartz schist in Kusumbari area

In the Kusumbari area the uranium mineralization is hosted by chlorite-biotite-quartz-schist and sheared granite. The chromium, copper and nickel content is significantly higher in the radioactive as well as non-radioactive zone. Although there is no correlation between the uranium and copper mineralization, locally uranium seems to be associated with copper, whereas the inverse relationship does not seems to be holds true. Table 8.6 indicates both the radioactive and non-radioactive schist have similar major elemental composition, whereas, in case of trace elements, the radioactive schist have higher Cr, Cu , Zn and Rb content as compared to non-radioactive portion.

Table 8.5: The Correlation matrix of major and trace element data of chl-bt-qtz schist, Kusumbari.

	SiO2	TiO2	Al2O3	Fe2O3(t)	MgO	MnO	CaO	Na2O	K2O	P2O5	Cr	Ni	Cu	Zn	Ga	Rb	Sr	Y	Zr	Nb	Pb	Ba	Ce	Th
TiO2	-0.472																							
Al2O3	-0.234	-0.244																						
Fe2O3(t)	-0.501	0.471	-0.624																					
MgO	-0.474	0.569	-0.634	0.709																				
MnO	-0.81	0.695	-0.026	0.429	0.578																			
CaO	-0.67	0.153	0.633	0.007	-0.124	0.452																		
Na2O	-0.173	-0.068	0.476	-0.58	-0.026	0.302	0.341																	
K2O	0.313	-0.203	0.154	-0.64	-0.133	-0.094	-0.391	0.531																
P2O5	-0.581	0.365	-0.408	0.93	0.533	0.433	0.302	-0.518	-0.756															
Cr	-0.315	0.39	-0.54	0.357	0.818	0.621	-0.136	0.371	0.241	0.2														
Ni	-0.073	-0.276	-0.265	0.545	-0.1	-0.103	-0.012	-0.664	-0.626	0.602	-0.248													
Cu	-0.225	0.226	-0.421	0.77	0.243	0.161	0.122	-0.7	-0.887	0.829	-0.107	0.745												
Zn	0.152	-0.351	0.737	-0.914	-0.517	-0.104	0.192	0.792	0.636	-0.837	-0.16	-0.601	-0.785											
Ga	-0.183	0.06	0.683	-0.595	-0.154	0.144	0.387	0.775	0.271	-0.549	-0.046	-0.697	-0.551	0.79										
Rb	-0.05	0.281	0.397	-0.35	-0.106	0.032	0.09	0.107	0.437	-0.336	-0.214	-0.657	-0.441	0.345	0.338									
Sr	-0.235	-0.169	0.878	-0.473	-0.608	0.072	0.744	0.405	-0.126	-0.178	-0.532	-0.105	-0.089	0.579	0.588	0.199								
Y	-0.071	0.048	0.255	-0.373	-0.045	0.351	0.148	0.589	0.155	-0.395	0.224	-0.262	-0.173	0.578	0.61	-0.123	0.332							
Zr	0.248	0.327	0.281	-0.445	-0.309	-0.052	0.044	0.018	0.295	-0.412	-0.31	-0.564	-0.279	0.317	0.246	0.828	0.235	0.068						
Nb	0.382	-0.219	0.005	-0.617	-0.003	-0.051	-0.354	0.732	0.733	-0.747	0.433	-0.591	-0.708	0.664	0.48	-0.036	-0.096	0.598	0.018					
Pb	-0.059	0.177	-0.496	0.112	0.631	0.41	-0.367	0.469	0.453	-0.092	0.918	-0.297	-0.297	0.043	0.046	-0.283	-0.522	0.329	-0.357	0.689				
Ba	-0.399	0.03	0.5	0.186	-0.351	-0.017	0.568	-0.432	-0.511	0.395	-0.685	0.38	0.378	-0.186	-0.094	0.277	0.501	-0.393	0.171	-0.856	-0.872			
Ce	-0.1	-0.186	0.501	-0.194	-0.566	-0.054	0.329	-0.251	0.047	-0.013	-0.561	0.245	0.004	0.139	-0.195	0.428	0.404	-0.201	0.422	-0.462	-0.655	0.707		
Th	-0.233	-0.108	0.952	-0.685	-0.565	0.122	0.588	0.606	0.306	-0.519	-0.361	-0.404	-0.542	0.824	0.74	0.439	0.802	0.425	0.383	0.183	-0.313	0.325	0.467	
U	0.237	-0.539	-0.077	-0.041	-0.159	-0.516	-0.215	-0.077	0.135	-0.067	-0.07	0.242	-0.264	-0.104	-0.304	-0.352	-0.299	-0.57	-0.518	0.002	0.031	-0.045	-0.063	-0.181

Similar to feldsapthic schist, the schist in the Kusumbari area shows fractionated REE pattern; LREE enrichment, HREE depletion and pronounced negative europium anomaly. The total REE content in the radioactive portion is significantly higher as compared to non-radioactive portion (Figure 8.7(a)).

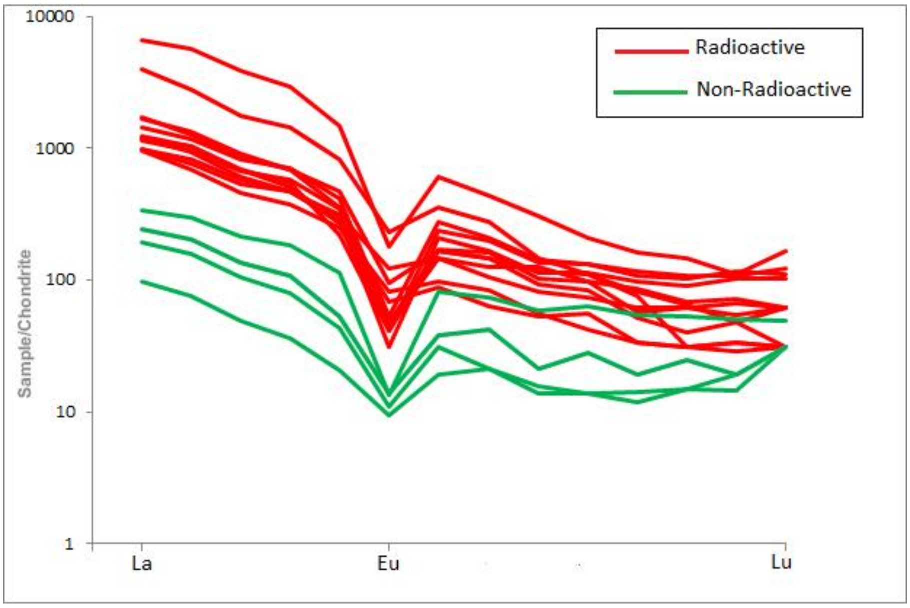

Figure 8.7 (a) The image shows chondrite normalized REE pattern for radioactive and non-radioactive samples of chlorite-biotite-quartz schist, Kusumbari, Mayurbhanj, Odisha.

Table 8.6 Major and trace element data of active and non-active subsurface samples of chlorite-biotite-quartz-schist, Kusumbari area.

Elements	Radioactive (n=5)			Non-Radioactive (n=5)		
	Mean	Max	Min	Mean	Max	Min
U_3O_8 (ppm)	234.2	760.0	50.0	<10	<10	<10
(wt. %)						
SiO2	64.44	69.60	55.22	63.30	66.56	56.98
TiO2	0.30	0.49	0.11	0.38	0.47	0.31
Al2O3	11.70	14.20	8.81	13.67	21.10	11.21
Fe2O3	10.25	17.46	4.44	9.32	14.41	4.16
MgO	1.81	4.42	0.83	1.67	2.76	0.65
MnO	0.02	0.04	0.01	0.02	0.03	0.02
CaO	1.50	1.86	1.15	1.63	3.03	0.47
Na2O	1.80	2.38	0.93	1.57	3.20	0.61
K2O	5.96	6.89	3.42	5.93	8.35	3.62
P2O5	0.77	1.43	0.21	0.70	1.30	0.29
	n=52			n=53		
(ppm)						
Cr	167.4	635.0	46.0	115.0	279.0	41.0
Ni	594.5	1902.0	193.0	597.3	1843.0	140.0
Cu	4039.9	19840.0	80.0	2051.4	4997.0	212.0
Co	108.5	305.0	37.0	nd	nd	nd
Zn	68.7	128.0	44.0	14.0	19.0	11.0
Ga	17.0	22.0	11.0	20.6	31.0	14.0
Rb	405.1	727.0	54.0	179.1	245.0	0.0
Sr	37.2	98.0	5.0	11.2	16.0	10.0
Y	114.4	131.0	80.0	118.6	139.0	103.0
Zr	107.4	239.0	50.0	132.9	255.0	80.0
Nb	55.8	92.0	21.0	45.8	84.0	24.0
Ba	601.1	1457.0	152.0	1451.9	2677.0	1023.0
Pb	25.2	83.0	5.0	152.9	311.0	97.0
Ce	508.5	563.0	454.0	460.0	1011.0	106.0
Th	19.1	101.0	5.0	20.0	24.0	16.0

8.4.2 Sulphur Isotope study of Kusumbari rocks

Six Sulphide fractions (SIL/18.19/239 to 243) were collected from core samples of chlorite-biotite-quartz-schist, chlorite-schist, sheared granite and undeformed dolerite from Kusumbari for sulphur isotope studies. The results for those samples collected from present study area given in Table- 8.7

δ^{14}S‰ (V-CDT) values (+ 6.1‰) on pyrite occurring along mylonitic foliation of sheared granite and in quartz-sulphide vein (+6.2‰) cutting across foliation in chlorite schist are similar. The geological set-up, mode of occurrence of pyrites and similarity of δ^{14}S values in granites and schist are suggestive of coeval origin, possibly related to high temperature magmatic fluids during granitization of metasediments.

Table 8.7 Sulphur isotope data for Sheared Romapahari Granite, biotite-chlorite-quartz schist, chlorite schist, and undeformed dolerite, Kusmubari area, Mayurbhanj dist., Odisha.

Lab Ref. No	Field Sample No	Rock Type	Mode of Occurrence of sulphides	δ^{14}S‰ (V-CDT)
SIL/18.19/239	KMB-10/247.00	chlorite-biotite-quartz-schist	Along foliation	7.7
SIL/18.19/240	KSP-1/187.10	Chlorite-schist	As quartz sulphide vein across foliation	6.2
SIL/18.19/241	KMB-13/44.00	Sheared granite	Along mylonitic foliation	6.1
SIL/18.19/242	KMB-13/94.00	chlorite-biotite-quartz-schist	Along foliation plane	8.3
SIL/18.19/243	KMB-14/198.80	underformed dolerite	In dolerite dyke	2.1
SIL/18.19/244	KMB-7/B5/44.01	chl-biotite-quartz-schist	Along foliation plane	7.6

$\delta^{14}S$ values (+7.6‰ to +8.3‰, n=3) on pyrites occurring along foliation in chlorite-biotite quartz schist are relatively higher. Such enrichment may be due to incorporation of minor amounts of evaporates-derived heavier sulphur from metasediments by the magmatic fluids during its passage through the metasediments.

The $\delta^{14}S$ values (+2.1‰, n=1) on pyrites from dolerites sample is unrelated to the inferred event and it might be late magmatic in character.

8.5 Discussion

In the Tilogoria area, the high concentration of Na_2O in mineralized feldspathic schist probably reflects uranium mineralization genetically related to soda metasomatism. The uranium mineralization in the Dumurdiha quartzite is also suggested to be the result of fluid activity. In Kusmubari similar to Tilogoria and Dumurdiha area the fractionated REE pattern and sulphur isotope data lend support to the metasediment-hosted uranium mineralization to be fluid origin. It has been observed in the metasediments of Dumurdiha and Kusumbari area there is significant decrease in sodic content (or feldspathisation) (Table 8.2 & 8.6) whereas there is an appreciable increase in tourmalinisation as indicated by field data and petro-mineralogical study (Figure 7.9h & 5.6b). These observation indicates that mineralization in these areas might represent the residual volatile component originated from the same source from which the earlier sodic fluids have been originated.

CHAPTER 9

CONCLUSION

Detailed geological mapping was carried out on 1:5000 scale to the decipher lithological dispositions of different lithounits exposed over an area of 32 sq Km. The mapping was carried out from Kesharpur in the north to Dumurdiha in south. The major lithounit exposed over northern part of the area is Romapahari Granite, which is easternmost extension of Mayurbhanj Granite. The granitic body intrudes into Singhbhum group of metasediments (metamorphosed to greenschist to amphibolite facies) which includes biotite-sericite-chl-quartz schist, hornblende-biotite-chlorite-quartz schist, feldspathic schist (schistose Soda Granite), magnetite-bearing quartzite, kyanite quartzite, and fuchsite quartzite. The presence of feldspathized schist in the area is related to the granitization of shear zone rocks during regional scale ductile deformation. To the north of the feldspathic schist the metasediments belongs to Chaibasa Formation and to the South the major lithounits are of Dhanjori Group of rocks. The uranium mineralization in the area is hosted by biotite-chlorite-quartz schist, feldspathic schist and hematite bearing quartzite.

A fairly detailed structural analysis was carried out along Kesharpur-Kusumbari-Tilogoria-Dumurdiha tract. The rocks exhibit well developed primary and secondary structures both in mega- and mesoscopic scale. On the megascopic scale the area exposes a large synformal structure plunging towards north. The core of the synform is occupied by the Romapahari Granite, whereas, the outer part consists of metamorphites of Chaibasa Formation and Dhanjori Group of rocks. The intrusion of the Romapahari Granite lacks chilled margin and the metasediments do not show any imprints of metasomatism. Therefore it is suggested that the granite is not emplaced in a molten condition, rather the melt mostly crystallized at depth a before its emplacement. The structural data of coarse grained variety of Romapahari Granite show certain similarity with the folded metasediments, while the fine granite does not show any geometrical congruence with the folded metasediments. It indicates that emplacement of coarse granite is pre- to syntectonic with reference to folding event whereas that of fine grained granite post-tectonic. The shear direction in the western part of the study area is along NW-SE direction, whereas in the eastern part it is along NE-SW direction, which indicates that either the shearing is a pre-tectonic w.r.t to folding or there is a layer parallel shearing due to large scale regional folding. Subsequently, the whole area is intersected by joint planes and quartz veins.

The host rock for uranium mineralization in Kusumbari area is biotite-chlorite-quartz-schist and sheared granite, in Tilogoria area it is feldspathic schist, and in Dumurdiha the host rock is ferruginous quartzite. Other than those at a very few exposures the radio-active quartz-chlorite and quartz-feldspathic veins also intruded into the different lithounits. The principal uranium mineral is uraninite. It occurs in disseminated form in association with apatite, biotite and chlorite. Some secondary minerals of uranium such as torbernite and uranophane have also observed in Dumurdiha area, which at places are associated with zircon, monazite, apatite and magnetite. Locally uraninte is associated with Ni, Mo, Cu, Fe and Zn sulphides and Fe oxides. The higher concentration of Co, larger value of Co/Ni, and Fe/(S+As) ~0.85 indicate epigenetic hydrothermal origin of sulphide phases. Similarly high U/Th ratio, and high Y content indicates high temperature, hydrothermal-magmatic origin of uranium mineralization.

In the Tilogoria area there is high concentration of Na_2O in feldspathized lithic unit. The radioactive feldspathic schist shows mild positive correlation between Na_2O

and U, and Al_2O_3 and U, while there is very mild negative correlation between U-CaO and no correlation between U and K_2O content. Hence, U content in rocks is somehow related to soda activity. High concentration of Na_2O, fractionated REE pattern, and elevated concentration of U, Cr, Ni, Cu etc. indicate mineralization in feldspathic schist is genetically derived from hydrothermal sources related to Na-metasomatism. The soda rich fluids might have originated from the partial melting of SBG-III during shearing. In the ferrugenized quartzite exposed in Dumurdiha, major oxide data indicates high concentration SiO_2 and Fe_2O_3 in radioactive as well as non-radioactive samples. Good concentration of CaO and P_2O_5 have been reflected only in radioactive samples which possibly reflect the apatite mineralisation in the shear zone which in turn, is spatially related to the uranium mineralisation. Similar to feldspathic schist high U/Th ratio in Dumurdiha area points towards hydrothermal origin. In Kusumbari area fractionated REE, and sulphur isotopic data indicates hydrothermal origin of ore minerals.

9.1 Genetic Model

The subsurface borehole data show the perceptible gradation of unaltered chlorite-biotite-quartz schist, partially feldspathised sheared biotite-chlorite-quartz schist, and completely feldspathized schist. The above observation indicates feldspathic schist in the area is the products of progressive addition and replacement of pre-existing schists within the shear zone by feldspathic materials rich in soda. The process of feldspathisation started to operate after intense shearing took place in the area. The process can be speculated as syn to post tectonic w.r.t to emplacement of Mayurbhanj granite when extensional tectonic are in existence. The high temperature soda rich fluid moved up along the schistosity planes within the biotite-chlorite-sericite schists of the shear zone. The presence of both deformed (sheared) and undeformed feldspar porphyroblasts indicate that the processes of shearing continued for some time during feldspathisation and thereby the early formed plagioclase porphyroblasts were sheared.

To explain the origin of sodic fluids for large scale feldspathization along entire shear zone Banerjee and Talapatra, (1966) has suggested if Singhbhum granite (14.3% perthitic orthoclase, 50.7% plagioclase, 29% quartz) is subjected to the melting the first fluid generated will be enriched in albite. He further suggested during the shearing the partial melting of basement Singhbhum Granite has took place which generates sodic fluid. These sodic fluids because of higher mobility compared to potassic fluids invaded through the shear planes and replaced the rock lying in the upper tectonic levels. The similarity in REE pattern of Singhbhum Granite Phase-III, Mayurbhanj Granite (which also evolved from SBG-III, Misra, 2002) and feldspathic schist, further supports the above contention. The relative enrichment of trace elements, like U, Cr, Ni etc in feldspathized zone could be explained based on the fact that the ascending sodic fluids in course of their passage through shear zone might have collected these elements from shear zone rocks such as sheared metabasalts and sheared metasediments of Chaibasa Formation and Dhanjori Group of rocks.

Similar to feldspathic schist in Tilogoria, the uranium mineralization in Dumurdiha area appears to be high to medium temperature fluids related. The fluids rich in U, Cu and REE complexes, purveyed into meta-sediments of Dumurdiha quartzite, when these complexes came in contact with reducing agents like ferrous ion (indicated by high Fe_2O_3), they get reduced and precipitate. The presence of apatite further fostered the supply of U4+ ion by forward shifting of the reduction reaction. This regenerative capture evidenced from the close association of apatite further explains the uranium mineralization in the close proximity to the apatite-magnetite mineralisation in this area.

In Kusmubari similar to Tilogoria and Dumurdiha area the fractionated REE pattern and sulphur isotope data lend support to the metasediment-hosted uranium mineralization to be magmatic fluid related. It has been observed in the metasediments of Dumurdiha and Kusumbari area there is significant decrease in sodic content (or feldspathisation) whereas there is an appreciable increase in tourmalinisation as indicated by field data and petro-mineralogical study. These observation indicates that mineralization in these areas might represent the residual volatile component originated from the same source from which the earlier sodic fluids have been originated.

9.2 Future Work

The present conclusion is strictly based on the geochemical data of specific minerals and whole rock geochemistry. Now to further confirm the hypothesis related to presence of sodic rich fluids the geochemistry and geothermometry of the fluids can be carried out.

REFERENCES

Acharya, S. (1984) Stratigraphic and structural evolution of the rocks of the iron ore basins in Singhbhum-Orissa iron ore province, India. 'Crustal Evolution of the Indian Shield and its Bearing on Metallogeny', Seminar Volume, Ind. SOC. Earth Sci., Calcutta, pp.19-28.

Acharyya, S. K., Gupta, A., & Orihashi, Y. (2008). U–Pb zircon dates (LA-ICP-MS) of some felsic magmatic rocks from the basal parts of the Dhanjori basin and their stratigraphic implication, East Singhbhum, India. In IAGR Conference Series, Vol. 5, pp.151-152.

Acharyya, S. K., Gupta, A., & Orihashi, Y. (2010). Neoarchean–Paleoproterozoic stratigraphy of the Dhanjori basin, Singhbhum Craton, Eastern India: And recording of a few U–Pb zircon dates from its basal part. Journal of Asian Earth Sciences, 39(6), pp.527-536.

AMD Annual report of quartz pebble conglomerate investigation, (field season 2017-18) - unpublished report.

AMD Annual report of quartz pebble conglomerate investigation, (field season 2018-19) - unpublished report.

Altschuler, Z. S., Clarke, R.S., & Young, E.J.(1958). Geochemsitry of Uranium in Apatite and Phosphorite. U.S. Geological Survey. Professional Paper 314-D. Shorter contribution to general geology, pp.85-87.

Augé, T., Cocherie, A., Genna, A., Armstrong, R., Guerrot, C., Mukherjee, M. M., & Patra, R. N. (2003). Age of the Baula PGE mineralization (Orissa, India) and its implications concerning the Singhbhum Archaean nucleus. Precambrian Research, 121(1-2), pp.85-101.

Balboni, E.; Jones, N.; Spano, T.; Simonetti, A.; Burns, P.C. (2016). Chemical and Sr isotopic characterization of North America uranium ores: Nuclear forensic applications. Appl. Geochem, 74, pp.24–32.

Bandyopadhyay, P. K., Chakrabarti, A. K., Deomurari, M. P., & Misra, S. (2001). 2.8 Ga old anorogenic granite-acid volcanics association from western margin of the Singhbhum-Orissa Craton, eastern India. Gondwana Research, 4(3), pp.465-475.

Banerji, A. K. (1962). Cross folding, migmatization and ore localization along part of the Singhbhum Shear Zone, south of Tatanagar. Economic Geology, 57, pp.50-71.

Banerji, A. K. (1964). Structure and stratigraphy of part of northern Singhbhum, south of Tatanagar, Bihar. Natl. Inst. Sci. India, Proc. 30A, pp.486-510.

Banerji, A. K. (1969). A reinterpretation of the geological history of the Singhbhum Shear Zone, Bihar. Geol. Soc. India, 10, pp.49-55.

Banerji, A. K. (1974). Role of basic volcanism in copper mineralisation along the Singhbhum shear zone, Bihar, Eastern India: IAGOD Symposium, 4th, Varna, Bulgaria, 1974, Proc, 1, pp.208-214.

Banerji, A. K. (1975). On the evolution of the Singhbhum nucleus. Geol. Mining Metall. Soc. India Quart. Jour. 47, pp.51-60.

Banerji, A. K. (1981). Ore genesis and its relationship to volcanism, tectonism, granitic activity, and metasomatism along the Singhbhum shear zone, Eastern India. Economic Geology, 76, pp.90-98.

Banerji, P. K. (1982). Stratigraphy, petrology, and geochemistry of some Precambrian basic volcanic and associated rocks of Singhbhum District, Bihar, and Mayurbhanj and Keonjhar districts, Orissa (Vol. 111). Geological Survey of India.

Banerji, A. K. (1977). On the Precambrian banded iron-formations and the manganese ores or the Singhbhum region, eastern India. Economic Geology, 72(1), pp.90-98.

Banerji, A. K., & Talapatra, A. K. (1966). Soda-granites from south of Tatanagar, Bihar, India. Geological Magazine, 103(4), pp.340-351.

Batchelor, R. A., & Bowden, P. (1985). Petrogenetic interpretation of granitoid rock series using multicationic parameters. Chemical geology, 48(1-4), pp.43-55.

Bajwah, Z.U.; Seccombe, P.K.; Offler, R. (1987). Trace element distribution, Co/Ni ratios and genesis of the Big Cadia iron-copper deposit, New South Wales, Australia. Miner. Depos., 22, pp.292–300.

Bhattacharya D.S. (1966). Structure of the rocks of the Sonepet valley, Singhbhum Bihar. Geol. Mining Metall. Soc. India Bull. 36, pp.1-21.

Bhattacharya D.S. (1978). Time relation of polymetamorphic recrystallisatio in the Precambrian rocks of the Sonepet valley. Geol. Soc. India.14, pp. 282-288.

Bhattacharya D.S., Pasyat, S., and Sarkar, A.N. (1976). Zones of metamorphism in western Singhbhum, Eastern India. Indian Jour. Earth Sci. 3, pp.26-36.

Bhattacharya, H. N. (1991). A Reappraisal of the Depositional Environment of the Precambrian Metasediments around Ghatsila-Galudih, Eastern Singbhum. Geological Society of India, 37(1), pp.47-54.

Bhola, K. L. (1965). Radioactive mineral deposits of India, in Proc. Symposium on Uranium Prospecting and Mining in India: Jadugoda, India Department of Atomic Energy, pp.2-41.

Bhola, K. L., Rama Rao, Y. N., Sastry, C. S., & Mehta, N. R. (1966). Uranium mineralization in Singhbhum thrust belt, Bihar, India. Economic Geology, 61(1), pp.162-173.

Bindeman, I. N., & Davis, A. M. (2000). Trace element partitioning between plagioclase and melt: investigation of dopant influence on partition behavior. Geochimica et Cosmochimica Acta, 64(16), pp.2863-2878.

Bose, M. K. (1994). Sedimentation pattern and tectonic evolution of the Proterozoic Singhbhum basin in the eastern Indian shield. Tectonophysics, 231(4), pp.325-346.

Bose, M. K. (2009). Precambrian mafic magmatism in the Singhbhum craton, eastern India. Journal of the Geological Society of India, 73(1), pp.13-35.

Bose, M. K., & Chakraborti, M. K. (1981). Fossil marginal bassin from the Indian shield: A model for the evolution of Singhbhum Precambrian belt, Eastern India. Geologische Rundschau, 70(2), pp.504-518.

Bose, P. K., Mazumder, R., & Sarkar, S. (1997). Tidal sandwaves and related storm deposits in the transgressive Protoproterozoic Chaibasa Formation, India. Precambrian Research, 84(1-2), pp.63-81.

Bowles JF. (2015). Age Dating from Electron Microprobe Analyses of U, Th, and Pb: Geological Advantages and Analytical Difficulties. Microsc Microanal. 21(5), pp.1114-22.

Bralia, A.; Sabatini, G.; Troja, F. (1979). A revaluation of the Co/Ni ratio in pyrite as geochemical tool in ore genesis problems. Miner. Depos,14, pp.353–374.

Cathelineau M (1981a). Les gisements d'uranium lies spatialement aux leucogranites Sud Armoncains et a leur encaissant metamorphique, Sci Terre Mem, Nancy, 42, pp.475.

Cathelineau M (1981b) Les gisements uraniferes de la presqu'ile Guerandaise (Sud Bretagne), Approche structurale et metallogenique, Mineral Deposita, 16, pp.227-240.

Chakraborty, K.L. and Majumder, T. (1986) Geological aspects of the Banded Iron Formation of Bihar and Orissa. J. Geol. SOC. India, v. 31, pp.305-313.

Chatterjee, P., De, S., Ranaivoson, M., Mazumder, R., & Arima, M. (2013). A review of the∼ 1600 Ma sedimentation, volcanism, and tectono-thermal events in the Singhbhum craton, Eastern India. Geoscience Frontiers, 4(3), pp.277-287.

Dahlkamp, F. J. (2013). Uranium ore deposits. Springer Science & Business Media.

Dasgupta, H. C., Rao, V. S., & Krishna, C. (1999). Chemical environments of deposition of ancient iron-and manganese-rich sediments and cherts. Sedimentary Geology, 125(1-2), pp.83-98.

Dasgupta, S. (2004). Modelling Ancient Orogens-An Example from North Singhbhum Mobile Belt. Geo1. Surv. India Spec. Publ, 84, pp.33-42.

De, A. (1964). Precambrian Dalma Dhanjori volcanicity of E. India and its stratigraphic significance. In Proceedings of the International Geological Congress (Vol. 10, pp.59-70).

De La Roche, H., Leterrier, J. T., Grandclaude, P., & Marchal, M. (1980). A classification of volcanic and plutonic rocks using R1R2-diagram and major-element analyses—its relationships with current nomenclature. Chemical geology, 29(1-4), pp.183-210.

Depiné, M.; Frimmelm, H.E.; Emsbo, P.; Koenig, A.E.; Kern, M. (2013). Trace element distribution in uraninite from Mesoarchaean Witwatersrand conglomerates (South Africa) supports placer model and magmatogenic source. Miner. Depos, 48, pp.423–435.

Dunn, J. A. (1937). The mineral deposits of eastern Singhbhum and surrounding areas. Mem. Geol. Surv. India, 69, pp.211-213.

Dunn, J. A. & Dey A. K. (1942). Geology and petrology of Eastern Singhbhum and surrounding areas. Mem. Geol. Surv. India, 69, pp.261-456.

Eriksson, Patrick G., Mazumder, R., Catuneanu, O., Bumby, Adam J., Ilondo, B. Ountsche., (2006). "Precambrian continental freeboard and geological evolution: a time perspective." Earth-Science Reviews 79.3: pp.165-204.

Foley, S., Tiepolo, M., & Vannucci, R. (2002). Growth of early continental crust controlled by melting of amphibolite in subduction zones. Nature, 417(6891), pp.837.

Frimmel, H.E.; Schedel, S.; Brätz, H. (2014). Uraninite chemistry as forensic tool for provenance analysis. Appl. Geochem, 48, pp.104–121.

Fritsche R. Amsrutz GC. Dahlkamp FJ (1988) Primare Uranerzminerale und ihre lagerstattengenetische Stellung, Deutsche Forschungsgemeinschaft. Final report. DFG Project Am 23/65, pp.212.

Ghosh, A. K. (1972). Trace element geochemistry and genesis of the copper ore deposits of the Singhbhum shear zone, eastern India: Mineralium Deposita, 7, pp.292-313.

Ghosh, D., & St Lambert, R. J. (1986). Rubidium-strontium and lead isotopic studies on the soda-granites from Mosaboni, Singhbhum Copper Belt, E. India. Indian journal of earth sciences, 13(2-3), pp.101-116.

Ghosh, S. K. and Sengupta, S. (1987). Progressive evolution in a ductile shear zone. J. Structural Geology, 9, pp.277-288.

Goswami, J. N., Mishra, S., Wiedenbeck, M., Ray, S. L., & Saha, A. K. (1995). 3.55 Ga old zircon from Singhbhum–Orissa iron ore craton, eastern India. Current Science, pp.1008-1012.

Gregory, D.D.; Large, R.R.; Halpin, J.A.; Lounejeva, E.B.; Lyons, T.W.;Wu, S.; Danyushevsky, L.V.; Sack, P.; Chappaz, A.; Maslennikov, V.V.; et al. (2015). Trace element content of sedimentary pyrite in black shales. Econ. Geol, 110, pp.1389–1410.

GSI Annual Report of Madansahi block, Mayurbhanj district, Odisha, (field season 2018-19) - unpublished report.

Hazen, R.M.; Ewing, R.C.; Sverjensky, D.A.(2009). Evolution of uranium and thorium minerals. Am. Mineral, 94, 1293–1311.

Hetherington, C.J. Harlov, D.E. (2013). Metasomatic thorite and uraninite inclusions in xenotime and monazite from granitic pegmatites, Hidra anorthosite massif, southwestern Norway: Mechanics and fluid chemistry. Am. Mineral, 93, pp.806–820

Iyengar S. V. P. and Anand Alwar M. A. (1965). The Dhanjori Eugeosyncline and its bearing on the stratigraphy of Singhbhum Keonjhar and Mayurbhanja Districts. D.N. Wadia Commn. Vol. Min. Kc Met. Inst. India, Calcutta, pp.138-162

Iyenger, S. V. P., Chandy, K. C., & Narayanaswamy, R. (1981). Geochronology and Rb-Sr systematics of the igneous rocks of Simlipal Complex, Orissa. Indian Journal of Earth Sciences, 8(1), pp.61-65.

Jaffey, A.H., Flynn, K.F., Glendenin, L.E., Bentley, W.C. & Essling, A.M. (1971). Precision measurement of half-lives and specific activities of 235U and 238U. Phys Rev C Nucl Phys 4, pp.1889–1906.

Keith, M.; Hackel, F.; Haase, K.M.; Schwarz-Schampera, U.; Klemd, R. (2016) Trace element systematics of pyrite from submarine hydrothermal vents. Ore Geol. Rev, 72, pp.728–745.

Koglin, N.; Frimmel, H.E.; Lawrie Minter,W.E.; Bratz, H. (2010). Trace-element characteristics of different pyrite types in Mesoarchaean to Palaeoproterozoic placer deposits. Miner. Depos., 45, pp.259–280.

Leng, C.B. (2017). Genesis of Hongshan Cu polymetallic large deposit in the Zhongdian area, NW Yunnan: Constraints from LA-ICPMS trace elements of pyritie and pyrrhotite. Earth Sci. Front, 24, pp.162–175.

Leroux, L.J. & Glendenin, L.E. (1963). Half-life of Th-232. In Proceedings National Conference on Nuclear Energy: Application of Isotopes and Radiation, Warren, F.L. (Ed.) 83–94. Pretoria, South Africa: Atomic Energy Board.

Liu, Z.; Shao, Y.; Zhou, H.; Liu, N.; Huang, K.; Liu, Q.; Zhang, J.; Wang, C. (2018). Major and Trace Element Geochemistry of Pyrite and Pyrrhotite from Stratiform and Lamellar Orebodies: Implications for the Ore Genesis of the Dongguashan Copper (Gold) Deposit, Eastern China. *Minerals*, *8*, pp.380.

Macmillan, E.; Cook, N.J.; Ehrig, K.; Pring, A. (2017). Chemical and textural interpretation of late-stage coffinite and brannerite from the Olympic Dam IOCG-Ag-U deposit. Mineral. Mag, 81, pp.1323–1366.

Mahalik, N. K. (1994). Geology of Contact between Eastern Ghats Belt and North-Orissa Craton, India. J. Geol. Soc. India, 44, pp. 41-51.

Martin, H., & Moyen, J. F. (2002). Secular changes in tonalite-trondhjemite-granodiorite composition as markers of the progressive cooling of Earth. Geology, 30(4), pp.319-322.

Mathur, S. N. (1964). Turbidites and sedimentary structures from Chaibasa Stage, Iron Ore Series, Singhbhum Dt., Bihar. India Geol. Survey Rec. 93, pp.263-264

Mazumder, R. (2005). Proterozoic sedimentation and volcanism in the Singhbhum crustal province, India and their implications. Sedimentary Geology, 176(1), pp.167-193.

Mazumder, R., & Sarkar, S. (2004). Sedimentation history of the Palaeoproterozoic Dhanjori Formation, Singhbhum, eastern India. Precambrian Research, 130(1), pp.267-287.

Mazumder, R., De, S., Ohta, T., Flannery, D., Mallik, L., Chaudhury, T., ... & Arima, M. (2015). Palaeo-Mesoproterozoic sedimentation and tectonics of the Singhbhum Craton, eastern India, and implications for global and craton-specific geological events. Geological Society, London, Memoirs, 43(1), pp.139-149.

Mazumder, R., Eriksson, P. G., De, S., Bumby, A. J., & Lenhardt, N. (2012). Palaeoproterozoic sedimentation on the Singhbhum Craton: global context and comparison with Kaapvaal. Geological Society, London, Special Publications, 365(1), pp.51-76.

Mazumder, R., Van Loon, A. J., Mallik, L., Reddy, S. M., Arima, M., Altermann, W & De, S. (2012a). Mesoarchaean–Palaeoproterozoic stratigraphic record of the Singhbhum crustal province, eastern India: a synthesis. Geological Society, London, Special Publications, 365(1), pp. 31-49.

Mei, J.M. (2000**).** Chemical typomorphic characteristic of pyrites from Zhilingtou gold deposit, Suichang, Zhejiang.Geoscience, 14, pp.51–55.

Meert, J. G., Pandit, M. K., Pradhan, V. R., Banks, J., Sirianni, R., Stroud & Gifford, J. (2010). Precambrian crustal evolution of Peninsular India: a 3.0 billion year odyssey. Journal of Asian Earth Sciences, 39(6), pp.483-515.

Mishra, S., Deomurari, M. P., Wiedenbeck, M., Goswami, J. N., Ray, S., & Saha, A. K. (1999). 207Pb/206Pb zircon ages and the evolution of the Singhbhum Craton, eastern India: an ion microprobe study1. Precambrian Research, 93(2-3), pp.139-151.

Misra S, (1993). Geochemistry and petrology of Mayurbhanj Granite of Bangriposi-Romapahari area, Mayurbhanj district, Orissa, India. Unpub Ph. D. thesis Univ. Calcutta

Misra S, (1999). The Mayurbhanj granite: its nature, tectonic setting, mode of emplacement and pressure-temperature of magma generation. Indian Journal of Geology, 71 (1 & 2), pp.33-52.

Misra S, (2002). Evolution of Mayurbhanj granite pluton, eastern Singhbhum, India: a case study of petrogenesis of a A-type granie in bimodal association. Journal of Asian Earth Sciences, 20(200), pp.965-989.

Mondal, S. K., Frei, R., & Ripley, E. M. (2007). Os isotope systematics of mesoarchean chromitite-PGE deposits in the Singhbhum Craton (India): Implications for the evolution of lithospheric mantle. Chemical Geology, 244(3-4), pp.391-408.

Moorbath, S., & Taylor, P. N. (1988). Early Precambrian crustal evolution in Eastern India: the ages of the Singhbhum Granite and included remnants of older gneiss.

Mukhopadhyay K, (1979). Geology of the Kesharpur Romapahari area with special reference to the mineralisation potentiality of the Romapahari Granite, Mayurbhanj district, Orissa, India. Unpublish M.Sc. thesis, Univ. Calcutta, pp.121.

Mukhopadhyay, D. (2001). The Archaean nucleus of Singhbhum: the present state of knowledge. Gondwana Research, 4(3), pp.307-318.

Mukhopadhyay, D., Deb, G.K. (1995). Structural and textural development in Singhbhum shear zone, eastern India. Proc. Indian Acad. Sci. Earth Planet Sci,104, pp.385–405

Mukhopadhyay, J., Ghosh, G., Nandi, A. K., & Chaudhuri, A. K. (2006). Depositional setting of the Kolhan Group: its implications for the development of a Meso to Neoproterozoic deep-water basin on the South Indian craton. South African Journal of Geology, 109(1-2), pp.183-192.

Murty, V.N. and Acharya, S. (1975) Lithostratigraphy of the Precambrian rocks around Koira, Sundargarh district, Orissa. J. Geol. SOC. India, v. 16, pp.55-68.

Naha, K. (1954). A note on the continuation of the Singhbhum shear belt into eastern Mayurbhanj. Science & Culture 20, pp.295-297.

Naha, K. (1956). Structural set-up and movement plan in parts of Dhalbhum, Bihar. Sci. Cult. (Calcutta), 22, pp.43-45.

Naha K, (1960). Granitic emplacement in relation to thrusting in south Dhalbhum and northeastern Mayurbhanj. Quart Jour Geol Min Metal Soc India, 32(3), pp.115-122.

Naha, K., & Ghosh, S. K. (1960). Archaean palaeogeography of eastern and northern Singhbhum, eastern India. Geological Magazine, 97(5), pp.436-439.

Naqvi, S. M., & Rogers, J. J. W. (1987). Precambrian geology of India. Oxford monographs on geology and geophysics. Oxford Monographs on Geology and Geophysics, pp.6.

Nelson, D. R., Bhattacharya, H. N., Misra, S., Dasgupta, N., & Altermann, W. (2007). New SHRIMP U–Pb zircon dates from the Singhbhum craton, Jharkhand–Orissa region, India. In Abstracts International Conference on Precambrian Sedimentation & Tectonics & 2nd Global Precambrian Sedimentation Syndicate Meeting. Indian Institute of Technology, Bombay (Vol. 47).

Olierook, H.K.H., Clark, C., Reddy, S.M., Mazumder, R., Jourdan, F., Evans, N.J. (2019). Evolution of the Singhbhum Craton and supracrustal provinces from age, isotopic and chemical constraints. Earth-Science Rev. 193, pp.237–259.

Ozha, M.K.; Pal, D.C.; Mishra, B.; Desapati, T.; Shaji, T.S. (2017). Geochemistry and chemical dating of uraninite in the Samarkiya area, central Rajasthan, northwestern India-implication for geochemical and temporal evolution of uranium mineralization. Ore Geol. Rev, 88, pp.23–42.

Parvej, Alam (2019). Characterisation of soda granites and related uranium metallogeny over rajgaon-gura sector, singhbhum shear zone, Jharkhand. Unpub. M.tech. thesis. Atomic Mineral Directorate, Eastern Region, Jamshedpur.

Pearce, J. (1983). The role of sub-continental lithosphere in magma genesis at destructive plate margins. Continental Basalts and Mantle Xenoliths.

Pearce, J. A., Harris, N. B., & Tindle, A. G. (1984). Trace element discrimination diagrams for the tectonic interpretation of granitic rocks. Journal of petrology, 25(4), pp.956-983.

Rai, K. L., Sarkar, S. N., & Paul, P. R. (1980). Primary depositional and diagenetic features in the banded iron formation and associated iron-ore deposits of Noamundi, Singhbhum district, Bihar, India. Mineralium Deposita, 15(2), pp.189-200.

Rene, M. (2008). Anomalous rare earth element, yttrium and zirconium mobility associated with uranium mineralisation. Terra Nova, v.20, pp.52–58.

Rogers, J. J. (1996). A history of continents in the past three billion years. The journal of geology, 104(1), pp.91-107.

Saha, A. K. (1972). Petrogenetic and structural evolution of the Singhbhum granite complex, eastern India. In Proceedings of the 24th International Geological Congress. pp.147-155.

Saha A. K, Bose R, Ghosh S N and Roy, (1977). Petrology and emplacement of the Mayurbhanj Granite batholith, eastern India. Bulletin of Geological Minning and Metallurgical Society of India, 49, pp.1-34.

Saha A. K., Ghosh S., Dasgupta D., Mukhopadya K., and Ray S L., (1984). Studies on crustal evolution of the Singhbhum-Orissa Iron Ore craton, in Monograph on crustal evolution. Indian Society of Earth Science, pp.1-74.

Saha, A. K., (1994). M-27. Crustal Evolution of Singhbhum-North Orissa, Eastern India. GSI Publications, 1(1).

Saha, A . K., (1975). The Mayurbhanj granite- a Precambrian batholith in Eastern India: Geol. Soc. India Jour.16, pp.137-41

Saha, A. K., & Ray, S. L. (1984). The structural and geochemical evolution of the Singhbhum granite batholithic complex, India. Tectonophysics, 105(1-4), pp.163-176.

Saha, A. K., Ray, S. L., & Sarkar, S. N. (1988). Early history of the Earth: evidence from the eastern Indian Shield. Precambrian of the Eastern Indian Shield. Mem. Geol. Soc. India, 8, pp.13-37.

Saha, A. K., (1979),Geochemistry of Archean granites of the Indian Shield. Geol. Soc. India Jour., 20, pp.375-392.

Sarkar, S. C. (1964). Geological conditions of the formation of copper deposits in the Mosabani area, Singhbhum, India. Moscow Univ. Pub., pp.5-16.

Sarkar, S. C. (1984). Geology and ore mineralisation of the Singhbhum copper-uranium belt, Eastern India. Jadavpur University.

Sarkar, A. N. (1982). Precambrian tectonic evolution of eastern India: a model of converging microplates. Tectonophysics, 86(4), pp.363-397.

Sarkar, S. C. (1966a). Ore deposits along Singhbhum shear zone and their genesis. Contributions to the geology of Singhbhum, pp.91-101.

Sarkar, S.C., Deb, M., and Roy Choudhury, K., (1971). Sulphide mineralisation along Singhbhum shear zone, Bihar. Soc. Mining Geologists, Japan, Spec. Issue, 2, pp.226-234

Sarkar,S .C., and Deb, M., (1974). Metamorphism of the sulphide of the Singhbhum copper belt, India the evidence from the ore fabric, Economic Geology, 69, pp.1282-1293.

Sarkar, S. C. (1986). The problem of uranium mineralization in Precambrian metamorphic shear tectonites–With particular reference to the Singhbhum copper-uranium belt Eastern India. Vein type uranium deposits. TECDOC-361, IAEA, Vienna, 9-20.

Sarkar, S. N., Ghosh, D., & St Lambert, R. J. (1986). Rubidium-strontium and lead isotopic studies on the soda-granites from Mosaboni, Singhbhum Copper Belt, E. India. Indian journal of earth sciences, 13(2-3), pp.101-116.

Sarkar, S. N. and Saha, A. K. (1983). Structure and Tectonics of Singhbhum-Orissa Iron Ore Craton, eastern India. Structure and Tectonics of the Precambrian Rocks. Recent Res. in Geol. 10, pp.1-25, Hindustan Pub., New Delhi.

Sarkar, S. N., Saha, A. K., & Subhasis, S. (1990). Structural pattern of Pala Lahara area, Dhenkanal district based on aerial photo interpretation and ground data. Indian journal of earth sciences, 17(2), pp.128-137.

Sarkar, Sanjib Chandra, and Anupendu Gupta (2012). Crustal evolution and metallogeny in India. Cambridge University Press.

Sengupta, S., Ghosh, S.K., (1997). The kinematic history of the Singhbhum Shear Zone. Proc. Indian Acad. Sci. Earth Planet. Sci. 106, pp.185–196

Sengupta, P. R. (1972). Study on mineralization in southeastern part of Singhbhum Copper Belt, Bihar. Memoirs of the Geological Suevey of India, 101, pp.1-82.

Sengupta, S., & Chattopadhyay, B. (2004). Singhbhum Mobile Belt-how far it fits an ancient orogen. Geol. Surv. India Spl. Publ, 84, 23-31.

Sengupta, S., Corfu, F., McNutt, R. H., & Paul, D. K. (1996). Mesoarchaean crustal history of the eastern Indian Craton: Sm-Nd and U-Pb isotopic evidence. Precambrian Research, 77(1-2), pp.17-22.

Sengupta, S., Paul, D. K., De Laeter, J. R., McNaughton, N. J., Bandopadhyay, P. K., & De Smeth, J. B. (1991). Mid-Archaean evolution of the eastern Indian craton: geochemical and isotopic evidence from the Bonai pluton. Precambrian Research, 49(1-2), pp.23-37.

Sengupta, S., Acharyya, S. K., & DeSmeth, J. B. (1997). Geochemistry of Archaean volcanic rocks from Iron Ore supergroup, Singhbhum, eastern India. Proceedings of the Indian Academy of Sciences-Earth and Planetary Sciences, 106(4), pp.327.

Shand, S. J. (1943). Eruptive rocks: their genesis, composition, classification, and their relation to ore deposits with a chaper on meteorites (No. 552.1 S43 1943).

Shannon, R.D. (1976). Revised effctive ionic radii and systematic studies of interatomic distances in halides and chalcogenides. Acta Crystallogr, 32, pp.751–767.

Streckeisen, A. L. (1973). Plutonic rocks, classification and nomenclature recommended by the IUGS subcommission on the systematics of igneous rocks. Geotimes, 18, pp.26–30.

Streckeisen, A.L, (1976). To each plutonic rock its proper name. Earth Science Review 12, pp.1-33.

Sunder-Raju, P.V., Hanski, E. and Lahaye, Y.(2015). LA-MC-ICP-MS dating of zircon from chromitite of the Archean Bangur Gabbro Complex, Orissa, India – Ambiguities and constraints. Acta Geologica, 13(4): pp.325-334.

Talapatra, A. K. (1966). Study of Soda-Granite and associated feldspathic rocks with reference to ore mineralization along the Singhbhum shear zone. Ph.D. thesis Univ. Calcutta.

Talapatra, A. K. (1968). Sulfide mineralization associated with migmatization in the south eastern part of the Singhbhum shear zone, Bihar, India: Economic Geology, 68, pp.156-165.

Talapatra, A. K. (1969). Study of feldspathic schists and Soda-Granites from the south-eastern part of the Singhbhum shear zone, eastern India. Quart. Jour. Geol. Min. Met. Soc. India, 41, pp.65-82.

Vinogradov, A., Tugarinov, A. L., Zhykov, C., Stapnikova, N., Bibikova, E., & Khorre, K. (1964). Geochronology of Indian Precambrian. In Report of the 22nd International Congress, New Dehli, 10, pp.553-567.

Vohra, C. P., Dasgupta, S., Paul, D. K., Bishui, P. K., Gupta, S. N., & Guha, S. (1991). Rb-Sr chronology and petrochemistry of granitoids from the south-eastern part of the Singhbhum craton, Orissa. Geological Society of India, 38(1), pp.5-22.

Whalen, J. B., Currie, K. L., & Chappell, B. W. (1987). A-type granites: geochemical characteristics, discrimination and petrogenesis. Contributions to mineralogy and petrology, 95(4), pp.407-419.

Winter, J. D. (2014). Principles of igneous and metamorphic petrology. Pearson Education.

Xu. G. Wang A, Gu Q. Zhang J. Zhang Z, Huang Y (1981). Some characteristics of uranium oxides in China. Bull Mindr, 104, pp.565-574.

Yuan, F.; Jiang, S.-Y.; Liu, J.; Zhang, S.; Xiao, Z.; Liu, G.; Hu, X. (2019). Geochronology and Geochemistry of Uraninite and Coffinite: Insights into Ore-Forming Process in the Pegmatite-Hosted Uraniferous Province, North Qinling, Central China. *Minerals*, *9*, pp.552.